FUEL AND CORE PHYSICS CONSIDERATIONS FOR A PRESSURE TUBE SUPERCRITICAL WATER COOLED REACTOR

FUEL AND CORE PHYSICS CONSIDERATIONS FOR A PRESSURE TUBE SUPERCRITICAL WATER COOLED REACTOR

BY

MICHAEL H. MCDONALD, B.Sc, Honours

A THESIS
SUBMITTED TO THE SCHOOL OF GRADUATE STUDIES
OF MCMASTER UNIVERSITY
IN PARTIAL FULFILLMENT OF THE REQUIREMENTS
FOR THE DEGREE
MASTER OF APPLIED SCIENCE

McMaster University

MASTER OF APPLIED SCIENCE (2011) MCMASTER UNIVERSITY
(Engineering Physics) HAMILTON, ONTARIO

TITLE:	Fuel and Core Physics Considerations for a Pressure Tube Supercritical Water Cooled Reactor
AUTHOR:	Michael H. McDonald B.Sc. Honours (Physics) University of Winnipeg
SUPERVISOR:	Dr. D. R. Novog Department of Engineering Physics McMaster University
NUMBER OF PAGES:	viii, 131

Abstract

The supercritical water cooled reactor (SCWR) is a Generation IV reactor concept that features light water coolant in a supercritical state. Canada is developing a pressure tube variant of the supercritical water reactor as an evolution of the CANDU reactor. The main advantages of the pressure tube SCWR are an improved thermal efficiency over current reactors, enhanced safety through passive safety features, and plant simplifications. The objective of this thesis was to investigate current fuel and core designs for the Canadian SCWR concept.

Simulations of 2-D lattice cells for fuel assemblies containing 43 and 54 fuel elements were performed using the neutron transport code WIMS-AECL. Safety parameters and fuel burnup performance were investigated here. Three dimensional full core simulations were performed using the diffusion code RFSP. These studies examined batch fueling, cycle length, radial and axial power profiles, linear element ratings, and reduction of axial power peaking through graded enrichment along the fuel channel. Finally, a study of reactivity transients was performed using the FUELPIN heat transfer/point kinetics code.

The main results of the studies show that the coolant density change that occurs as water passes through the pseudocritical point strongly affects fuel performance. It is concluded that the 54 element assembly design is acceptable in terms of coolant void reactivity performance with lattice pitch smaller than 26 cm. To meet the burnup target, a fuel enrichment of about 5% is required. From the RFSP studies, this level of fuel enrichment will provide an operating period of 370 days between refueling. Relatively high axial power peaking is observed at the beginning of cycle conditions. A main finding is that the proposed reactor power level of 2540 MW_{th} produces unacceptably high linear element ratings. This is confirmed using the FUELPIN code. A reduction in linear element rating is suggested for consideration.

Contents

List of Figures

List of Tables

Chapter 1

Introduction

The goal of this thesis is to present some of the first evaluations of the fuel and core preconceptual designs for the Canadian Generation IV supercritical water cooled reactor (SCWR). Lattice and full core calculations have been performed using the modern neutron transport code WIMS-AECL and diffusion code RFSP. Also presented is a first available analysis of fuel powers and temperatures during a loss of regulation transient. This was performed using the FUELPIN heat transfer/point kinetics computer code. This thesis has been organized as a logical progression of calculations, starting from the basic lattice cell calculation, building up to the full core simulation which draws upon the previous lattice calculations, and then an evaluation of linear element ratings and selected reactivity transients. From both the core and lattice cell calculations, the linear element rating can be determined, and this is then furthered in calculations of fuel and clad temperatures during normal operation and loss of regulation accidents.

Chapter two introduces the Canadian SCWR design through a review of literature and work previously conducted on the SCWR. Also included is a review of other supercritical water cooled reactor designs being pursued by other countries.

Chapter three outlines the computer codes used and some of the theory and equations used

by these codes. Listed here are the equations for neutron transport and diffusion as well as point kinetics. The methodology of the calculations is described here as well.

Chapter four presents the results of a lattice cell comparison between 43 and 54 fuel element assembly geometries. A suitable choice for the fuel design is determined and results of fuel burnup and coolant void reactivity are presented here. A discussion is made to compare online refueling to batch refueling and the effect this will have on fuel burnup.

Chapter five discusses the full core simulations performed using the fuel assembly geometry found in chapter four. Discussed here is the refueling strategy employed as well as radial and axial core power profiles. Important for safety analysis, the linear element rating is calculated for the maximum power fuel channel.

Chapter six draws upon the linear power rating found in chapter five and extends this to the calculation of fuel and clad temperatures during normal operation and reactivity initiated transients through the use of point kinetics and a one-dimensional heat transfer analysis.

Finally, chapter seven summarizes the conclusions reached here and gives some possibilities for future work in this area.

1.1 Generation IV Reactor Initiative

With an ever increasing world population and increasing growth in energy consumption by developing nations, significant pressure is being placed on the world's energy resources. Coupled with these increased energy demands, there are also great concerns over climate change and sustainability. Reserves of oil are declining worldwide, while coal and natural gas burning are significant sources of greenhouse gas emissions, with coal fired power plants in particular being phased out in many areas. Clean and sustainable electricity generation is seen as a top priority, and a shift away from traditional fossil fuel burning to more "green" solutions is becoming commonplace. Renewable

sources such as wind and solar power currently do not come close to providing the energy density needed to meet either current or future demand. Nuclear power, by comparison, is relatively clean in that it is not a significant source of greenhouse gases, and can provide enormous amounts of reliable and cost effective electrical energy.

It is certain that nuclear energy will need to play a prominent role in terms of future energy generation. There have been many advances in nuclear power through the years. The first generation, prototype nuclear power reactors were developed and built in the 1950s. Most current operating power reactors are of the Generation II and III type, each generation evolving and advancing from the previous. Looking ahead to the future, many countries are currently researching and planning for a new generation of innovative and advanced nuclear power reactors, the so-called Generation IV nuclear reactors.

An international collaboration involving thirteen countries, known as the Generation IV International Forum (GIF), aims to leverage resources to research and design an advanced Generation IV reactor for deployment internationally around the year 2030.
The goals of the Generation IV project can be grouped into four broad categories [1].

Sustainability

Sustainability includes the clean generation of electricity as well as the minimization of "nuclear waste" through advanced fuel cycles, or technology that works to reduce current waste, e.g. fast reactors.

Economics

Generation IV nuclear systems must be economical in that they have overall cost advantages over other forms of electricity generation.

Safety and Reliability

As with any nuclear power plant, Generation IV systems will strive to offer improvements in

safety, where possible using passive safety features. In particular, post-Fukushima there is an elevated sensitivity to safety features in the Generation IV designs.

Proliferation Resistance

Generation IV reactors and fuel cycles used should be designed in such a way that the diversion of nuclear materials for weapons purposes is unattractive or unfeasible.

1.1.1 Generation IV reactor systems

Six vastly different reactor candidate designs have been identified as promising Generation IV reactor types. The Generation IV reactors under consideration by GIF are:

GFR: Gas-cooled Fast Reactor

The GFR is a direct cycle reactor concept featuring a helium coolant and gas turbine. The reference design is for a 600 MWth reactor with an outlet temperature of 850°C and high thermal efficiency of 48%. It features a fast (i.e. high energy) neutron spectrum that can be used to transmute actinides and ultimately reduce radiotoxicity of current spent nuclear fuel [1].

VHTR: Very High Temperature Reactor

The VHTR is a helium gas cooled reactor with a thermal neutron spectrum from graphite moderation. It is expected to feature coolant outlet temperatures above 1000°C The reference design features a thermal power of 600 MW.

LFR: Lead-cooled Fast Reactor and SFR: Sodium Cooled Fast Reactor

Both reactors are fast neutron spectrum reactors with liquid metal coolants. Both are expected to feature closed fuel cycles and are suited for management of actinides. The LFR is rated slightly higher in safety due to the inert coolant, while there is more operational experience for sodium cooled reactors worldwide. The LFR has many proposed plant sizes ranging from small 50-150

MWe plants up to large 1200 MWe plants. The SFR has similar options: a smaller 150 MWe-500 MWe plant, or larger 500 MWe-1500 MWe plants [1].

MSR: Molten Salt Reactor

The MSR is a thermal-to-epithermal spectrum reactor featuring a liquid fuel that is made up of sodium, zirconium and uranium fluorides [1] and is an efficient actinide burner. The heat generated is transferred via a heat exchanger. The reference design is for a 1000 MWe core.

SCWR: Supercritical-Water Cooled Reactor

The SCWR is a light water cooled reactor that features a fluid in a supercritical state as coolant to increase reactor efficiency over current light water reactors. Thermal spectrum and fast spectrum designs exist as well as pressure tube and pressure vessel designs. The supercritical water cooled reactor is the subject of this thesis.

1.2 Supercritical Water Cooled Reactor

For nuclear power plants, a major portion of the power generation cost over the lifetime of the reactor is the relatively high capital cost of the reactor (typically 50-60% for light water reactors [12]). In addition, most currently operating nuclear power plants generate electricity with a thermal efficiency of around 30-33%. Simplification of plants and increases in thermal efficiency will help to make nuclear power a more economically favourable option.

The supercritical water cooled reactor is a pressurized light water reactor that operates above the thermodynamic critical point of water, i.e. 647 K and 22.1 MPa (Figure 1.1). In doing so, the thermal efficiency can be raised to values over 40% [2, 1]. Also, since such reactors can employ direct cycles, there can be significant plant simplifications, i.e. no secondary side and associated steam generators may be needed. The plant simplifications can reduce plant capital costs as well as improve safety. Further still, many modern fossil fuel power plants currently use supercritical water in their electricity generation cycle. As a result, the turbine technology and balance of plant components for supercritical water are available already.

In addition to electricity production, the SCWR is well suited to other applications. Hydrogen production, expected to be a growing industry in the future, is currently done mostly through processing of hydrocarbons. This process is unsustainable and works against the movement to reduce carbon emissions. A promising alternative involves direct production of hydrogen through a thermochemical cycle. This process requires high temperatures like those reached in the SCWR. An overview of this technology is given by Rosen et al. in [3]. The high temperatures may also find utility for process heat in any number of industries, e.g. desalinization.

The use of a supercritical water coolant in a nuclear reactor is not a new concept. In fact, there exist designs from the late 1950s and 1960s proposing the use of supercritical water in nuclear power reactors [5]. A good review of previous early designs is given by Oka in [6].

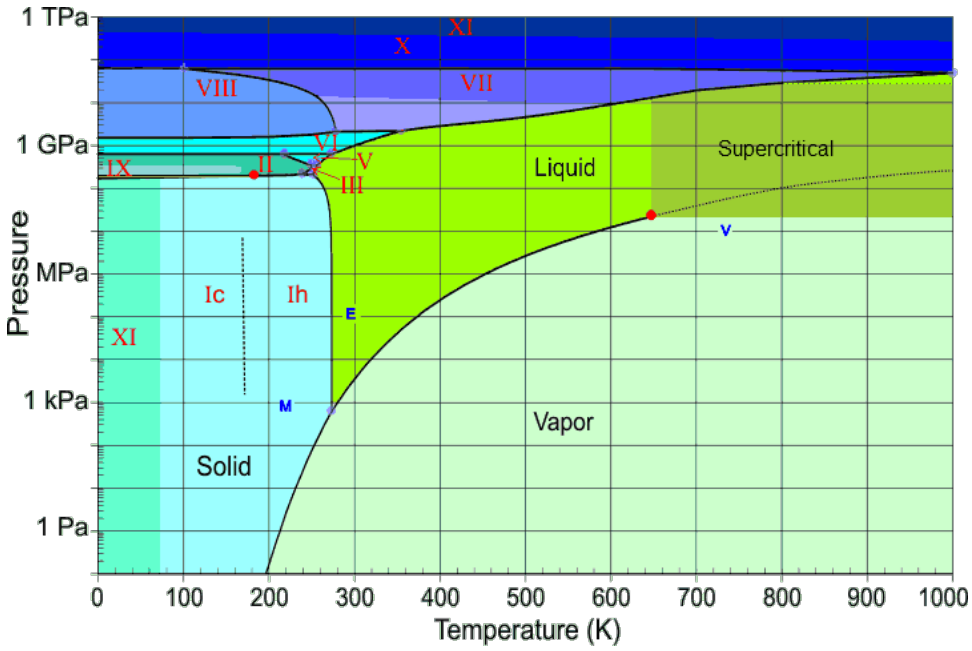

Figure 1.1: Phase Diagram for Water (from [4])

All designs can be placed into two categories: the pressure vessel type reactor, where the fuel, moderator and coolant are all contained within a large thick-walled vessel to withstand the high pressures, or a pressure tube type reactor where the fuel and high pressure coolant are contained in many tubes passing through a calandria vessel that contains the moderator at low (or atmospheric) pressure. Further, the designs can be distinguished by neutron energy spectrum with some SCWR designs featuring a fast (high energy) neutron spectrum and other designs utilizing thermal neutron energies for the bulk of the fission events.

In Canada, there is a long history of successful CANDU (CANada Deuterium Uranium) pressure tube (PT) type reactors designed by Atomic Energy of Canada Limited (AECL). A unique feature of the CANDU reactor is the use of a heavy water moderator and coolant, chosen for its lower neutron absorption cross-section compared to light water. As an evolution of the CANDU design,

the Canadian SCWR concept is a pressure tube design featuring a thermal neutron spectrum, heavy water moderator and light water coolant. Herein, the acronym SCWR shall refer to the Canadian pressure tube conceptual design unless otherwise specified.

Chapter 2

Background and Literature Review

First generation nuclear power reactors in Canada emerged in the 1960s. A prototype nuclear power plant called NPD ("Nuclear Power Demonstration") began operation in 1962, demonstrating the technology for commercial production of electricity through nuclear fission. In 1967, a larger prototype, the Douglas Point reactor, began operation. Both first generation reactors taught many lessons to the Canadian nuclear industry and provided much of the technology that went into the design of the CANDU reactor. Key features of the CANDU design are pressure tubes containing fuel and pressurized heavy water coolant, a low pressure heavy water moderator system, and on-power refueling using natural uranium fuel.

After the successes of the first generation reactors in Canada, the CANDU reactor design was developed and refined, and deployment of Generation II reactors began in 1971. In the years to follow, other CANDU plants would be built in Canada, and around the world.

Generation III reactors in Canada are currently being developed by AECL and include the Enhanced CANDU 6 reactor which builds on the features of the current CANDU reactors while improving safety and performance. Another Generation III reactor, sometimes referred to as Generation III+, is the Advanced CANDU reactor (ACR). While retaining the heavy water moderator,

pressure tubes, and online refueling of the CANDU reactor, it features light water coolant and enriched fuel design to meet more demanding requirements [7].

As part of the Generation IV International Forum, Canada is participating in the development and selection of the next generation reactor technology, or Generation IV. The SCWR concept is the main focus of the Canadian Generation IV effort and is being designed by AECL as an evolution of the CANDU reactor concept using pressure tubes and separate low pressure moderator. Canada is also conducting research into the materials aspect of the VHTR concept, as there is some synergy in this area with the SCWR.

2.1 Features of Canadian Pressure Tube SCWR

There exist a number of differences between current CANDU reactors and the Canadian SCWR concept.

Due to the high pressures of the supercritical water coolant, on-power refueling, a main feature of current CANDU reactors, is not practicable (i.e., closure seals, fuel machine pressures make the design unattractive). The reactor will thus be fueled in batches offline, similar to current operating pressurized water reactors (PWR) and boiling water reactors (BWR). Also, since the reactor will not be fueled online, the core shall be positioned in a vertical orientation rather than the current horizontal fuel channels in the CANDU reactor. An inlet plenum will be used at the top of the core, while outlet feeders will be used at the coolant outlet [8]. The vertical orientation will facilitate the fueling from the top of the reactor. Reactivity suppression strategies similar to those used in LWRs will need to be used for a batch fueled reactor.

The corrosive nature of the supercritical water coolant precludes the use of zircaloy-IV as a fuel sheath material as is standard in current operating CANDU reactors. While a large amount of materials research is currently being undertaken for the SCWR, the current clad used in physics

calculations is stainless steel 310. While stainless steel offers more corrosion protection than zirconium alloys, it comes at a cost of having a much higher neutron absorption, which presents a penalty in neutron economy. An alternative, under development, may be the use of zirconium alloys with a protective coating [16], or the use of zirconium alloy clad at the high coolant density region of the core where the coolant is less corrosive, and switching to stainless steel clad near the point of the channel where the transition to the supercritical state occurs. The use of light water as coolant increases the penalty on neutron economy, as light water has a larger neutron absorption cross-section than heavy water.

The use of batch fueling, as well as the above penalties to neutron economy mean that the fuel material for the reactor must be enriched, again a departure from the natural uranium fueled CANDU reactor. A major focus of this work is to perform neutronic calculations with the new SCWR fuel design and materials.

The enrichment level of the fuel is based predominantly on the fuel burnup target. Currently, the target exit burnup for the fuel set by AECL is 45 MWd/kg. While the focus of this thesis is enriched uranium fuel, the current fuel type being pursued by AECL is a plutonium-thorium mixture. The choice to use thorium fuel for the SCWR increases its sustainability, as thorium is around three times more abundant in the earth than uranium. Further, many chemical properties of thorium dioxide are superior to uranium dioxide including chemical stability, thermal conductivity, and fission product release [18]. These advantages may be reduced however, when other chemical species, e.g. plutonium "driver" fuel, are admixed with the ThO_2.

2.2 Fuel Channel Designs

Two fuel channel designs have been proposed by AECL: the so-called High Efficiency Channel (HEC) and the Re-Entrant Channel (REC)[2].

2.2.1 High Efficiency Channel

In the High Efficiency Channel design shown in Figure 2.1, the pressure tube is in direct contact with the moderator. This is in contrast to the current use of calandria tubes in current CANDU reactors. For the HEC, a ceramic insulator is located on the inside surface of the pressure tube. The current material choice for the insulator is yttria stabilized zirconia. The use of the insulator protects the pressure tube from the corrosive supercritical water coolant and allows the pressure tube to be made of a zirconium based alloy. In addition, the insulator prevents unwanted heat loss to the moderator. In this thesis, only the high efficiency channel concept has been examined.

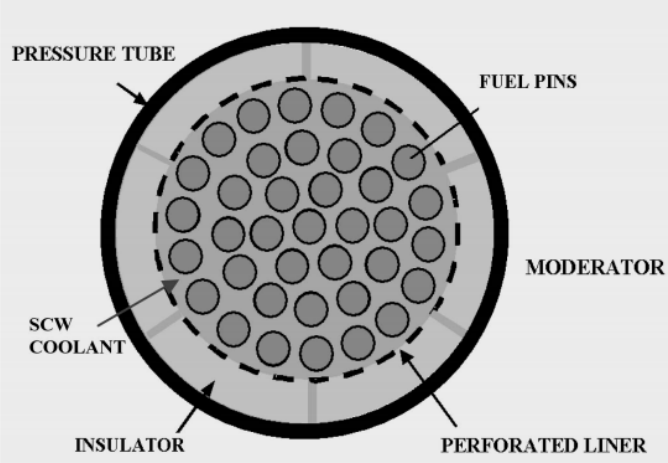

Figure 2.1: High Efficiency Channel Concept (from [2])

2.2.2 Re-Entrant Channel

The re-entrant channel design shown in Figure 2.2 features an inner tube within a pressure tube. The coolant first flows through the annulus created by these two concentric tubes, where it then turns around at the end of the channel and flows back through the fuel area. In this way the pressure tube is kept at a lower temperature, again allowing zirconium alloys to be used.

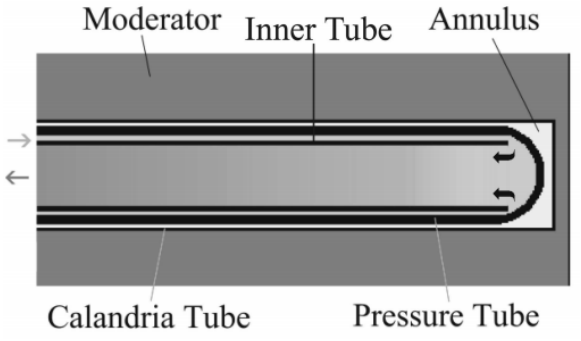

Figure 2.2: Re-entrant Channel Concept (from [2])

2.3 Table of SCWR Parameters

Table 2.1 lists a number of overall parameters of the SCWR that were assumed for the analysis in subsequent chapters.

2.3.1 Coolant Density

As water passes through the critical point, it experiences an abrupt change in many physical properties including density, thermal conductivity, and viscosity. The critical temperature and pressure of water are 373.95°C and 22.064 MPa respectively. In some literature, mention is made of the pseudocritical point. For pressures above the critical pressure, the "pseudocritical point" is the temperature where the fluid exhibits a maximum in specific heat for a given pressure [9]. In general, the temperature corresponding to the pseudocritical point increases slightly with increasing pressure above the critical pressure.

Of particular interest for reactor physics is the density change through the pseudocritical point. The density corresponding to the coolant temperature range in the SCWR fuel channel is shown graphically in Figure 2.3 [1].

[1]Data from MS Excel macro by Dr. B. Spang, http://www.cheresources.com/iapwsif97.shtml

Parameter	Value
Moderator	Heavy Water (Low pressure)
Coolant	Light Water (25 MPa pressure)
Reactor Power	2540 MW (thermal)
Thermal Cycle	Direct Cycle
Coolant Inlet Temperature	350°C
Coolant Outlet Temperature	625°C
Coolant Flow Rate	approx. 1300 kg/sec
Coolant Inlet Density	625.5 kg/m^3
Coolant Outlet Density	67.58 kg/m^3
Core length	5 m
Number of fuel channels	300

Table 2.1: Table of parameters for SCWR

2.4 Other SCWR Concepts

2.4.1 Boiling Water Reactor

While the Boiling Water Reactor does not use supercritical water as a coolant, there are many similarities between it and the SCWR. Firstly, BWRs employ direct thermodynamic cycles similar to the SCWR design. Another similarity is a large density variation of coolant axially across the core as the coolant is allowed to boil in the core. Issues such as coolant instabilities found in operating BWR reactors may also be found in the SCWR as a result of the coolant density variation. An area of current thermalhydraulic research for the SCWR is focused on this phenomenon. Furthermore, BWRs also employ direct power generation cycles similar to the proposed SCWR concept. The BWR provides a long history of operational experience that can be drawn upon in the design of the SCWR.

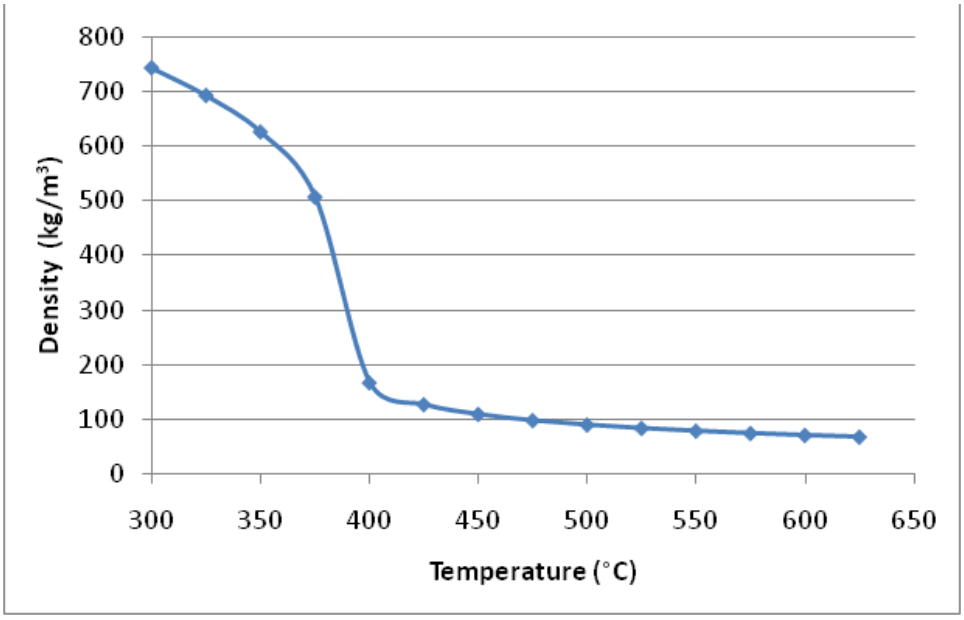

Figure 2.3: Density Of Water at 25 MPa

2.4.2 Japanese SCWR

The development of the Japanese SCWR concept, referred to as "Super Light Water Reactor" or "Super LWR", was started in 1989 at the University of Tokyo [11]. Both fast and thermal neutron spectrum versions of the design have been developed by Oka et al. [12].

The design is a pressure vessel type reactor with a once-through coolant design similar to a BWR. Coolant is fed through inlet nozzles, is heated in the core, and passes through outlet nozzles where it is delivered directly to the turbine system. The reactor pressure is 25 MPa with inlet temperature of 290°C and outlet 510°C.

The fuel assembly is made up of 192 fuel rods and a square, low-temperature water rod to provide moderation. It is shown in Figure 2.4. The fuel is uranium dioxide pellets encased in a stainless steel clad. For the equilibrium core, the reload fuel uranium enrichment is 7.2% [11] to

meet the burnup target of 45000 MWd/tonne. The average linear element rating of the fuel is 18 kW/m, while the design criteria states that the maximum linear element rating is to be 40 kW/m [12]. Kamei et al [10] report a maximum linear heat generation rate of 38.9 kW/m in their studies of fuel and core design. The length of the assembly is 4.2 m. The core will contain 372 of these assemblies and will generate 1725 MWe at 42.7% efficiency.

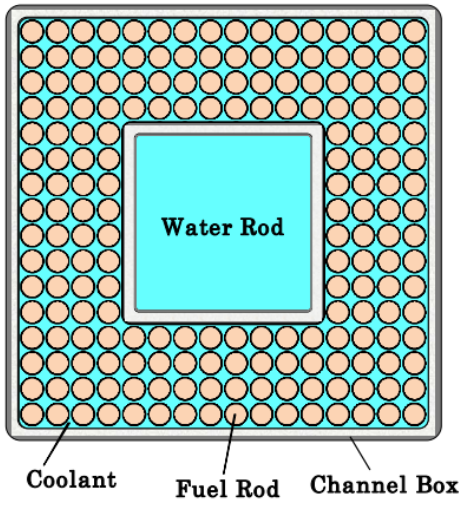

Figure 2.4: Fuel Assembly for Japanese Super LWR (from [11])

Physics analysis that has been done to date on the Super LWR includes cell and assembly burnup calculations using the transport code ASMBURN, and core burnup calculations using a two energy group diffusion code COREBN. This represents a level of analysis similar to that which has been presented in this thesis for the Canadian SCWR. For the Super LWR, the control rods have been designed and included in the full core simulations which represents a step up from the current level of detail for the Canadian preconceptual design.

The method to simulate the equilibrium core using batch refueling is nearly identical to that performed in this report using the code RFSP. For the Super LWR, the refueling scheme is a three

batch scheme with one additional fourth cycle assembly placed in the center of the core for flux flattening. It is a so-called "low leakage" fuel loading pattern, where as many as possible third cycle assemblies are placed in the core periphery. It has been found previously that placing the assemblies with the highest reactivity in the core periphery (a strategy used to flatten the radial power distribution) led to higher enrichments being required [10], or alternatively a burnup penalty. The fuel assemblies feature axially varied enrichments to reduce the axial power peaking along the assembly, a concept that is explored in this thesis for the pressure tube SCWR. Figure 2.5 shows the two types of axial enrichments used in the simulations presented in [10]. 40 of the rods in an assembly are the gadolinium doped rods, while the remainder are the undoped variety. Shown in Figure 2.6 is the result for the core-average axial power profile for beginning, middle, and end of cycle using the assemblies with the aforementioned fuel rods. The results for power peaking factors are similar to the results shown in Chapter Five of this thesis for the fuel channel of the Canadian SCWR.

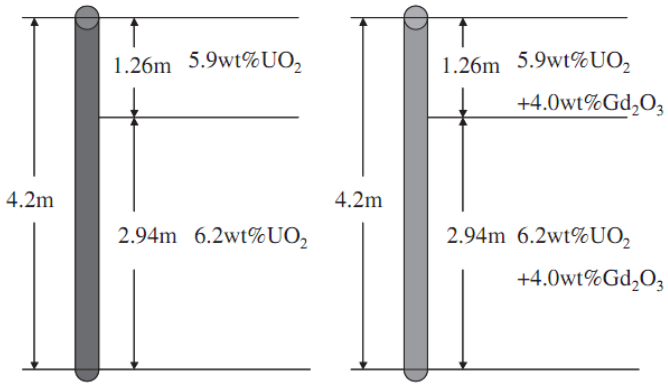

Figure 2.5: Axial Enrichments for Japanese Super LWR (from [10])

Safety analysis has been performed for the Super LWR for a selection of postulated events and is documented in [12]. Abnormal transients including decrease in coolant flow rate, abnormality in

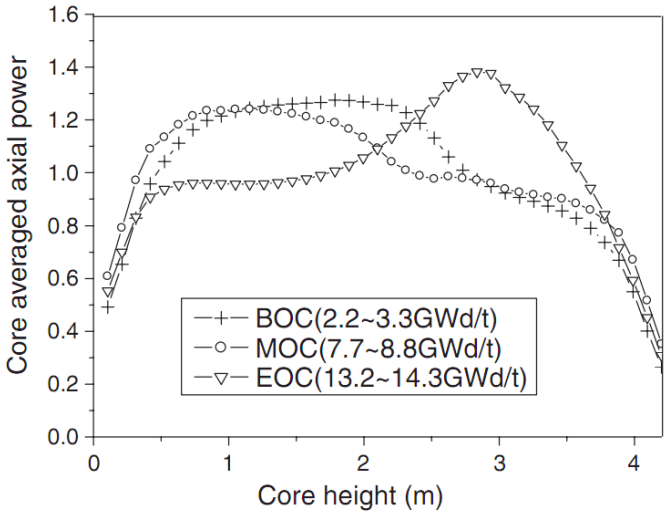

Figure 2.6: Axial Power Profile for Japanese Super LWR (from [10])

reactor pressure, abnormality in reactivity and accidents including decrease in coolant flow rate, control rod ejections at high and low power, and loss of coolant accidents have been described. A significant source of uncertainty in these calculations is the heat transfer coefficient to the supercritical water. Currently there is an IAEA program examining convective heat transfer in supercritical water.

2.4.3 European SCWR

The European supercritical water cooled reactor design is called the "High Performance Light Water Reactor" (HPLWR) and is also a pressure vessel design. Like other SCWR concepts the coolant pressure is 25 MPa. Coolant inlet and outlet temperatures are 280°C and 500°C respectively, which represents the same temperature rise as the Japanese concept [13]. The aim of the reactor is the generation of 1000 MWe. The core features a sophisticated coolant flow path made up of three different sections featuring intensive coolant mixing between sections. The coolant first flows

through the central "evaporator" region of the core where it passes through the pseudocritical point. It then mixes in the upper mixing chamber and flows down through the first "superheater" region where it enters the lower mixing chamber and flows back up through the second superheater region in the core periphery. The supercritical coolant is then delivered directly to the turbines for electricity generation.

The HPLWR fuel assembly is shown in Figure 2.7. It is similar to the Super LWR assembly, featuring a water box for moderation but containing fewer (40), stainless steel clad fuel rods. The active fuel height is equivalent to the Japanese design at 4.2 m. Calculations show that an average discharge burnup of 32.5 MWd/kgU can be achieved with average 6.2% uranium enrichment fuel [14]. The target burnup however is 60 MWd/kg [15]. It has been found [15], that enrichments of up to 9.5% are required to achieve the desired burnup. Assemblies range in enrichment from 3% to 7%, while in addition, some feature gadolinium doped rods. Similar to the Super LWR, axially varied enrichment are used for reduction of axial power peaking.

Physics analysis has been performed for the equilibrium core using the codes KARATE and SPROD [13]. A hot channel assessment has been performed in which a maximum linear element rating calculated for the fuel in the HPLWR is 36.5 kW/m, while the limit that has been proposed is 39 kW/m [14]. This maximum in linear element rating is expected to come in the evaporator region of the core, which is similar to the result found in this thesis for the Canadian SCWR, where the maximum linear element rating is found to occur in the higher density coolant region of the fuel channel. For this safety analysis the HPLWR steady state peak cladding temperature limit has been set at 630°C [15], this is about 100°C less than the Super LWR limit and that used in the analysis in this thesis. The average axial linear element ratings for the three regions of the core is shown in Figure 2.8.

Safety analysis has been performed for many postulated events for the HPLWR. Results given in [15] show the analysis of partial and total loss of feedwater, loss of offsite power, and loss of

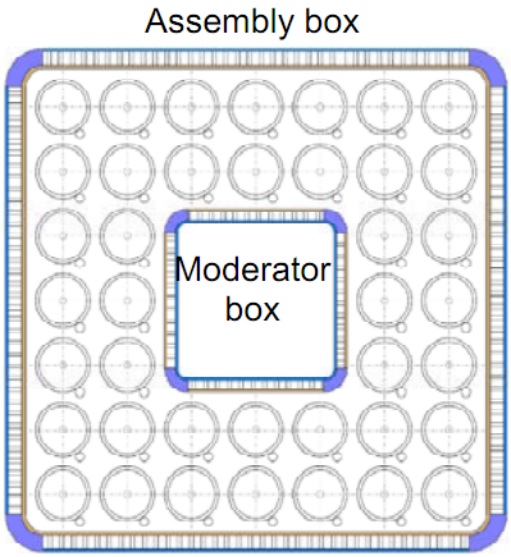

Figure 2.7: Fuel Assembly for European HPLWR (from [13])

coolant accidents. For a comparison to the work presented here, i.e. reactivity initiated accidents, the event of control rod ejection is discussed. For the control rod ejections, two cases were reported: a slow ejection of 1.0 seconds, and a rapid ejection of 0.1 seconds. The maximum reactivity inserted occurred in the 0.1 s case and was approximately 2.8 mk. The maximum clad temperature was found to be 860°C while the pellet centerline temperature was found to reach 2600°C [15] which is below the limits defined, however the fuel centerline temperature represents a small margin to melting.

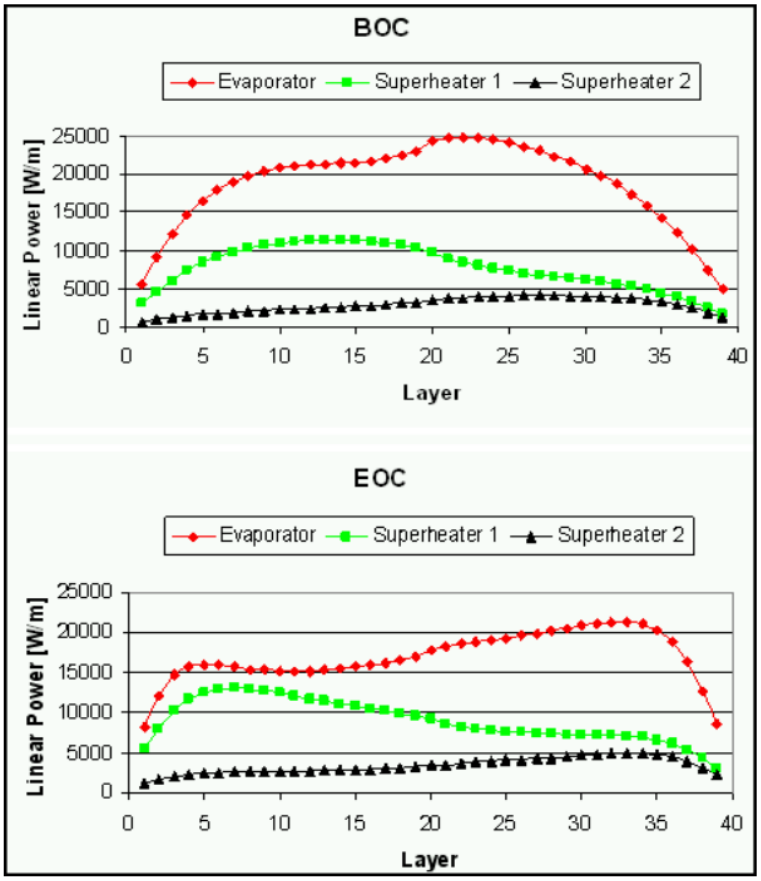

Figure 2.8: Average Axial power profile for European HPLWR (from [14])

2.5 Canadian SCWR Literature

Early research into reactor physics for the Canadian SCWR focused on fuel and lattice scoping studies with a 43-element fuel bundle similar to that designed for the Advanced CANDU Reactor. The parameters investigated in these studies included discharge burnup, coolant void reactivity, lattice pitch, enrichment, and burnable neutron absorber (BNA) concentration [16]. Alongside the 43 element bundle, a new 54 element design was conceived, featuring a large, unheated centre pin. Studies were performed using enriched uranium as well as a plutonium-thorium mixture fuel. These

two bundle designs are compared in this thesis with the enriched uranium fuel only. Key results found in [16] were that:

- There is a large penalty in neutron economy from the use of stainless steel clad
- Both coolant void reactivity and burnup increase with increasing moderator to fuel ratio, i.e. both can not be simultaneously optimized
- For the Pu-Th fuel, an average Pu concentration of 9.2% gives a burnup of 40 MWd/kg
- Burnup for three batch-refueling is at least 25% lower than for online refueling
- The 54 element design is a more efficient design in terms of burnup and CVR than the 43 element design

Later studies investigated the maximum linear element rating of the 54 element bundle [17]. The results shown in this paper indicate that the linear element rating is unacceptably high for this design, reaching nearly 80 kW/m. Similar findings are presented in this thesis. The linear element rating limit is imposed to reduce the temperatures of the fuel, thereby limiting fission gas release that can cause issues with fuel clad integrity. A limit of 40 kW/m for the maximum LER is set and justified in [17].

To reduce the linear element rating, the number of fuel channels has been increased from 300 to 336. Also, new fuel designs were investigated using element subdivision, thus dividing the power up between more elements. A 78-element design is proposed in [17] and is found to have a maximum linear element rating of 37 kW/m, a large improvement over the 54 element design. Another proposed design is the use of annular fuel elements in the outer ring of the fuel assembly. In this design, the fuel pellets in the outer ring are annular and clad on the outside and inside with coolant being allowed to flow through the centres of the elements. While this does not reduce the linear

element rating, it allows the fuel to operate at lower temperatures and satisfies the goal of reduced fission gas release. The results in this paper indicate that for annular fuel operating at a maximum LER of 120 kW/m, the maximum fuel temperature is 1100°C, this is found to be equivalent to solid-rod CANDU fuel operating at 35 kW/m [17].

The most recent literature on the SCWR cements the 78 element design as the new reference design for the SCWR. It is found to offer similar performance in terms of CVR and fuel burnup as the 54 element design, with superior performance in linear element rating [18]. The work documented in this thesis addresses the 54 element design work.

The evolution of the fuel design for the SCWR is shown pictorially in Figure 2.9.

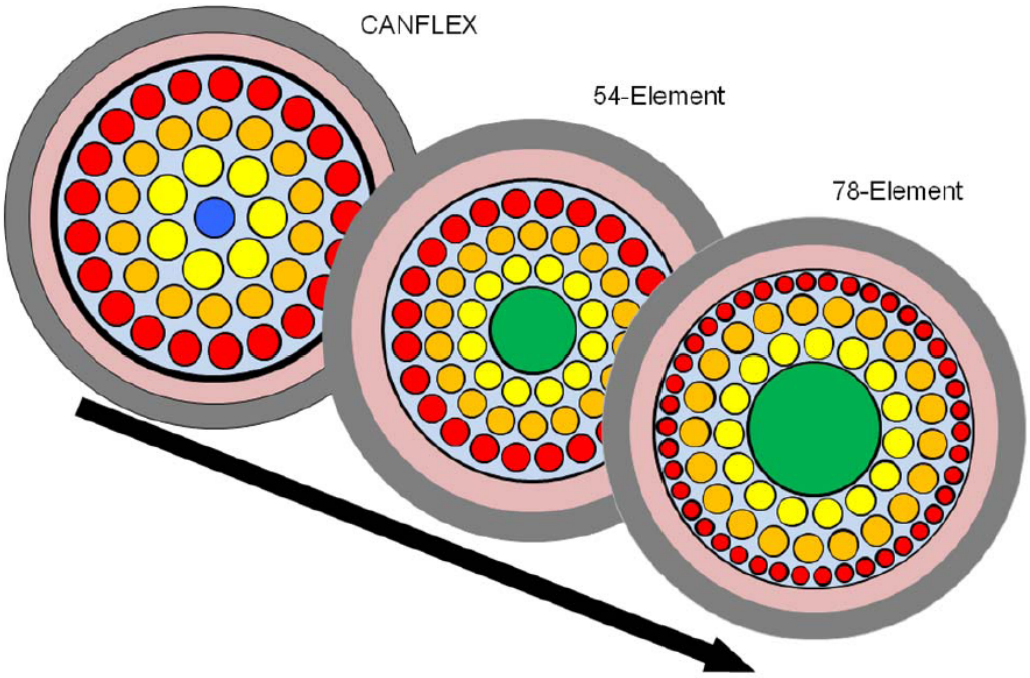

Figure 2.9: Evolution of SCWR fuel design (from [18])

Chapter 3

Calculation Methodology, Codes and Theory

3.1 Lattice Cell Calculation

The calculation method for reactor physics calculations begins with a two-dimensional model of a lattice cell. The lattice cell can be thought of as a slice of a fuel channel and includes the moderator, pressure tube, insulator, liner tube, and fuel bundle geometry with coolant. A diagram of a lattice cell is shown in Figure 3.1.

3.1.1 WIMS-AECL

The lattice cell is modelled with a computer code called WIMS-AECL (Winfrith Improved Multigroup Scheme - Atomic Energy of Canada Limited) version 3.1. WIMS-AECL is a two-dimensional neutron transport code used to calculate many lattice properties including k-infinity (k-effective) values, neutron flux distribution, fuel burnup and radial power densities for user defined geometries and fuel compositions. The multigroup nuclear data library used for the WIMS-AECL calculations

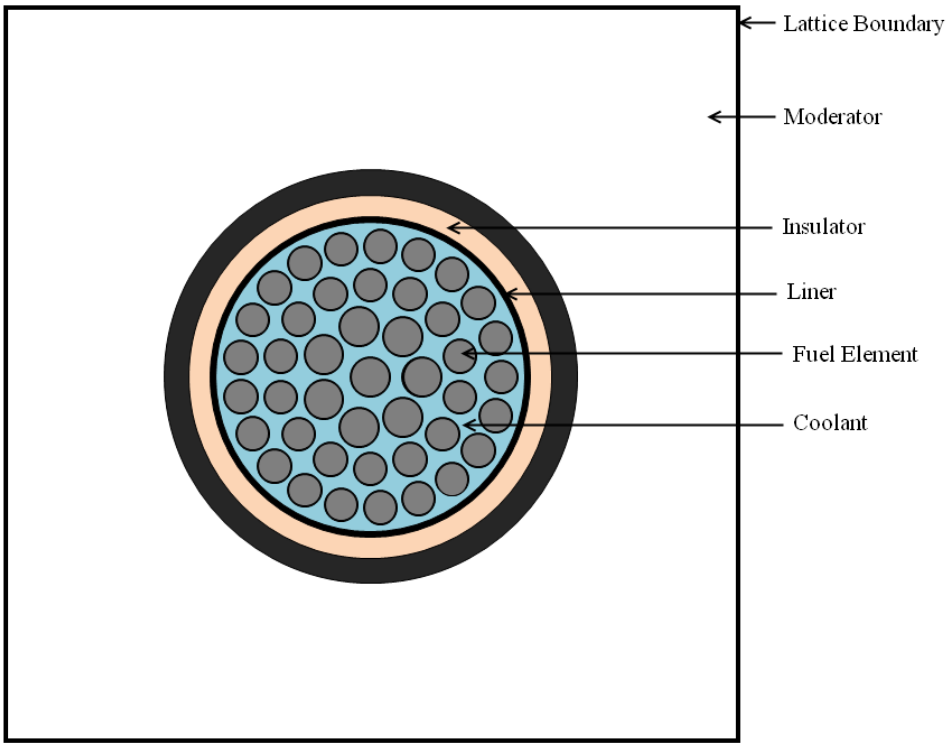

Figure 3.1: Lattice Cell

is the ENDF/B-VII cross-section library. WIMS-AECL has the ability to perform calculations in up to 89 energy groups, and for the studies presented here, all 89 energy groups were used.

The WIMS-AECL calculation can be thought of as a number of steps, and, while a basic overview of the calculation is given here, for a more detailed description of the calculation procedure, the reader is suggested to consult the WIMS-AECL theory manual [19]:

First, the case specific macroscopic cross-sections are prepared. This involves a self-shielding calculation based on the geometry of the lattice cell and if required, a group condensation. This is followed by the main transport solution yielding the neutron flux and multiplication factor for the lattice cell. WIMS-AECL also has the capability to perform burnup calculations. By specifying

the power level, the absolute flux may be determined which is required to determine the reaction rates. The reaction rates allow WIMS-AECL to track the nuclides present throughout the time step the burnup calculation is to be performed. WIMS-AECL will perform a transport solution at each interval specified and in this way, the neutron multiplication factor as a function of burnup may be determined.

Neutron Transport Equation

The main equation being solved by WIMS-AECL is the neutron transport equation. The solution of the neutron transport equation yields the neutron flux distribution and neutron multiplication factor. Essentially, the equation balances the loss and production of neutrons. It can be written in the form:

$$\begin{aligned}[\Omega \cdot \nabla + \Sigma_t(\mathbf{r}, E)]\, \psi(\mathbf{r}, E, \Omega) - \int_0^\infty dE' \int_{4\pi} d\Omega'\ \Sigma_s(\mathbf{r}, E' \to E, \Omega' \to \Omega)\psi(\mathbf{r}, E', \Omega') \\ = \frac{1}{k}\ \chi(E) \int_0^\infty dE' \int_{4\pi} d\Omega'\ \nu(\mathbf{r}, E)\Sigma_f(\mathbf{r}, E)\psi(\mathbf{r}, E', \Omega') \end{aligned} \tag{3.1}$$

where,

$\psi(\mathbf{r}, E, \Omega)$	=	Neutron Flux Distribution
$\mathbf{r}$	=	Position vector
Ω	=	Direction unit vector specifying azimuthal and polar angle
E	=	Neutron Energy
Σ_t	=	Total macroscopic cross-section at position $\mathbf{r}$, energy E
Σ_f	=	Fission macroscopic cross-section at position $\mathbf{r}$, energy E
k	=	Multiplication factor
χ	=	Fission spectrum
ν	=	Number of neutrons produced per fission, dependent on energy
Σ_s	=	Scattering cross-section from energy E' to E and direction Ω' to Ω
∇	=	Spatial gradient
$\int_{4\pi}$	=	Angular integration over unit sphere ($\int_{4\pi} = \int_0^{2\pi} d\phi \int_0^{\pi} \sin\theta \; d\theta$)

Term by term, this equation represents:

First term: Loss of neutrons from position $\mathbf{r}$, energy E, in direction Ω by either neutron movement (gradient term) or any neutron absorption (total cross-section term)

Second term: Increase of neutrons at position $\mathbf{r}$, energy E, in direction Ω by neutrons scattering from some other energy E' and/or direction Ω' to energy of interest E and direction of interest Ω.

Third term: Increase of neutrons at position $\mathbf{r}$, energy E, in direction Ω by fission events.

Here the production and loss of neutrons is balanced by the neutron multiplication factor, k, an important result of the WIMS-AECL calculation. WIMS-AECL solves the transport equation in steady state by solving an integral form of the transport equation through a collision probabilities approach. This method is detailed in the WIMS-AECL theory manual [19] and is not covered here.

3.2 Reactor Core Calculation

Performing a three-dimensional full core neutron transport calculation modelled in the resolution described in the previous section would be prohibitively expensive computationally. Using as a basis the results of the lattice physics calculation, full core 3D calculations can be performed using a neutron diffusion computer code. The diffusion code used here is called RFSP (Reactor Fuelling Simulation Program)[21].

3.2.1 RFSP

The output of a WIMS-AECL calculation includes cross-sections for each material (region) of the lattice cell for each burnup step input into the code. These can be *homogenized* to produce a set of cross-sections for the overall lattice cell. This homogenization of cross-sections over the lattice cell is commonly done with a set of utilities developed by AECL called WIMS Utilities [20]. WIMS Utilities takes as an input the results of a WIMS-AECL calculation and outputs a table of two-group cross-sections specific to the overall lattice cell. Cross-sections produced for each energy group are: absorption, downscattering, upscattering, transport, production yield ($\nu\Sigma_f$). The transport cross-section is related to the diffusion coefficient D as $\Sigma_{tr} = \frac{1}{3D}$. In addition, so-called F and H factors are included in the cross-section tables. The F factor is the ratio of fuel-average to cell-average thermal neutron flux, and the H factor is the energy produced from each energy group for a given flux[21].

In RFSP, a 3D reactor is constructed out of a set of parallelepipeds. Each parallelepiped is supplied with a set of two-group cross sections from the WIMS-AECL calculation and the cross-sections are assumed constant over the entire volume.

Neutron Diffusion Equation

The diffusion equation is an approximation to the neutron transport equation and assumes that neutrons diffuse from regions of high concentration to low concentration, not unlike gaseous particles. The movement is assumed to depend on the concentration gradient and is described by Fick's Law. In practice, for CANDU reactor analysis, a two group representation of the above equation has proven to be sufficient in accurately predicting the core neutronics behaviour. The steady state diffusion equations solved by RFSP are:

$$-\nabla \cdot D_1(\mathbf{r})\nabla\phi_1(\mathbf{r}) + (\Sigma_{a1}(\mathbf{r}) + \Sigma_{12}(\mathbf{r}))\,\phi_1(\mathbf{r}) - \Sigma_{21}(\mathbf{r})\phi_2(\mathbf{r}) - \frac{1}{k_{\text{eff}}}\left(\nu\Sigma_{f1}(\mathbf{r})\phi_1(\mathbf{r}) + \nu\Sigma_{f2}(\mathbf{r})\phi_2(\mathbf{r})\right) = 0$$

$$-\nabla \cdot D_2(\mathbf{r})\nabla\phi_2(\mathbf{r}) + (\Sigma_{a2}(\mathbf{r}) + \Sigma_{21}(\mathbf{r}))\,\phi_2(\mathbf{r}) - \Sigma_{12}(\mathbf{r})\phi_1(\mathbf{r}) = 0 \tag{3.2}$$

RFSP solves the two-group diffusion equation using a finite-different solution method. This method is detailed in [21]. The output of an RFSP calculation includes flux profiles radially and axially, channel powers, bundle powers and core excess reactivity.

3.3 Chronicle of a Calculation

This section endeavours to document the procedure used in calculating the results discussed in the following chapters.

A note on nomenclature: unlike the CANDU reactor, where it is common to fuel the reactor by replacing individual fuel bundles each day on power, the SCWR will be batch fueled offline. This will require a shuffling of all bundles in a channel to a new channel. To avoid confusion, the fuel in a channel shall be referred to as an assembly and shall be thought of as one continuous 5 metre long segment, rather than individual bundles. It is however still divided into 0.5 metre long sections for lattice physics analysis and into ten segments for full core simulations. Shown in Figure 3.2 are the assembly subdivisions used for the RFSP analysis, and the five axial positions simulated in WIMS-AECL and referred to throughout this work.

The first step in the calculation sequence is a WIMS-AECL lattice calculation. As discussed previously, there is a large change in coolant density along a SCWR fuel channel. The coolant at the inlet end of the channel will be in a "liquid like" higher density state, while the coolant at the outlet end will be in a "gas like" lower density state. To account for the density change along assemblies, each WIMS-AECL calculation is performed at five "slices" along a fuel assembly. The coolant temperatures and densities at each position, from [25], are shown in Table 3.1.

Position	**Location From Coolant Inlet**	**Coolant Density**	**Coolant Temperature**
1	0.5m	592 kg/m^3	632 K
2	1.5m	382 kg/m^3	656 K
3	2.5m	161 kg/m^3	675 K
4	3.5m	89 kg/m^3	774 K
5	4.5m	69 kg/m^3	881 K

Table 3.1: Coolant Temperatures and Densities at 5 positions along fuel channel

Moving from the lattice calculation to the full core calculation involves the construction of a full

core model in RFSP. The full core RFSP modelled here contains 300 fuel channels. For the full core model, each fuel channel is divided into ten sections comprising a fuel assembly. The cross-section tables for each axial node in the channel come from the five positions modelled in WIMS. That is, sections 1 and 2 of the fuel assembly are made up of fuel tables from position 1 WIMS data, sections 3 and 4 are composed of position 2 WIMS data, and so on. In this way the coolant density roughly resembles, in a stepwise fashion, the actual distribution along a fuel channel. This is shown in Figure 3.3.

RFSP is typically used in analysis of online refueled CANDU reactors. As the SCWR is to be three cycle batch fuelled, it was necessary to develop a method to simulate the process of batch refuelling in RFSP. This is done by calculating the irradiations for an equilibrium core, i.e. irradiations of once and twice irradiated assemblies present at the beginning of a new operating cycle. These irradiations are determined via an iterative procedure. First, an initial simulation is run with all fresh fuel to get an estimate of irradiation values for the end of a cycle. After deciding on a suitable refueling scheme, one can 're-arrange' the assemblies into the desired pattern for the start of the next cycle. After a number of iterations in which the assemblies at the end of each cycle are arranged according to the scheme, the irradiations at the end of cycle eventually converge on their equilibrium values. This method is further described in Chapter Five. The simulation of the equilibrium core is then used to determine the channel powers and radial power profile.

Scripts were written in Perl (Appendix D) that assist in taking the RFSP output irradiations and creating an input according to any user-specified refueling scheme. This allowed different schemes to be simulated relatively easily.

An important result of the calculations is the determination of the maximum linear element rating (LER) of a fuel element in the core. This requires information from both WIMS results and RFSP results. Of most importance is the maximum linear element rating in the core. In the case of batch refuelling, this generally occurs in the highest power channel. As the calculation of LER

requires information from the WIMS calculation results, the linear element ratings are calculated for the five axial positions simulated in WIMS.

A flow chart decribing the calculations is shown in Figure 3.4.

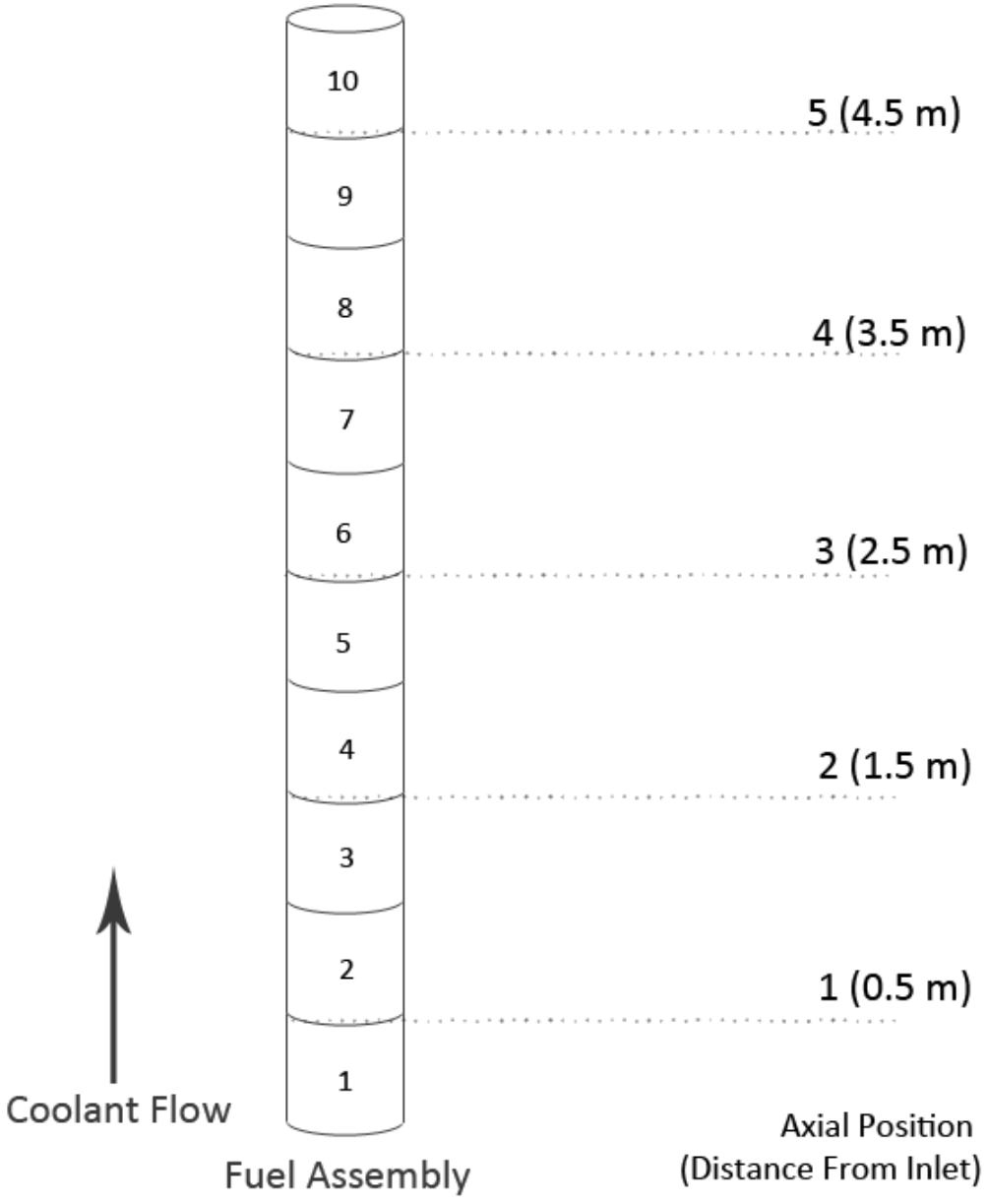

Figure 3.2: Axial Positions used in WIMS simulations and assembly subdivision for RFSP calculations

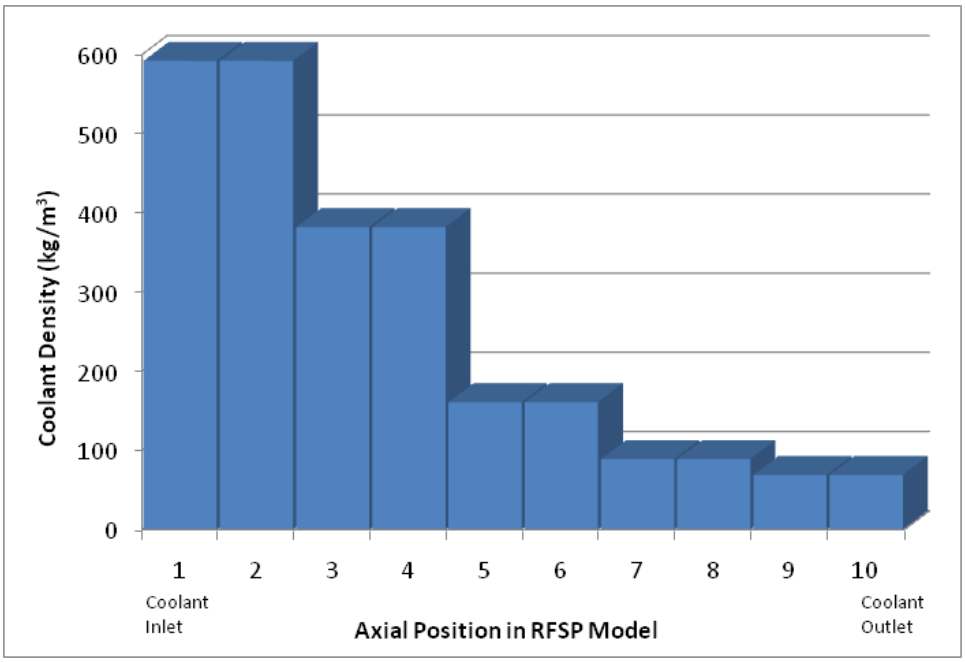

Figure 3.3: Density Change in RFSP model

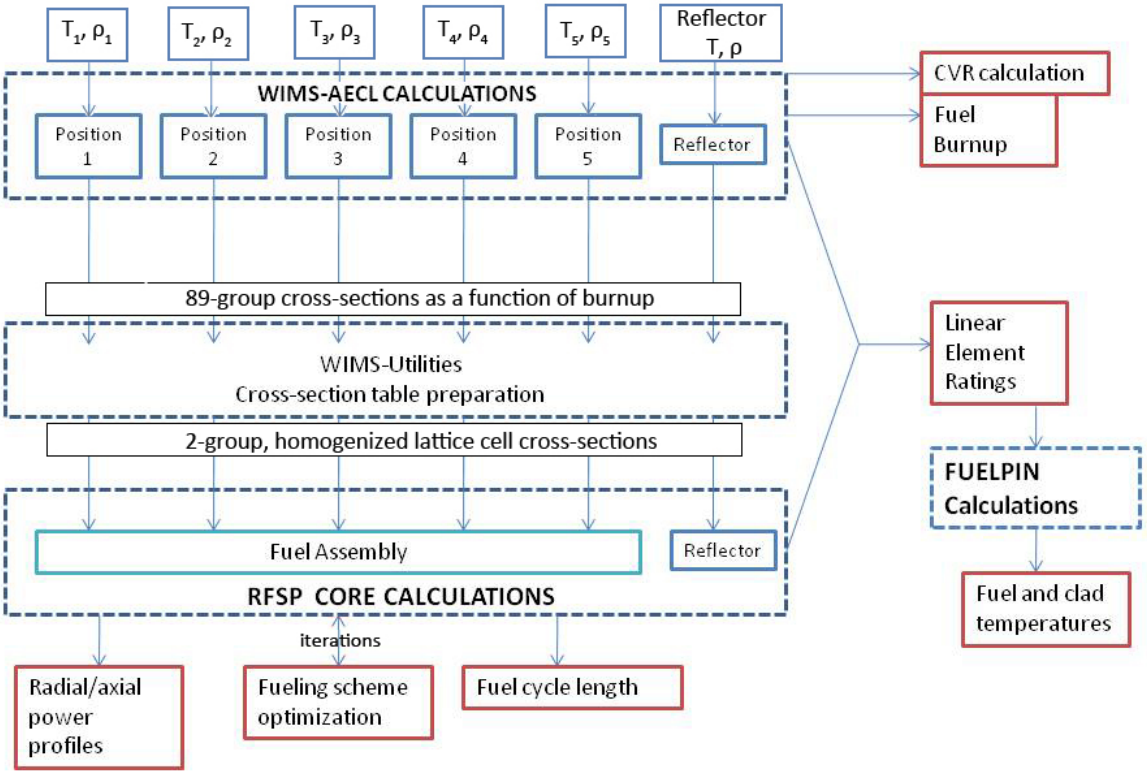

Figure 3.4: Calculation Sequence Outline

3.4 Loss of Regulation Transient Analysis

Safe reactor operation relies on remaining below certain thermal limits during normal operation. Along with the lattice and core calculations, analysis was done on loss of regulation transients. Analysis of peak clad and fuel centerline temperatures was performed with a computer code called FUELPIN [22] which has been used in the past for CANDU reactor licensing.

3.4.1 FUELPIN code

FUELPIN is a code designed to predict fuel and clad temperatures during a transient change in fuel power in the core. The code simulates a single fuel element of user-specified geometry and initial conditions, including coolant conditions, power level, coolant density. The code assumes UO_2 fuel and includes temperature dependent properties for the fuel. No temperature dependence is modelled for the coolant; as power increases, there is no coolant density feedback built into the code. The code predicts the fuel and clad temperatures by solving the one dimensional heat transfer equation. The transient input for the studies in this thesis are input as a positive reactivity insertion rate. To compute the power, FUELPIN uses a point reactor kinetics model.

Heat Transfer Equation

In three dimensions, heat transfer in a solid with thermal conductivity k, and volumetric heat generation q''' is governed by,

$$\nabla \cdot k\nabla T + q''' = 0 \tag{3.3}$$

Where T is the temperature.

The FUELPIN code solves this equation in the radial direction only, simplifying the above equation

to:

$$\frac{1}{r}\frac{d}{dr}\left(kr\frac{dT}{dr}\right) + q''' = 0 \tag{3.4}$$

A full explanation of the method employed by FUELPIN is given in [22], but it is important to note that the code solves the equation using linear element power, removing the dependence of temperature on pellet radius, and further accounts for the flux depression that occurs in the pellet. The boundary condition on the outer edge of the clad is a convective heat transfer boundary which requires knowledge of the heat transfer coefficient. As there is a large degree of uncertainty at present, two values were chosen for the FUELPIN analysis.

Point Reactor Kinetics Model

The point kinetics model is a model that provides a method to calculate the time evolution of neutron flux amplitude and delayed neutron precursor concentrations. The name point kinetics implies a space independent reactor. The equations used in FUELPIN are:

$$\frac{dN}{dt} = \left[\frac{(\rho(t) - \beta)}{\Lambda}\right] N(t) + \sum_{i=1}^{n} \lambda_i C_i(t) \tag{3.5}$$

$$\frac{dC_i}{dt} = -\lambda_i C_i(t) + \left(\frac{\beta_i}{\Lambda}\right) N(t) \tag{3.6}$$

where

t = time

N = neutron flux amplitude

ρ = reactivity ($\rho = \frac{k-1}{k}$ written in terms of the reactor multiplication constant)

β = delayed neutron fraction

β_i = fraction associated with the ith group of delayed neutron precursors

Λ = prompt generation time

λ_i = decay constant associated with ith group of delayed neutron precursors

C_i = delayed neutron precursor for ith group

n = number of delayed neutron precursor groups

Chapter 4

Lattice Cell Calculations

4.1 Fuel Design Considerations

In this chapter, results for two different fuel assembly designs are presented. The first is a 43 element assembly and the second is a 54 element fuel assembly. There are a number of considerations when designing a fuel assembly for the SCWR, many of which are interrelated. Summarized below are the main considerations examined here.

Fuel Burnup

Fuel burnup is a measure of the amount of energy extracted from an amount of fuel. It is commonly measured in units of energy per mass of initial heavy element, e.g. megawatt days per tonne-heavy element. In general, approximately 200 MeV of energy is released from a single U-235 fission event, this translates into approximately 0.95 MWd/gram fissioned.

For this research, the core average burnup target is taken as 30000 MWd/t. Since the core is to be batch fueled, this number represents the sum of burnups from the three cycles the fuel is present in the core. The current AECL target average burnup is 45000 MWd/t [17], this is the same target

as the Japanese SCWR concept [12]. 30000 MWd/t is chosen for this research as it is more in line with current BWR burnup levels and represents a reasonable level given the limits of today's fuel carrier technologies.

Coolant Void Reactivity

Coolant void reactivity (CVR) is the change in reactivity upon loss of coolant from a fuel channel. In a pressure vessel type reactor, a loss of coolant is a loss of moderation, and the effect of coolant voiding is an addition of negative reactivity. In a pressure tube type reactor, separation of coolant and moderator means that a loss of coolant is not a loss of moderation. The effect this has on reactivity is dependent on the fuel channel design, fuel material, fuel burnup, and coolant properties. In current operating CANDU reactors, voiding of coolant from a channel results in a positive reactivity insertion. For the SCWR, the coolant has a wide range of densities along the channel, so tailoring the CVR to have a small value will ensure stability during operation. Ideally, for the channel, the overall CVR will be small and negative i.e. 0 mk to -5 mk.

As discussed in the previous chapter, WIMS lattice calculations were performed at 5 positions axially to account for the coolant density variation. A burnup-averaged coolant void reactivity value for the each fuel channel position, $i = 1, 2, ..., 5$, was calculated as:

$$\mathrm{CVR}_i = \frac{\int \mathrm{CVR}\ d\mathrm{BU}}{\int d\mathrm{BU}} \tag{4.1}$$

Here, the integration is performed numerically over the range of burnup from 0 burnup (fresh

fuel) to the discharge burnup. The channel average CVR result reported here is the average of the five CVR_i values. The discharge burnup is arrived at by using the average integrated k-infinity value from WIMS. This value is defined in the same way as above equation, with the k_∞ value in place of CVR. This quantity is calculated automatically by WIMS at each burnup step. The integrated k-infinity value is used to calculate the discharge burnup for fuel in an online-fueled CANDU reactor. For this work, the burnup where the average integrated k_∞ value is equal to 1.04 is said to be the discharge burnup for an online fueled reactor. 40 mk excess reactivity was chosen to account for leakage and absorption from reactivity control devices.

The linear reactivity model [23] can be used to relate burnup for an online fueled reactor to a batch fueled reactor.

In the linear reactivity model, reactivity is approximated as a linear function of burnup, B:

$$\rho = \rho_0 - AB \tag{4.2}$$

where A is some constant and ρ_0 is the initial "excess" core reactivity.

Assuming all fuel operates at the same core average power, for an n-batch core, at the end of a cycle, the freshest batch will have reached a burnup, B_c, the next oldest, $2B_c$, all the way to the oldest batch which will have been burned nB_c. The mean reactivity of the core ρ_s can be computed by averaging batch reactivities:

$$\rho_s = \frac{1}{n}\sum_{j=1}^{n}\rho_j \tag{4.3}$$

ρ_s can be found by summing equation 4.2 over n-batches:

$$\begin{aligned} \rho_1 &= \rho_0 - AB_c \\ \rho_2 &= \rho_0 - 2AB_c \\ &\vdots \\ \rho_n &= \rho_0 - nAB_c \end{aligned}$$

Using the summation $\sum_{j=1}^{n} j = \frac{n(n+1)}{2}$, and solving for the discharge burnup, B_d,

$$B_d = nB_c = \left(\frac{2n}{n+1}\right) B_1 \tag{4.4}$$

since $B_1 = \frac{\rho_0}{A}$.

In the case of online refueling, $n = \infty$ and we get $B_{d,\text{online}} = 2B_1$, and for $n = 3$ in the SCWR case, $B_{d,\text{3-batch}} = 1.5B_1$. This means that the burnup achieved by the batch refueled SCWR will be 3/4 of the value predicted for the online fueled reactor ($B_{d,\text{3-batch}} = \frac{3}{4}B_{d,\text{online}}$), i.e. when the WIMS integrated k_∞ value reaches 1.04. In calculating the burnup for the SCWR in WIMS calculations, the integrated k_∞ value was averaged over the 5 axial positions. To calculate the burnup for the batch fueled reactor, 3/4 of the burnup value at the time where the average integrated k_∞ was equal to 1.04 was calculated. This is the burnup value reported in the following results.

Fuel Type and Enrichment

The fuel type in the models presented here is uranium dioxide (UO_2) fuel. Natural uranium is predominantly comprised of the isotope uranium-238, with only 0.7 weight percent being uranium-

235. Uranium-235 has a much larger thermal fission cross-section than uranium-238 and is the main source of fissions in fresh fuel for a thermal reactor. Uranium enrichment is a process by which the weight percent of U-235 is increased via isotopic separation. Apart from CANDU reactors which use natural uranium fuel, most nuclear reactors use enriched uranium fuel. The fuel enrichment is one of the main factors influencing fuel burnup. All other things being equal, increasing the fuel enrichment increases the fuel burnup achievable. A typical PWR reactor uses enrichments of around 3.5%, while a BWR reactor fuel assembly typically consists of five or six axial sections with different distributions of fuel compositions [30].

Lattice Pitch

The lattice pitch is the distance, centre to centre, of adjacent fuel channels. The choice of lattice pitch affects several factors. First, due to the use of a heavy water moderator, the choice of lattice pitch affects economics, as a larger lattice pitch means more heavy water will be required in the calandria. However, too small of a lattice pitch is impractical as there must be space to accommodate coolant feeder tubes at one end of the core, as well as space to include reactivity control devices interstitially between channels. From a neutronics point of view, an increased lattice pitch provides more neutron moderation and thus affects the neutron spectrum. It also affects the coolant void reactivity, typically an increased lattice pitch increases the coolant void reactivity by decreasing the fuel to moderator ratio. In a pressure tube reactor with separate moderator, decreasing the lattice pitch means that the moderating effect of the coolant becomes more important. This typically means that decreasing the lattice pitch reduces the coolant void reactivity. The current reference lattice pitch is a 25 cm square, significantly smaller than the 28.575 cm lattice pitch for the CANDU reactor [24].

4.2 Fuel Bundle Comparison

The following results are for a comparison of the 43-element fuel assembly design and a 54-element fuel assembly design. Both designs are shown in Figure 4.1. The most dramatic difference between the two designs is the large centre pin in the 54-element bundle. The composition of this central pin is zirconia that is clad in stainless steel, i.e. it is not fissile and hence not considered a fuel element. Its purpose is to shift the three rings of fuel elements outward (reducing the moderator to fuel ratio) and displace coolant at the center of the bundle to reduce coolant void reactivity. Apart from this, the two designs share many common features. The geometry and materials compositions are presented in Table 4.1. Material temperatures used in the WIMS calculations are the same used for studies in [16, 25, 17], and are specified in Table 4.2. While these temperatures are expected to qualitatively reflect trends within the fuel channel, accurate temperature values will require coupled physics and thermalhydraulics calculations, which represents an area for future work.

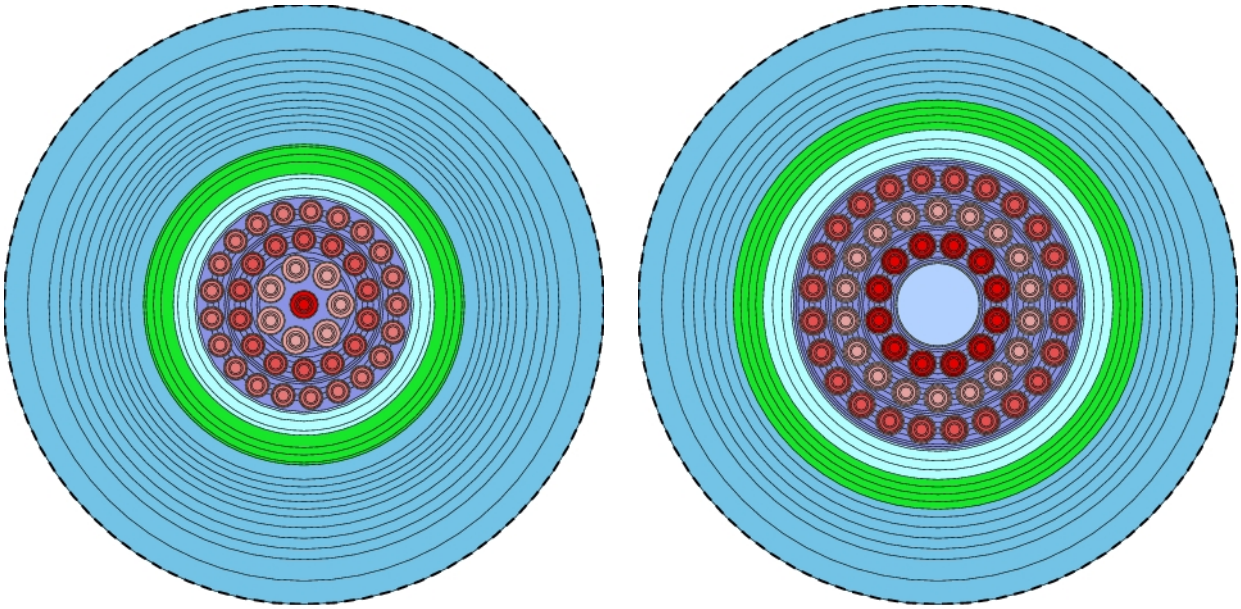

(a) 43 element fuel (b) 54 element fuel

Figure 4.1: 43 and 54 Element Fuel Designs

Materials		
	43 Element Bundle	**54 Element Bundle**
Moderator	D_2O	D_2O
Coolant	H_2O	H_2O
Pressure Tube	Zircaloy IV	Zircaloy IV
Insulator	ZrO_2 (70% porosity)	ZrO_2 (70% porosity)
Fuel sheath and Liner Tube	Stainless steel 310	Stainless steel 310
Fuel	UO_2 (various enrichment)	UO_2 (various enrichment)
Centre Pin	UO_2	ZrO_2
Geometries		
Geometry Reference	[24]	[25, 16, 17]
Lattice Pitch	Variable (reference 25 cm square)	Variable (reference 25 cm square)
Pressure Tube Thickness	1.4 cm	1.4 cm
Insulator Thickness	1 cm	1 cm
Liner Thickness	0.1 cm	0.1 cm
Pitch Circle Radius Outer Ring	4.4 cm	5.9 cm
Pitch Circle Radius Intermediate Ring	3.1 cm	4.4 cm
Pitch Circle Radius Inner Ring	1.7 cm	2.87 cm
Fuel Element Radius Outer Ring	0.57 cm	0.68 cm
Fuel Element Radius Intermediate Ring	0.57 cm	0.68 cm
Fuel Element Radius Inner Ring	0.68 cm	0.68 cm
Center Fuel Element Radius	0.68 cm	2 cm
Clad Thickness	0.04 cm	0.06cm

Table 4.1: Materials and Geometry for 43 and 54-element fuel

Axial Position (m)	**Clad Temp (K)**	**Liner Temp (K)**	**Insulator Temp (K)**	**Pressure Tube Temp (K)**	**Moderator Temp (K)**
0.5	796.35	632.35	554.88	477.55	342.16
1.5	808.30	656.30	570.83	485.51	342.16
2.5	817.76	675.27	583.46	491.82	342.16
3.5	867.04	774.05	649.25	524.65	342.16
4.5	920.63	881.45	720.78	560.35	342.16

Table 4.2: Material temperature information used in WIMS calculations

4.3 Results

Tables 4.3 and 4.4 show the results of WIMS calculations performed for 43 and 54 element designs with varied lattice pitch and fuel enrichment.

43 Element Bundle	Lattice Pitch 24 cm	Lattice Pitch 25 cm	Lattice Pitch 26 cm
Enrichment 4%	CVR: + 1.49 mk Burnup: 32029 MWd/t	CVR: +1.85 mk Burnup: 32493 MWd/t	+2.18 mk 32778 MWd/t
Enrichment 5%		CVR: +1.57 mk Burnup: 42440 MWd/t	
Enrichment 6%		CVR: +1.17 mk Burnup: 51697 MWd/t	

Table 4.3: CVR and Burnup data for 43 element fuel assembly

54 Element Bundle	Lattice Pitch 24 cm	Lattice Pitch 25 cm	Lattice Pitch 26 cm
Enrichment 4%	CVR: -1.696 mk Burnup: 22031 MWd/t	CVR: -0.696 mk Burnup: 24273 MWd/t	+0.073 mk 25916 MWd/t
Enrichment 5%		CVR: -0.434 mk Burnup: 34885 MWd/t	
Enrichment 6%		CVR: -0.279 mk Burnup: 44672 MWd/t	

Table 4.4: CVR and Burnup data for 54 element fuel assembly

As seen in the tables, the 30000 MWd/t burnup target can be achieved using the 43 element fuel assembly design with 4% fuel enrichment. For the 54 element design, the achievable burnup is reduced, and to achieve the burnup target, a higher enrichment (between 4% and 5%) will be required. Further, the effect of reducing the lattice pitch is found to reduce the achievable burnup in all cases, while acting to also reduce coolant void reactivity.

The results show a larger overall CVR for the 43 element fuel design. In the 43 element bundle, the CVR values could be reduced through the use of a centre element doped with a neutron absorbing element such as dysprosium. However, this would add an additional penalty to fuel

burnup. In addition, while the table shows channel average burnup and CVR values, there is a wide range of CVR values from inlet to outlet end of the fuel channel due to the coolant density variation. This spread is exacerbated in the 43 element design, where a nearly 40 mk difference between position 1 and 5 is seen at 0 MWd/t burnup, while the values are almost identical for positions 1 and 5 in the 54 element design at 0 burnup. The case for 4% enriched fuel is shown for the 43 and 54 element designs in Figures 4.2a and 4.2b respectively. In these figures, the coolant void reactivity for axial position one (0.5 m) and position five (4.5 m) are shown, i.e. the two extremes in coolant density in the fuel channel. As can be seen, for the 43 element fuel design, the CVR exhibits a much larger positive value at position one. The smallest magnitude CVR values occur in position five in all cases, as the coolant density difference between normal operation and voided conditions is minimized here. While not shown in the figures here for simplicity, the CVR values for the other three axial positions are bounded by the values for positions one and five.

For comparison, the plots of CVR vs. burnup are shown for the 6% initial enrichment case in Figures 4.3a and 4.3b. The results show the same overall trend as the 4% enrichment case, although with a larger difference in CVR between position 1 and 5 for the 43 element fuel design. Also shown in Figure 4.4, is the case of a larger, 26 cm lattice pitch and the 54 element assembly design. Here we see the moderator to fuel ratio is large enough to make the CVR quite positive (around 13 mk) at axial position 1 for fresh fuel, although as with the other 54 element cases, the CVR decreases with burnup. It can therefore be concluded that for the 54 element assembly design to meet the desired CVR target, a lattice pitch below 26 cm must be used.

The 54 element design is able to provide a smaller CVR value at every position axially without addition of burnable poison through reducing the moderator to fuel ratio. However, as shown in this report, confirming the results found in [16], doing so reduces the fuel burnup achievable. While the 54 element design gives this penalty to fuel burnup, it is shown to produce acceptable CVR values without the addition of any burnable poison to the fuel. While it may be possible to design a 43

element assembly with acceptable CVR characteristics, this would require axial sections featuring different levels of burnable absorber addition.

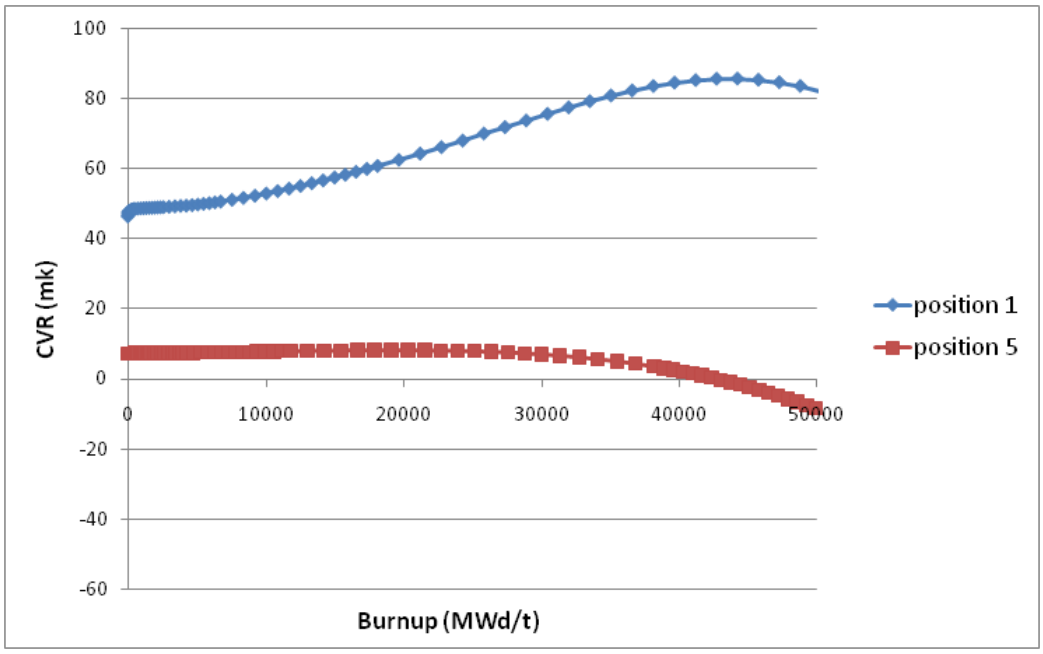

(a) CVR for 43 element fuel bundle at axial positions 1 and 5, 4% enrichment

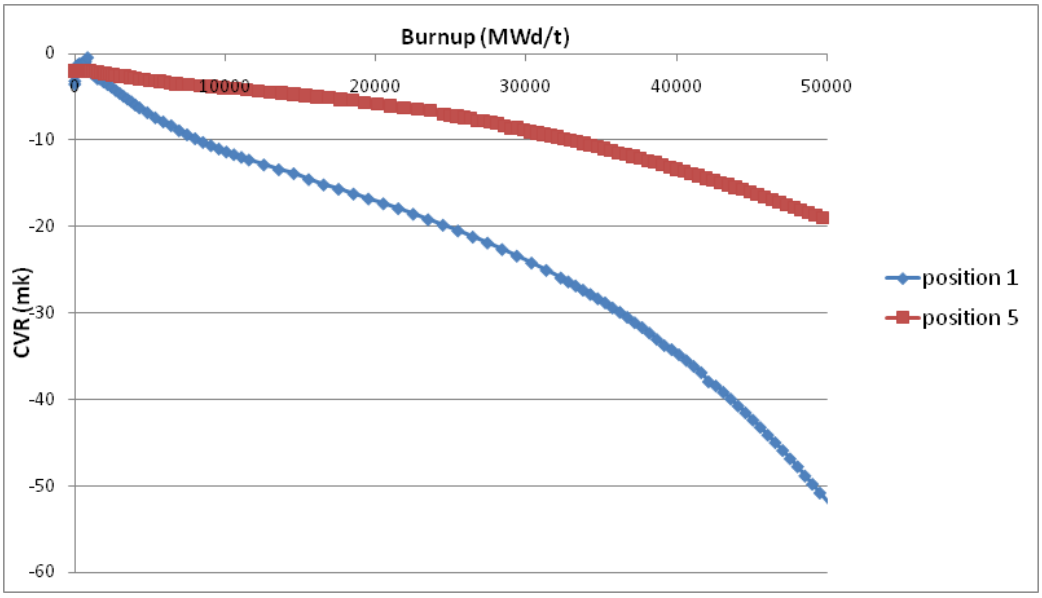

(b) CVR for 54 element fuel bundle at axial positions 1 and 5, 4% enrichment

Figure 4.2: Comparison of CVR at high and low density coolant locations for 43 and 54 element bundle, 4% enrichment

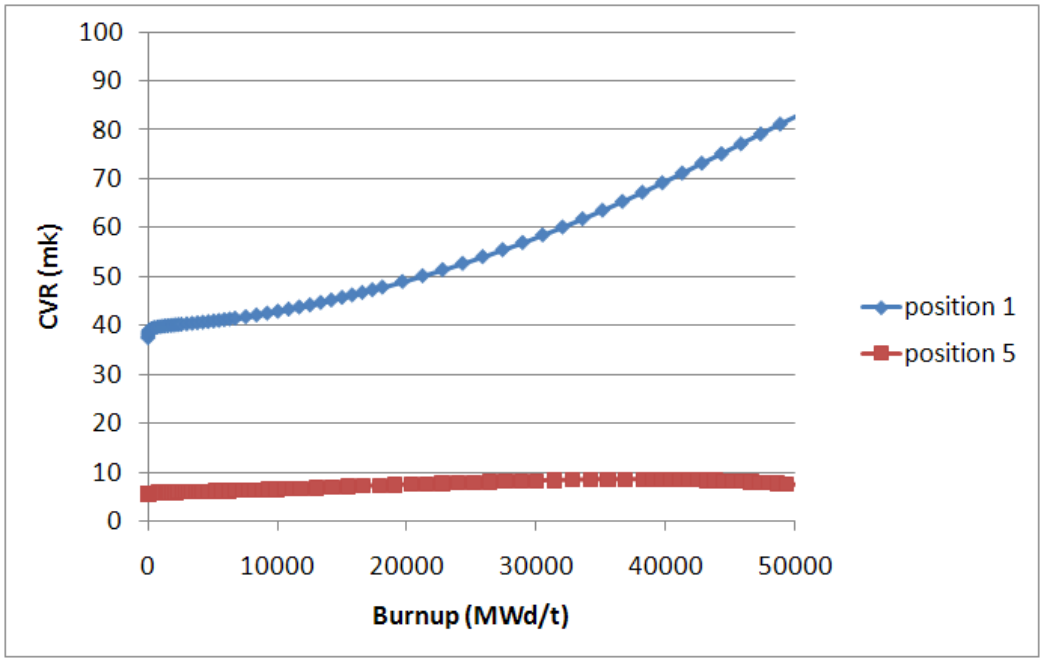

(a) CVR for 43 element fuel bundle at axial positions 1 and 5, 6% enrichment

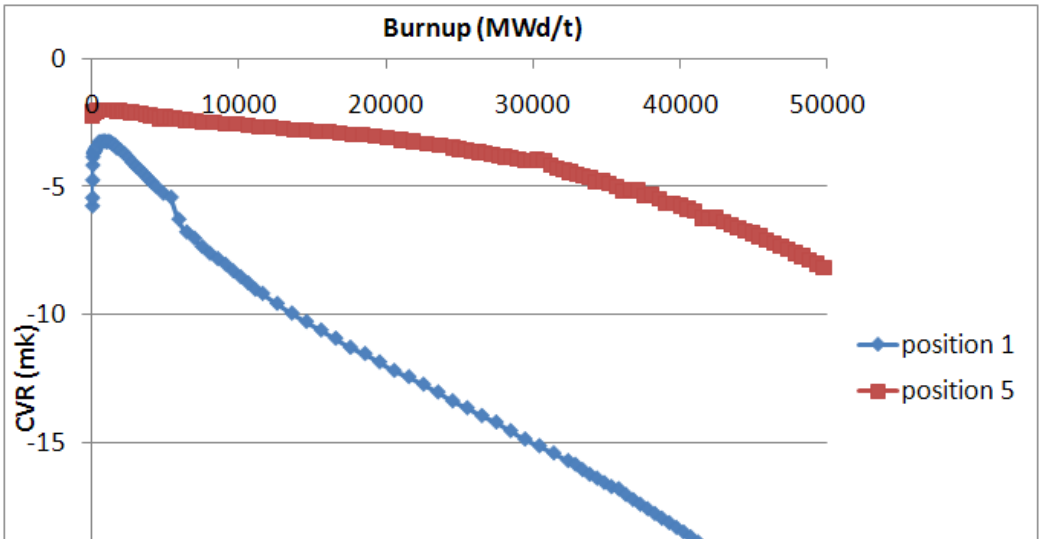

(b) CVR for 54 element fuel bundle at axial positions 1 and 5, 6% enrichment

Figure 4.3: Comparison of CVR at high and low density coolant locations for 43 and 54 element bundle, 6% enrichment

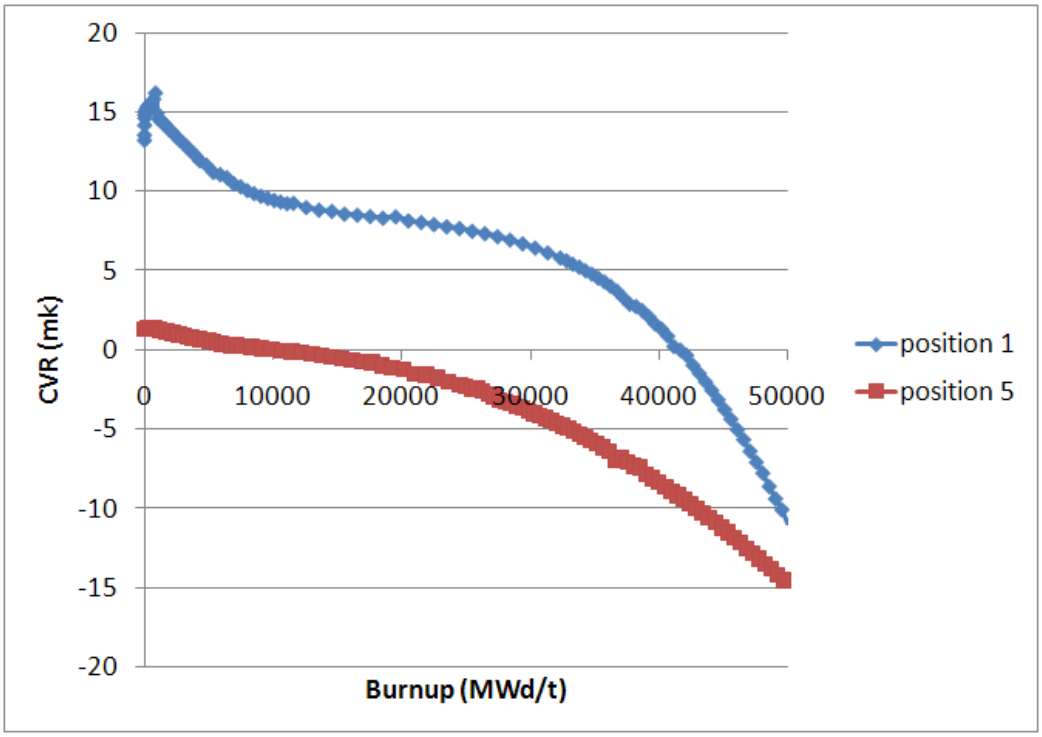

Figure 4.4: CVR for 54 element fuel bundle at axial positions 1 and 5, 6% enrichment, 26 cm lattice pitch

4.4 Power Profile Within Assembly

For fuel designs featuring concentric rings of fuel elements, e.g. CANDU type fuel, it is important to determine the relative power produced by each ring of fuel. This has implications for the linear element rating, a main safety parameter, which is explored further in Chapter 5 and 6. Typically, in a CANDU type fuel bundle, the highest power is produced by the outer ring of fuel elements. As the fuel burns up, the outer elements produce less power while the inner elements increase in power.

Figures 4.5 and 4.6 show the radial assembly power profiles for the 43 and 54 element fuel design for 4%, 5% and 6% enrichment levels and at fresh and a 30000 MWd/t burnup level and for positions 1 (Figs. 4.5a and 4.6a) and 5 (Figs. 4.5b and 4.6b). The results indicate that in all cases the most power is produced in the outer ring of fuel elements. As enrichment increases, more power is produced in the outer elements. With burnup, the inner elements increase in power while the outer elements decrease. This difference is found to be reduced with burnup for the lower coolant density (position 5) section of the fuel channel. The same overall trends are observed in both the 43 and 54 element cases.

The effect of increased lattice pitch on assembly power profile is shown in Figure 4.7. Here it is shown that an increased lattice pitch of 26 cm produces the same overall profiles as the 25 cm lattice pitch. This is the case for both axial position 1 and 5.

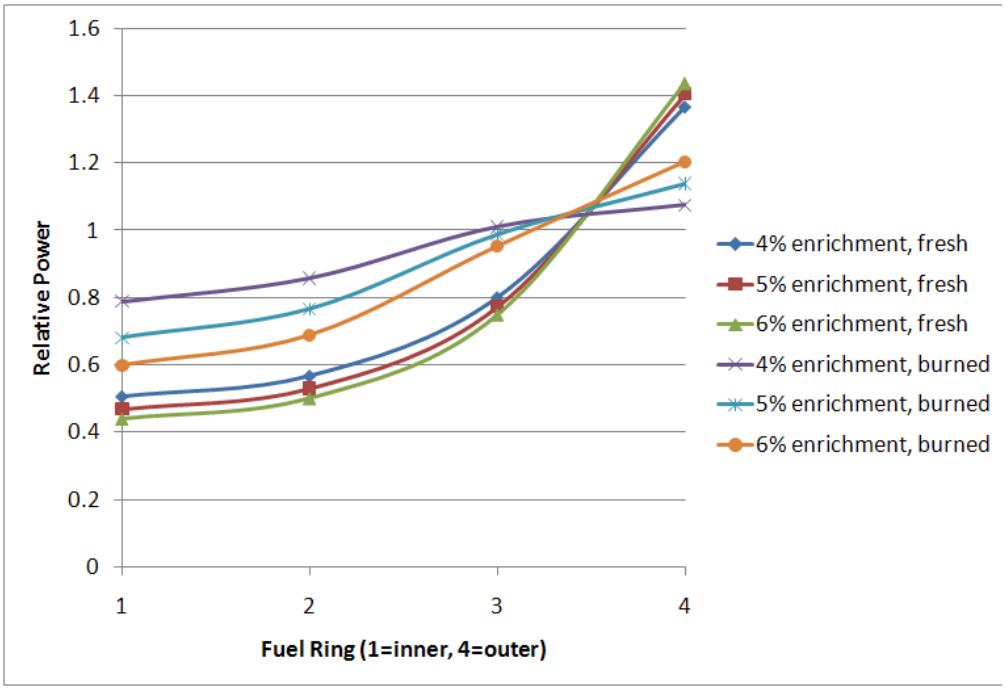

(a) Radial Power Profile within fuel assembly, axial position 1, 25 cm lattice pitch

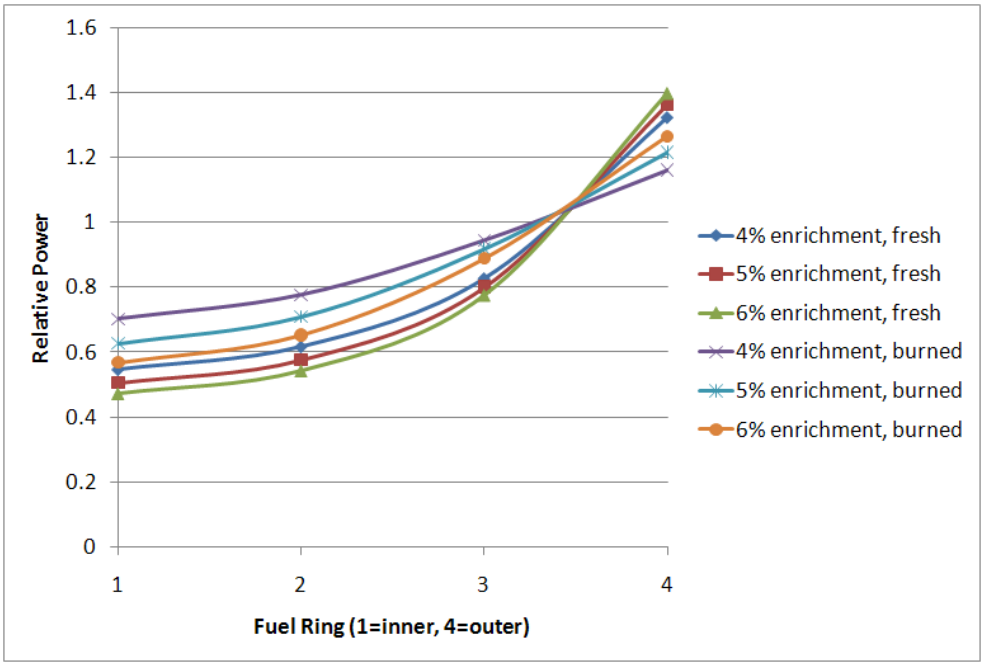

(b) Radial Power Profile within fuel assembly, axial position 5, 25 cm lattice pitch

Figure 4.5: 43 Element Assembly power profiles for high and low density channel locations

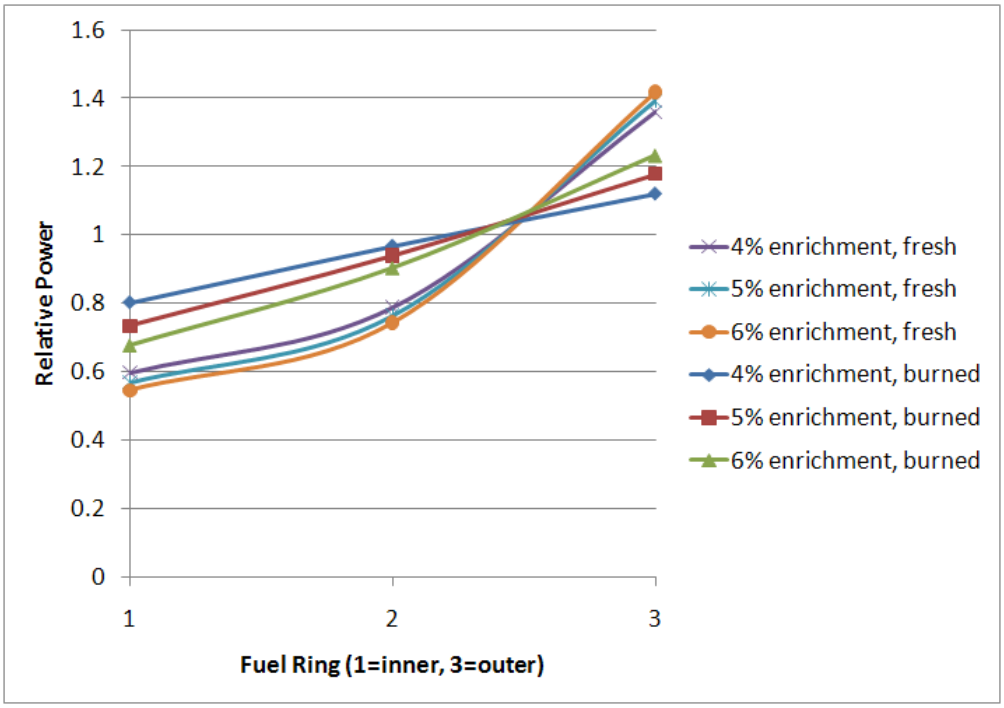

(a) Radial Power Profile within fuel assembly, axial position 1, 25 cm lattice pitch

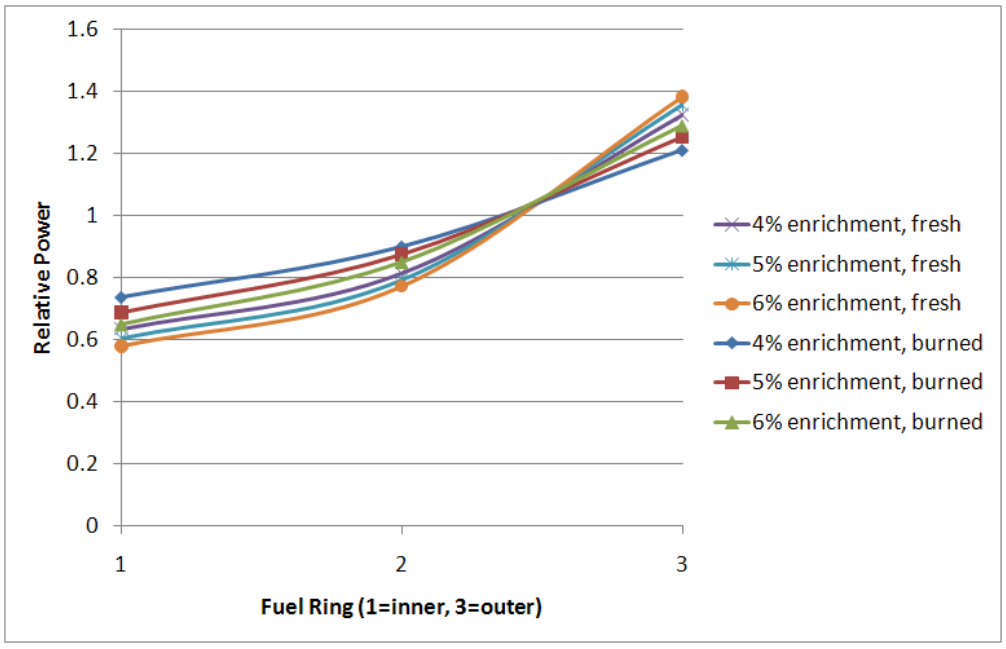

(b) Radial Power Profile within fuel assembly, axial position 5, 25 cm lattice pitch

Figure 4.6: 54 Element Assembly power profiles for high and low density channel locations

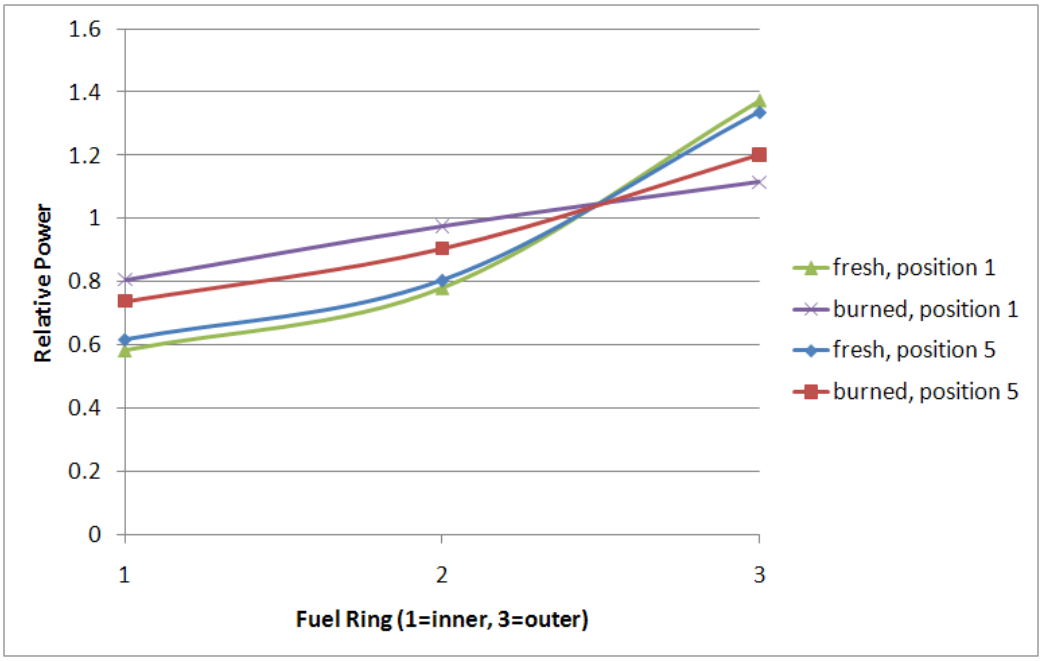

Figure 4.7: Radial Power Profiles for axial positions 1 and 5, 4% enrichment, Lattice pitch 26 cm

Chapter 5

Full Core Calculations

5.1 Core Design Considerations

The full core calculations have been performed with RFSP to assess the power profiles across the core radially and axially, to assess the batch cycle and refueling schedule and also to determine the maximum linear element ratings (LER) of the fuel.

The main parameters in the core model are the number of fuel channels, the length of the core, and core thermal power. Early literature on the SCWR [2] featured a core of 300, 5 m long channels with thermal power output of 2540 MW. More recently [17], the number of channels has been expanded to 336 in order to reduce the average channel power, in an effort to reduce maximum LER. In this work however, only the 300 channel design with 54 element fuel has been modelled. A heavy water reflector region around the core is also included in the model. The cross-section values for this reflector region were prepared from a WIMS-AECL model of a lattice cell, with an "extra" heavy water region located around the lattice cell. The flux and cross-section values for this extra heavy water region were processed with WIMS-Utilities to form reflector cross-section tables that were then input into RFSP.

The number of fuel channels has other implications besides linear element ratings and channel powers. Increasing the number of channels will increase the time it takes to perform the shuffle of fuel assemblies during refueling, while decreasing the number of channels makes it harder to achieve a flattened power profile via modifying the refueling strategy.

Of note, since the core is to be three-batch fueled and the core is fourfold symmetric, the number of fuel channels must be a multiple of 12 to allow all batches to be used in the refueling.

The cross-section tables input into RFSP were prepared using WIMS-Utilities using the output from the WIMS calculation of the 54 element design fuel described in Chapter 4. The core layout used in the RFSP model in the xy plane (reactor face view) is shown in Figure 5.1 with the locations of the fuel channels depicted by the white squares. Each parallelepiped used in making up the core has dimensions 25 cm x 25 cm x 50 cm. Ten parallelepipeds are placed in the z direction, giving the core a length of 5 m. Each parallelepiped contains the homogenized cross-sections prepared by WIMS-Utilities. In the z-direction, the core is divided into 5 "zones" to account for the coolant density variation. Each zone contains two parallelepipeds and contains the cross-sections prepared from the 5 axial positions simulated in WIMS. The overall coolant density profile is that given in Figure 3.3. For consistency, the same coolant density profile is used at all times for all the core simulations. An area for future work may be to update the density profile axially according to burnup state of the core and according to different fueling schemes, particularly the axially graded enrichments, which will affect the coolant density profile through altering the axial power profile.

Two modules of the RFSP code were used. The DATA module, data block GEOMETRY, was used to create the geometry and layout of the core model. The fuel and reflector properties files are read in using this module. The data block FLUX/POWER is used to initialize the thermal and fast fluxes. The other module used in the RFSP SCWR calculations is the SIMULATE module. This module performs a core-follow, simulating a power burnup history from a known initial condition and proceeding for a user input number of time steps.

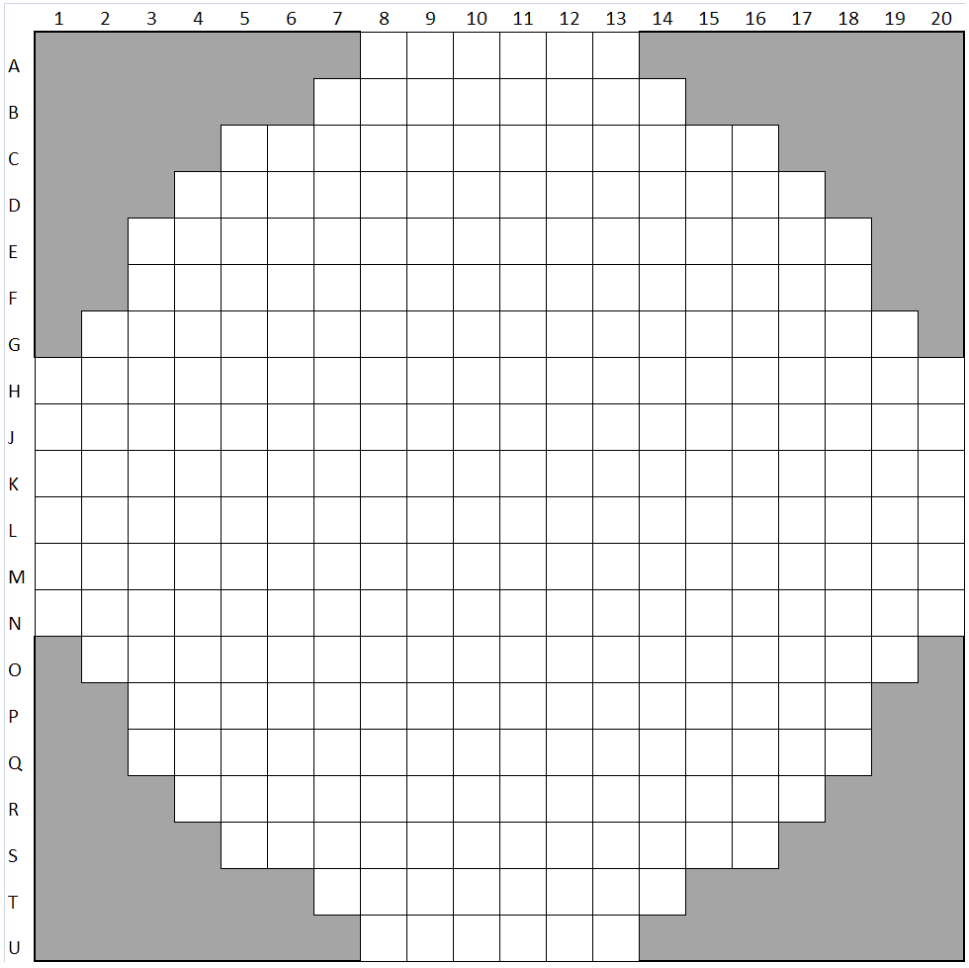

Figure 5.1: 300 Channel Core Layout

RFSP also has the capability to model reactivity control devices in the form of control rods (and liquid zone control in the case of CANDU reactors). At this stage in the preconceptual design of the SCWR, no control devices have been designed, thus the results presented here are for a bare core, free of devices. In determining the cycle length, a reactivity allowance is made for the presence of devices as described in the following section.

5.2 Cycle Length

Calculations were performed with RFSP to determine the length of an operating cycle, that is, the time period the reactor can operate (measured in full power days) between refueling operations. As a result of the fuel burnups calculated in the previous chapter, this calculation was performed with the initial enrichments of 4%, 5% and 6%. The resulting plot, Figure 5.2 shows the change in excess reactivity with respect to cycle length for each initial enrichment.

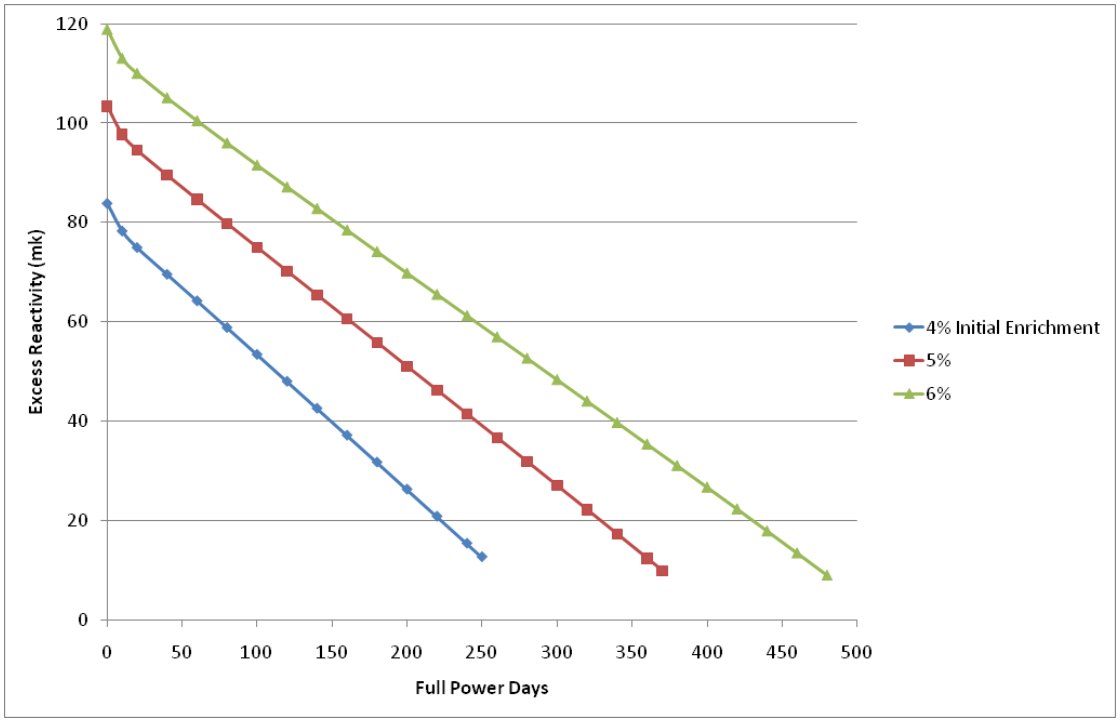

Figure 5.2: Excess Reactivity vs. Full Power Days for various initial enrichment

The cycle length for a given fuel enrichment, is defined here as the number of full power days it takes to reach an excess reactivity of 10 mk. The 10 mk margin is chosen to account for the presence of control devices in the core. The cycle lengths determined from this assumption are 250

full power days for the 4% enrichment case, and 370 and 480 full power days for the 5% and 6% enrichment cases respectively.

5.3 Refueling Scheme and Radial Power Profile

In preparation for creating a refueling scheme, a brief review of batch fueling schemes was conducted. Glasstone [26] examines the advantages and disadvantages of a number of schemes:

Batch irradiation, where the whole core is replaced at the end of a cycle does not allow efficient fuel utilization. *Center-to-Outside loading*, where fresh material is loaded into the center of the core, allows neutrons to be used most efficiently and hence provides the highest burnups, however this results in high power peaking at the center of the core and consequently large variations in power. *Outside-to-center loading* places the fresh fuel material in the core periphery, and *scatter loading* distributes various enrichments uniformly around the core. For both these schemes, the power radially across the core is flattened at the expense of poorer neutron economy. Most common in light water reactors is a modified scatter loading pattern [26]. This scheme is essentially a combination of outside-to-center loading and scatter loading. At the end of a cycle, highly irradiated fuel toward the inside of the core is replaced with fresher fuel previously at the core edge, while new fuel is placed in the core edge.

In many references, a common strategy is to reduce the channel power factor. This is defined as:

$$\text{Channel Power Factor} = \frac{\text{Channel Power}}{\text{Average Channel Power}} \tag{5.1}$$

The inverse of this is the so-called "form factor". For a 300 channel core and 2540 MW thermal power output, the average channel power can be calculated to be 8.47 MW_{th}.

Chen, et al. [27] describe a procedure whereby the fueling scheme optimization is calculated mathematically. Their results agree with the modified scatter loading scheme in that: i) highest

reactivity assemblies are loaded to the periphery of the core and ii) the remainder of the assemblies are divided into two groups and loaded in a checkerboard pattern on the inner region of the core. Chang and Sesonske [28] give an analysis of a"low-leakage" fuel management scheme where they also take into account power peaking factors as an objective function

For the Japanese SCWR, Kamei et al. [10] mention a low-leakage fueling scheme. In their scheme they attempt to place more highly irradiated bundles in the core periphery (i.e. a center-to-outside fueling scheme) citing the need for higher enrichments if an outside-to-center scheme is employed. One parameter from which the fueling scheme is evaluated is the distribution of coolant outlet temperatures. A flat distribution of temperatures ensures there are no hot-spots in the core.

In determining a refueling scheme to use in the SCWR full core simulations, the maximum (peak) radial channel power factor was chosen as the parameter to be optimized. Having this factor as close to 1 as possible ensures a flat power profile across the core, i.e. all channels operating at close to the same power. This is important as it is common to have limits on maximum channel power. By having all channels producing a power as close to the average as possible, it is possible to maximize the power produced by the reactor while keeping the maximum fuel temperatures as low as possible. The optimization was done manually through adjusting the refueling pattern. This represents an area for future work, that is, a more rigorous optimization strategy, most likely in combination with BNA addition. In [16], it is stated that at this point in the design a peak channel power factor of 1.4 would be acceptable for the analysis of the SCWR design. Shown in Figures 5.4 - 5.6, are the quarter-core power distributions for beginning of cycle and end of cycle for the three enrichment cases. As the core is fourfold symmetric, the other three quarters of the core are identical. In all cases the same refueling scheme was used. This scheme is shown in Figure 5.3 for a quarter of the core, with the other quadrants again being symmetric. In this figure, the labels within the channel represent the previous channel the assembly was located in while "F" refers to locations where a fresh assembly is placed. This scheme was optimized for the 4% initial assembly

enrichment and yielded a peak channel power factor of 1.26 for this case.

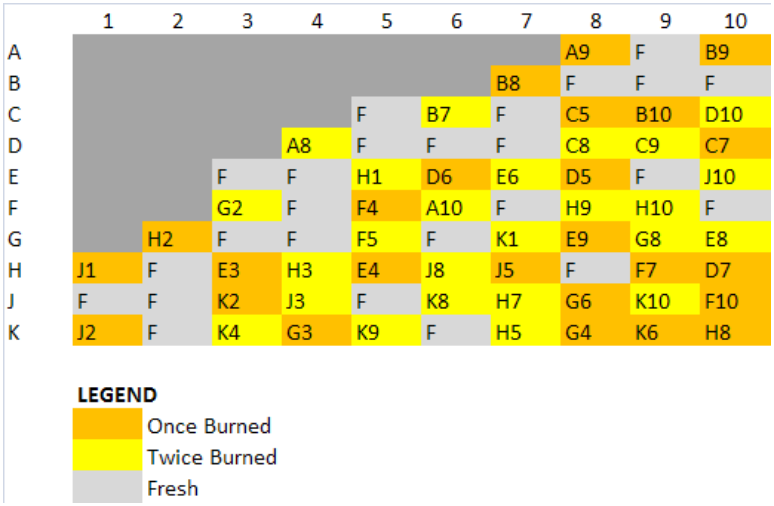

Figure 5.3: Refueling scheme used in full core simulations

As the fueling scheme was optimized for the 4% enrichment case, much higher peak channel power factors are noticed in the 5 and 6% enrichment cases. This is a result of the longer cycle lengths; as the cycle length is increased, the difference in reactivity between fresh and burned assemblies becomes larger. Without changing the refueling scheme, this will impact the channel power factors, i.e. higher reactivity assemblies will be placed closer to lower reactivity assemblies. A further area for work is to adopt differing batch fueling patterns for different initial enrichment levels. Figure 5.7 shows the power profile across the centre of the core (row K), normalized to the average channel power of the core (8.647 MW). As can be seen, the outer core provides the highest power at the beginning of cycle due to the fresher bundles being preferentially located there. By the end of cycle however, the power distribution has flattened due to fuel burnup.

At this point, no neutron absorbing materials (poisons) have been added in any of the models. Of course, due to the excess reactivity at the beginning of a cycle, some type of shim (commonly boron in PWRs) will need to be added to the moderator for global reactivity suppression and

	1	2	3	4	5	6	7	8	9	10
A								1.06	1.20	1.08
								0.95	1.05	0.97
B		BOC					1.17	1.21	1.24	1.23
		EOC					1.04	1.07	1.10	1.10
C					1.26	1.02	1.22	1.06	1.04	0.93
					1.10	0.92	1.10	0.99	0.99	0.90
D				1.01	1.19	1.22	1.21	0.91	0.87	0.94
				0.90	1.06	1.10	1.12	0.90	0.89	0.97
E			1.26	1.19	0.95	1.03	0.92	0.96	1.04	0.84
			1.10	1.06	0.89	0.99	0.92	0.99	1.09	0.92
F			1.02	1.22	1.03	0.89	1.06	0.83	0.81	0.99
			0.92	1.10	0.99	0.91	1.10	0.91	0.91	1.11
G		1.17	1.22	1.21	0.92	1.06	0.83	0.88	0.77	0.76
		1.04	1.10	1.12	0.92	1.10	0.92	1.01	0.91	0.91
H	1.06	1.21	1.06	0.91	0.96	0.83	0.88	0.97	0.83	0.81
	0.95	1.07	0.99	0.90	0.99	0.91	1.01	1.13	1.02	1.01
J	1.20	1.24	1.04	0.87	1.04	0.81	0.77	0.83	0.74	0.81
	1.05	1.10	0.99	0.89	1.09	0.91	0.91	1.02	0.94	1.04
K	1.08	1.23	0.93	0.94	0.84	0.99	0.76	0.81	0.81	0.82
	0.97	1.10	0.90	0.97	0.92	1.11	0.91	1.01	1.04	1.06

Figure 5.4: Quarter core channel power distribution for beginning and end of cycle, 4% initial enrichment

adjusted throughout the cycle as the fuel burns up to maintain criticality. Additionally, some burnable poison may be added to fresh fuel assemblies (localized reactivity suppression) in order to reduce the radial peak channel factor. This has been done in both Japanese and European designs using gadolinia doped fuel rods. Any poisons added to fuel must be done judiciously however, due to the already large penalty on neutron economy from the stainless steel clad. The use of burnable poisons within the fuel and moderator remains an area for future work.

5.3.1 Refueling simulation with RFSP

To simulate batch refueling in RFSP, an iterative procedure was used. After defining a core geometry, the "core" is simulated (i.e. run at the 2540 MW power level) with all fresh fuel assemblies for a predetermined time period (which is typically a guess at the cycle length). After this simulation

	1	2	3	4	5	6	7	8	9	10
A								1.18	1.42	1.22
								0.95	1.10	0.98
B		BOC					1.26	1.38	1.43	1.42
		EOC					1.03	1.11	1.15	1.14
C					1.41	1.04	1.35	1.10	1.07	0.93
					1.13	0.88	1.13	0.97	0.98	0.87
D				1.01	1.30	1.32	1.28	0.86	0.82	0.90
				0.86	1.09	1.14	1.15	0.85	0.85	0.94
E			1.41	1.30	0.92	1.02	0.86	0.90	1.00	0.76
			1.13	1.09	0.85	0.98	0.88	0.98	1.11	0.89
F			1.04	1.32	1.02	0.81	1.02	0.73	0.70	0.92
			0.88	1.14	0.98	0.86	1.12	0.88	0.88	1.14
G		1.26	1.35	1.28	0.86	1.02	0.71	0.77	0.64	0.63
		1.03	1.13	1.15	0.88	1.12	0.87	1.01	0.89	0.89
H	1.18	1.38	1.10	0.86	0.90	0.73	0.77	0.87	0.70	0.67
	0.95	1.11	0.97	0.85	0.98	0.88	1.01	1.18	1.03	1.01
J	1.42	1.43	1.07	0.82	1.00	0.70	0.64	0.70	0.60	0.67
	1.10	1.15	0.98	0.85	1.11	0.88	0.89	1.03	0.93	1.06
K	1.22	1.42	0.93	0.90	0.76	0.92	0.63	0.67	0.67	0.67
	0.98	1.14	0.87	0.94	0.89	1.14	0.89	1.01	1.06	1.08

Figure 5.5: Quarter core channel power distribution for beginning and end of cycle, 5% initial enrichment

is completed, a Perl script (Appendix D) is run that extracts the "cycle exit" irradiations for each fuel channel and creates input irradiations according to a user defined fueling scheme, placing fresh assemblies in the channels required and shuffling the other assemblies according to the scheme. The RFSP simulation is then run again with the "start of cycle" irradiations for the same time period. By iterating through this procedure a number of times, the equilibrium irradiations for the core are converged upon. As convergence is approached, the cycle length is tuned to achieve the desired excess reactivity at the end of cycle. It is this equilibrium core that is presented in this work.

	1	2	3	4	5	6	7	8	9	10
A								1.26	1.59	1.32
								0.94	1.13	0.97
B		BOC					1.31	1.51	1.58	1.56
		EOC					1.02	1.14	1.18	1.17
C					1.50	1.03	1.43	1.13	1.10	0.93
					1.16	0.85	1.16	0.96	0.96	0.84
D				1.00	1.37	1.39	1.33	0.82	0.77	0.87
				0.82	1.12	1.17	1.18	0.82	0.81	0.93
E			1.50	1.37	0.88	1.00	0.81	0.86	0.98	0.70
			1.16	1.12	0.81	0.97	0.86	0.97	1.14	0.87
F			1.03	1.39	1.00	0.75	0.99	0.67	0.63	0.87
			0.85	1.17	0.97	0.82	1.14	0.87	0.86	1.18
G		1.31	1.43	1.33	0.81	0.99	0.63	0.70	0.56	0.54
		1.02	1.16	1.18	0.86	1.14	0.84	1.02	0.88	0.87
H	1.26	1.51	1.13	0.82	0.86	0.67	0.70	0.80	0.62	0.58
	0.94	1.14	0.96	0.82	0.97	0.87	1.02	1.22	1.04	1.02
J	1.59	1.58	1.10	0.77	0.98	0.63	0.56	0.62	0.51	0.58
	1.13	1.18	0.96	0.81	1.14	0.86	0.88	1.04	0.92	1.07
K	1.32	1.56	0.93	0.87	0.70	0.87	0.54	0.58	0.58	0.57
	0.97	1.17	0.84	0.93	0.87	1.18	0.87	1.02	1.07	1.09

Figure 5.6: Quarter core channel power distribution for beginning and end of cycle, 6% initial enrichment

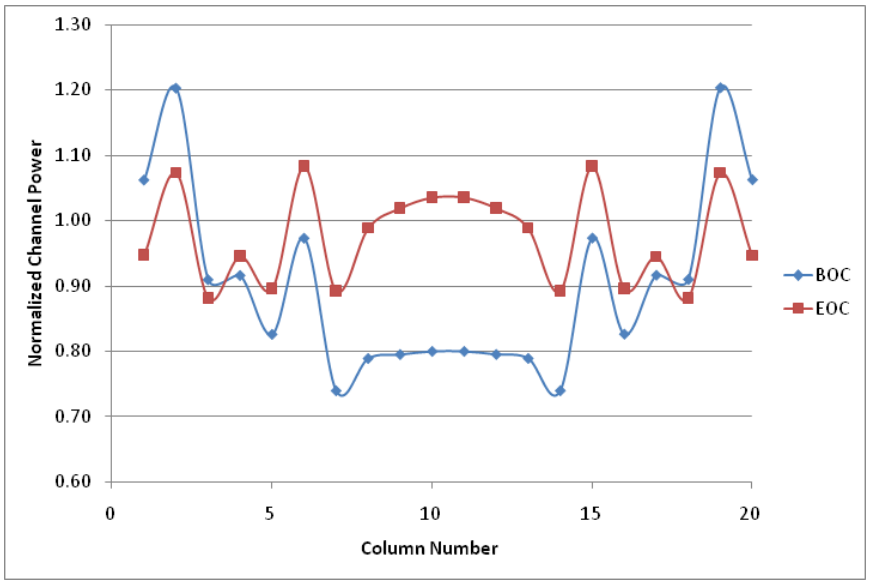

Figure 5.7: Radial Power Profile across center of core, 4% initial assembly enrichment, no reactivity devices present

5.4 Axial Power Profile

While the refueling scheme can be used to make some adjustment to radial channel power factors, it has little effect on the power profile along the fuel channel.

In the following sub-sections, axial power profiles are shown for an assembly as it is followed through its three cycles in the core. The assembly chosen is that which has the highest power initially, i.e. at the beginning of its first cycle. In each figure, the powers for beginning of cycle (BOC) and end of cycle (EOC) are shown for the highest initial power assembly in the core for the length of time it is in the core. For the refueling scheme used, the highest power assembly is located at core position M19. This was found to be the case regardless of initial enrichment, that is, it is dependent only on refueling scheme. For cycle 2 this assembly is moved to position L20, and finally moved to position O14 for the final cycle.

As can be seen here, at the beginning of cycle, a large power peak is seen near the 2 m point of the channel. In this area the coolant is in the higher "liquid like" density state. As the burnup will occur more rapidly at this peak position at the beginning of cycle, as burnup proceeds, the peak shifts and the overall profile becomes flatter towards the end of cycle.

5.4.1 4% Initial Enrichment

Shown in Figure 5.8, are the axial power profiles for the beginning and end of cycle for a 4% initial enrichment assembly. The highest power at the beginning of cycle and occurs near the coolant inlet side of the fuel channel. The highest power produced by the assembly occurs at the beginning of the first cycle. As the assembly is subdivided into ten "bundles" for the RFSP calculation, an axial peaking factor, defined as the maximum "bundle" power to average bundle power can be calculated. In the case of 4% enrichment, this maximum axial peaking factor is computed to be 1.25 at beginning of cycle 1, reducing to 1.11 at the end of the first cycle.

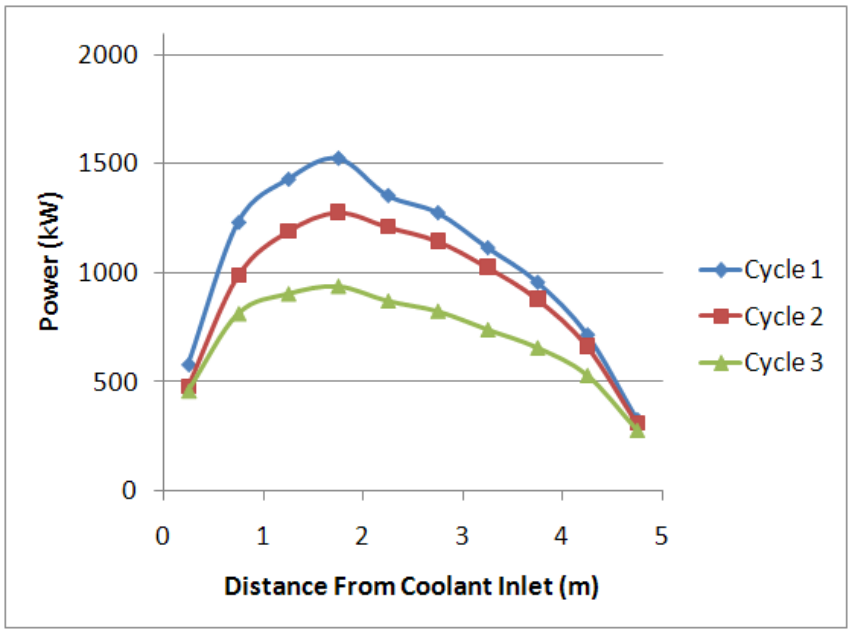

(a) Beginning of Cycle Powers

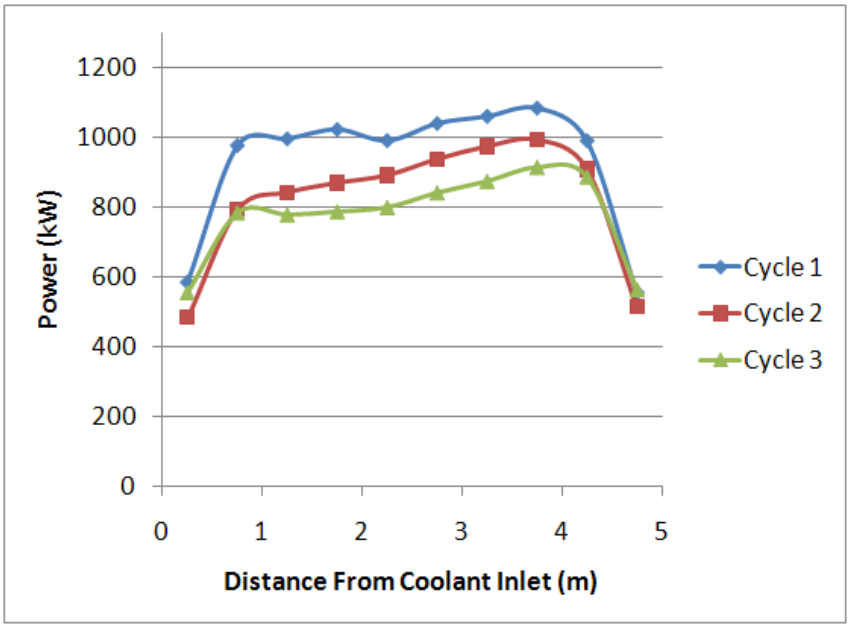

(b) End of Cycle Powers

Figure 5.8: Axial Power Profiles 4% initial enrichment assembly

5.4.2 5% Initial Enrichment

Figure 5.9 shows the axial power profiles for the beginning and end of cycle for the 5% initial enrichment assembly. The same shape of axial power profile is seen as in the 4% enrichment case although the power peak is much larger in this case. This maximum axial peaking factor is calculated to be nearly 1.5. This occurs at the beginning of cycle one for a fresh assembly. At the end of cycle one, this factor is reduced to 1.15.

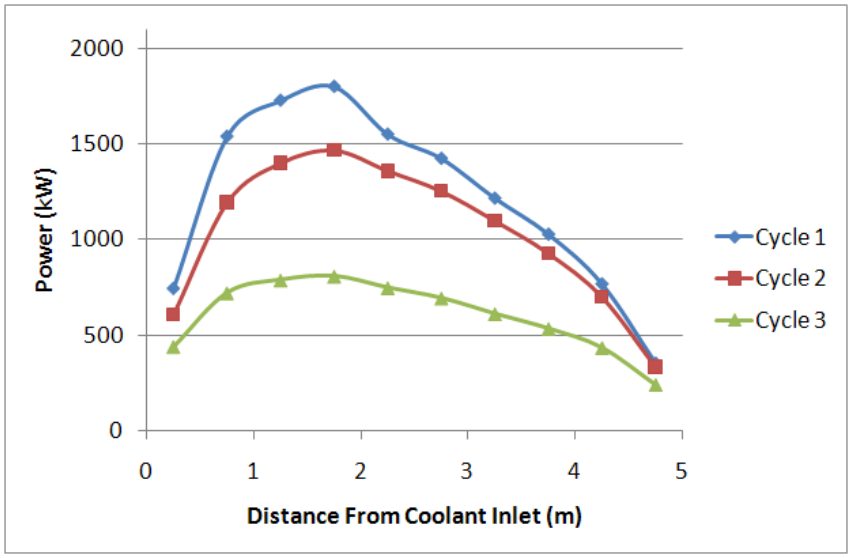

(a) Beginning of Cycle Powers

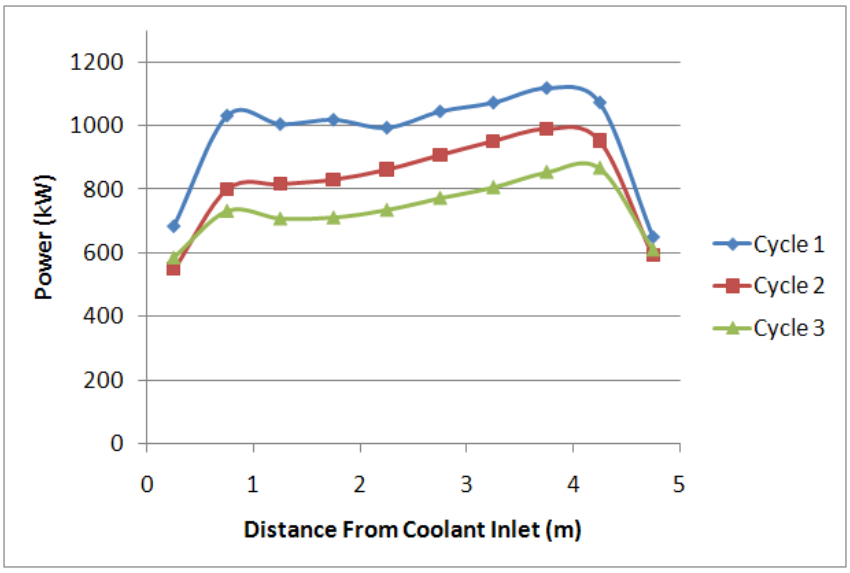

(b) End of Cycle Powers

Figure 5.9: Axial Power Profiles 5% initial enrichment assembly

5.4.3 6% Initial Enrichment

In the case of a 6% enrichment assembly, the power peaking becomes very large. In this case, the maximum channel peaking factor is calculated to be approximately 1.7. In both the 5% and 6% enrichment cases, at the end of cycle, the power profile exhibits peaks at the both the inlet and outlet ends of the channel, with the outlet peak being slightly higher. At the end of cycle one the channel peaking factor has been reduced to 1.2. By the end of cycle in all three enrichment cases, the overall power levels are nearly identical. This is confirmed by the similar peaking factors observed in all three cases at EOC.

To try to reduce the large axial power peaks, absorbing control rods could be used at these peak positions. Another option is axially graded enrichment. This method is used in boiling water reactors due to a similar coolant density variation. Typical BWR assemblies feature five or six axial sections with different U-235 enrichments and gadolinia concentrations [30]. Some sensitivity simulations were done in RFSP of some various axial gradations in enrichment.

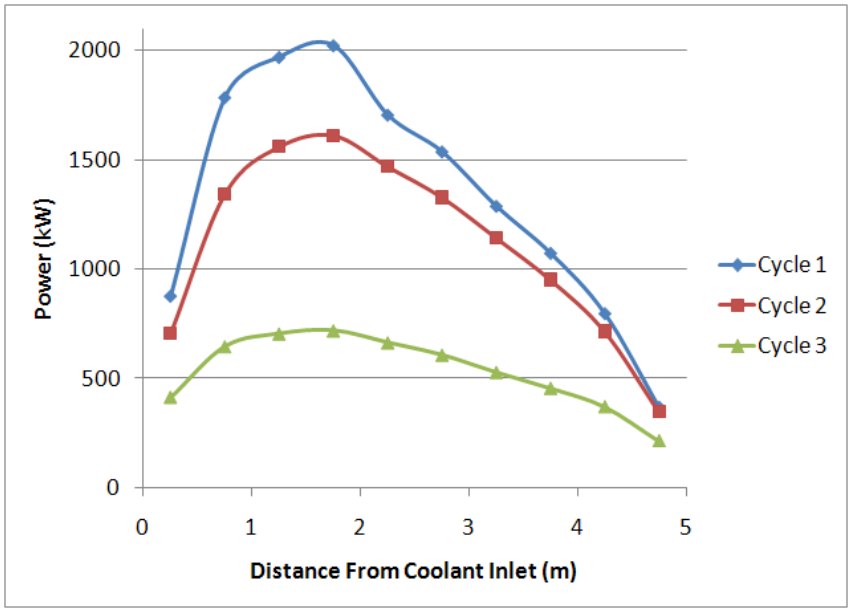

(a) Beginning of Cycle Powers

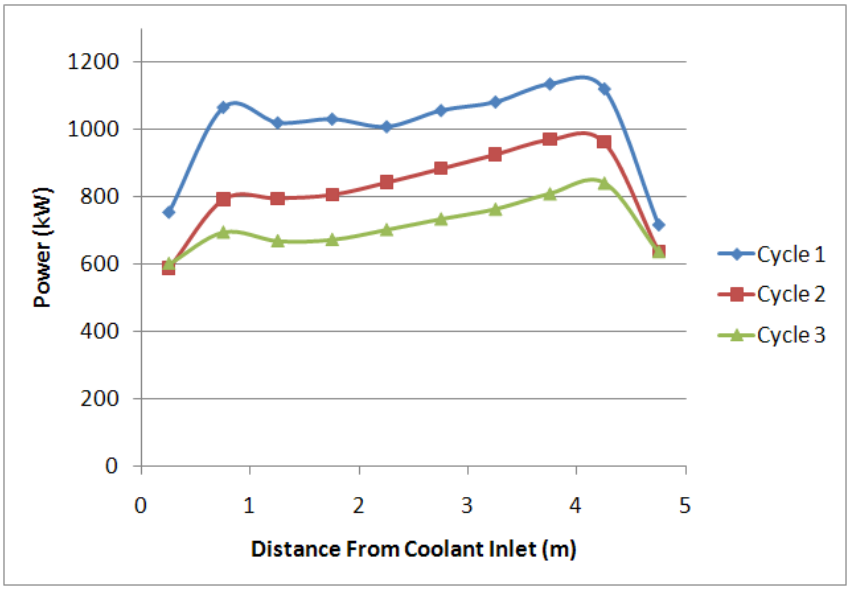

(b) End of Cycle Powers

Figure 5.10: Axial Power Profiles 6% initial enrichment assembly

5.5 Axially Graded Enrichment Cases

The goal of altering the enrichment axially is to reduce the peak in power shown in the previous section. As first attempts, shown in Figures 5.11 and 5.12, the enrichment was graded such that the peak occurs at the downstream end of the fuel channel. This is a disadvantageous position to have the power peak, as the heat transfer is reduced in this region due to high coolant temperatures and also the possibility of degraded convective heat transfer coefficients. Figure 5.13, shows a much flatter power profile, demonstrating that axially graded enrichment can be used to adjust the channel power peaking.

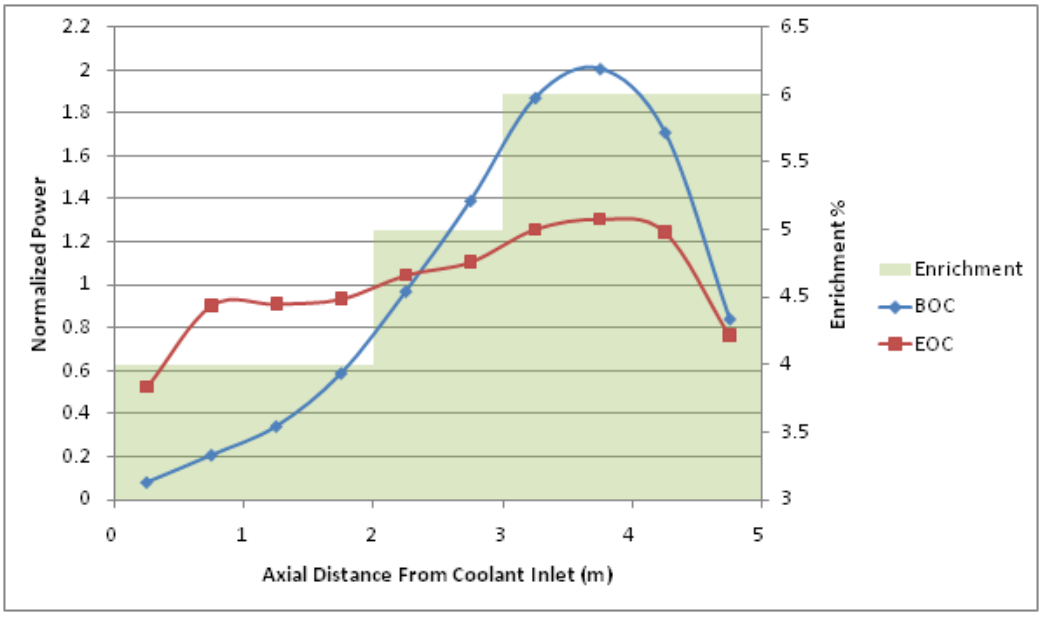

Figure 5.11: Axial Power Profile: Graded Enrichment Scheme 1

These results indicate that the axial power profile can be shaped through graded enrichment. A variation of 1% enrichment has a very strong effect on power, so variations of less than 1% may need to be considered in future work. While this will add to the fuel manufacturing cost, it is

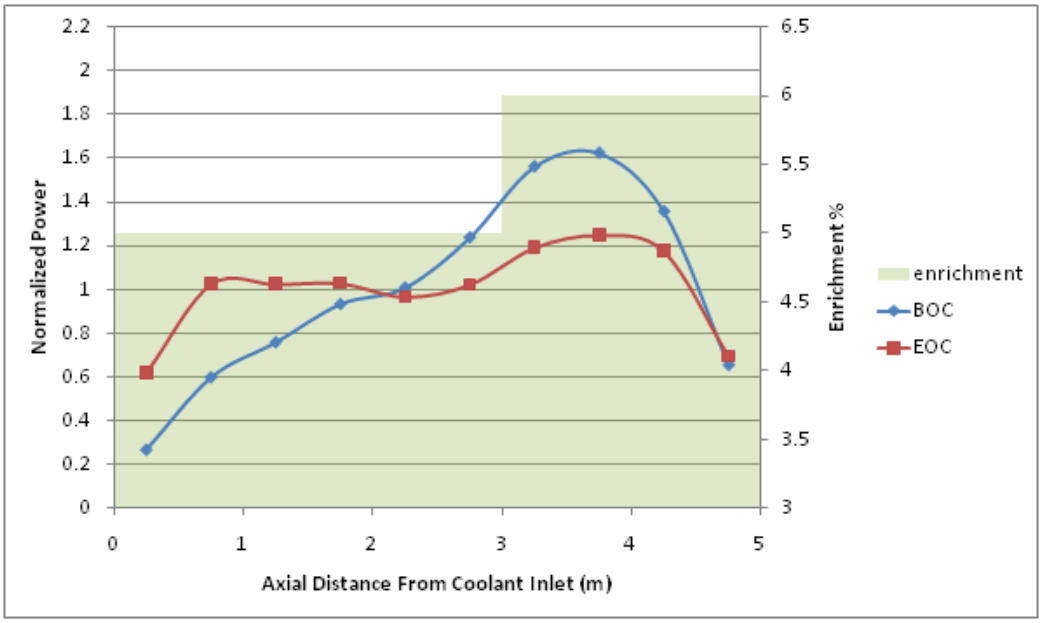

Figure 5.12: Axial Power Profile: Graded Enrichment Scheme 2

demonstrated to be an appropriate alternative to burnable poison addition. Further, the position at which the axial peak occurs will be important, as the heat transfer coefficient will change along the channel. It may be beneficial from a thermalhydraulic point of view to have the axial peaking occur at the higher coolant density end of the channel.

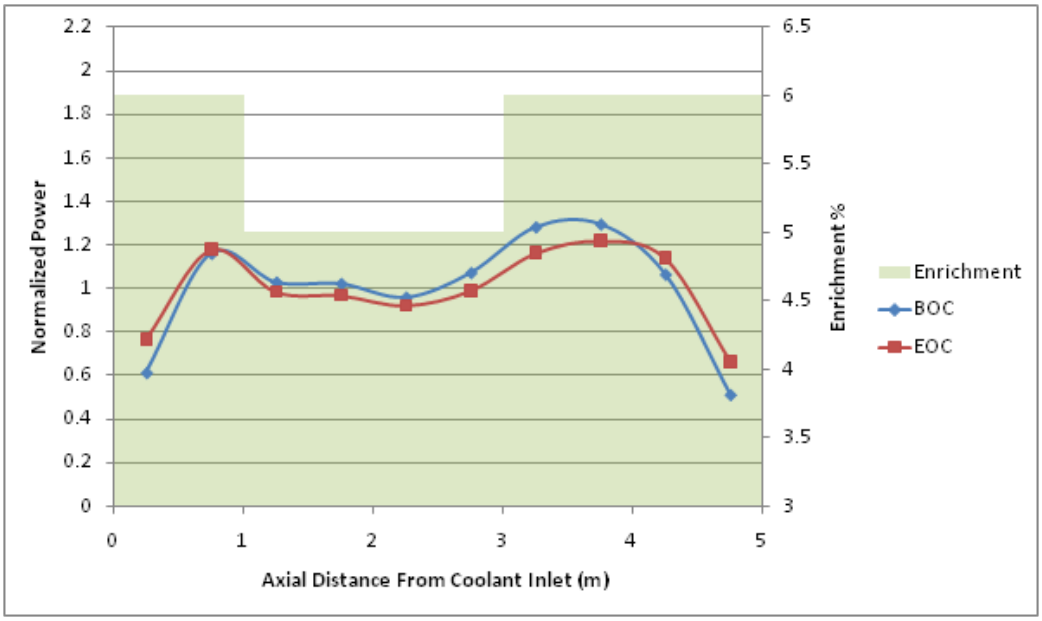

Figure 5.13: Axial Power Profile: Graded Enrichment Scheme 3

5.6 Linear Element Ratings

A result of performing lattice calculations in WIMS is the output of the relative powers for each ring of fuel. This is significant for CANDU style fuel made up of concentric rings of fuel elements as the power produced will vary by ring. Typically, most of the power is produced in the outer ring of fuel elements. These relative powers can be used along with a channel power profile from an RFSP calculation to determine the linear element ratings of the highest power fuel element in the core. The linear element rating is defined as the power produced per unit length of the fuel element.

Commonly, limits are placed on the maximum linear element rating in order to reduce fuel temperature. Uranium dioxide has a melting point of approximately 2840°C and it is required that during normal operation of a reactor and for transients, the fuel not experience centerline melting

(ideally with a large margin to melting). In addition there will be limits placed on the maximum temperature the fuel sheath can reach. By limiting the linear element rating of the fuel, a margin to these limits can be set.

Another motive for reducing linear element rating is to reduce the fission gas release from the fuel pellet for hypothetical events where the fuel becomes damaged. A large amount of fission gas released from the fuel can cause challenges to the integrity of the fuel element. The mechanism of fission gas release depends mostly on fuel temperature. At lower temperatures, most of the fission gas produced remains within the grain boundaries of the fuel. At higher fuel temperatures, fission gas can diffuse more easily to the fuel-clad gap. It has been noted in [29] for CANDU fuel, that above 40 kW/m, the rate of fission gas release is increased. Moreover, for higher burnup fuel ($>$ 25 MWd/kg U), fission gas release rates are even more increased. It is therefore particularly important to limit the maximum linear element rating in the SCWR as the fuel will have a much higher burnup than in traditional CANDU reactors.

The linear element ratings were computed for the five axial position simulated with WIMS-AECL using the powers computed with RFSP. Of interest is the maximum linear element rating in the core. This was computed by first locating the maximum power channel from the RFSP simulation. As all the channels will have the same overall axial power profile shape, the profile and powers from the highest power channel were used to include the highest overall "bundle" powers reached in the core. Next, the power at the five axial positions simulated in WIMS were calculated. By using the relative powers for the three fuel rings from WIMS and the power information from RFSP, the linear element ratings were computed as a function of burnup. The linear element rating for a fuel element in ring $i = 1,\ 2,\ 3$ at position along the channel $j = 1 \ldots 5$ is computed as:

$$\text{Linear Element Rating } i,j = \frac{\text{Power at Position } j \text{ (From RFSP)}}{\text{Number of fuel elements in assembly (54)}} \times \text{Relative Power of Ring } i \text{(From WIMS)} \tag{5.2}$$

Shown in Figures 5.14 - 5.18 are the calculations of linear element ratings for the 4% enrichment assemblies at all five axial positions and for the three rings of fuel in the assembly: inner, intermediate and outer. A simplifying assumption that was used here was that the assembly power stays at its initial BOC power value for the entire cycle. This assumption is conservative for the first section of the assembly, as the power reduces here during a cycle, while towards the end of the channel the power increases towards the end of the cycle. As the largest axial power peak occurs at BOC near the 2 m point in the fuel channel, the overall maximum linear element rating will also occur here.

From these results, it is seen that the maximum linear element rating occurs near the 1.5 meter point of the channel, as can be expected from the axial power profile. In addition, for the 4% enrichment case, the linear element rating is approximately 67 kW/m, well above the target of 40 kW/m. As the LER limit has been exceeded for a 4% enriched assembly, the limits will therefore be exceeded in the 5% and 6% enrichment cases. For the 6% enrichment case, the power peak is approximately 1.3 times the 4% case so the maximum LER can be estimated to be around 89 kW/m for this extreme case. Overall, these results show a reduction in the linear element rating may need to be considered for the SCWR. This can be accomplished in many ways, including increasing the number of fuel channels or reducing overall core power, as well as options such as subdividing the fuel assembly into more fuel elements, annular fuel pellets, or graded enrichments within the assembly axially or radially.

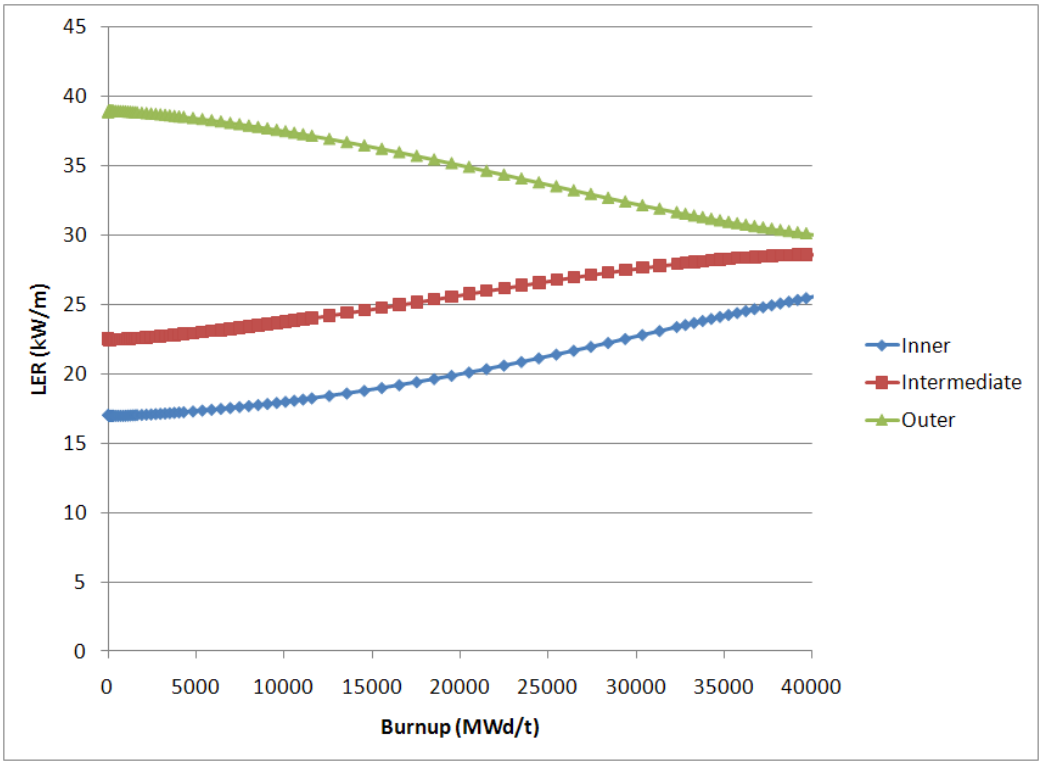

Figure 5.14: Linear Element Rating vs. Burnup for Axial position 0.5 m

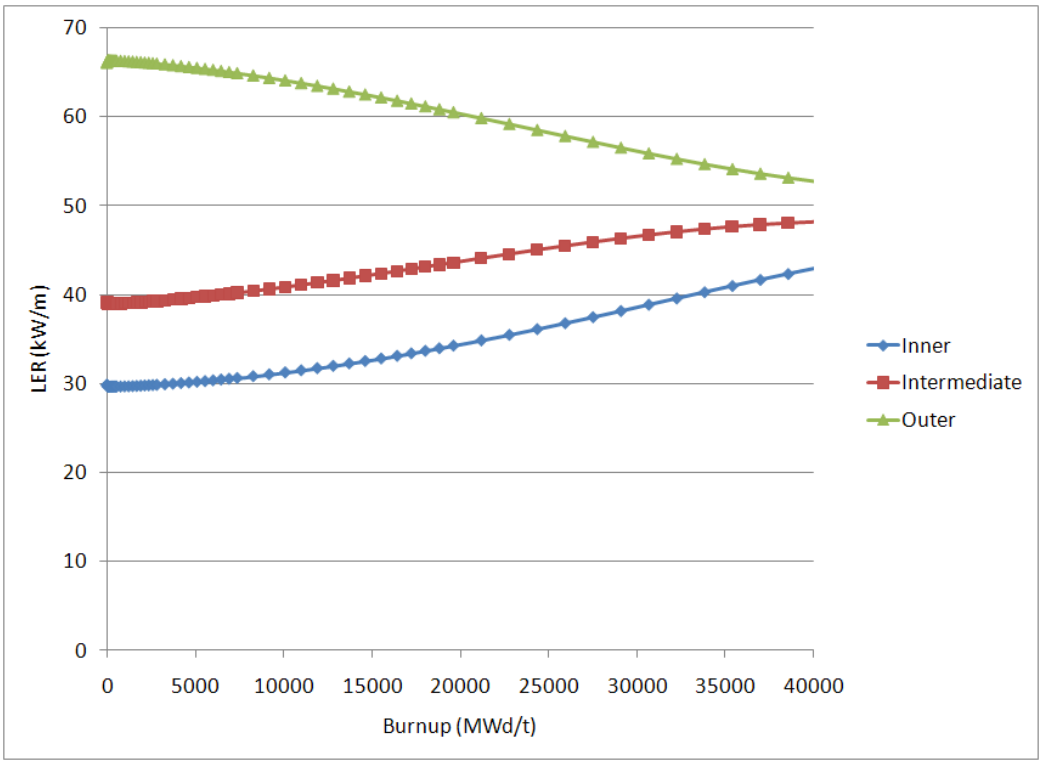

Figure 5.15: Linear Element Rating vs. Burnup for Axial position 1.5 m

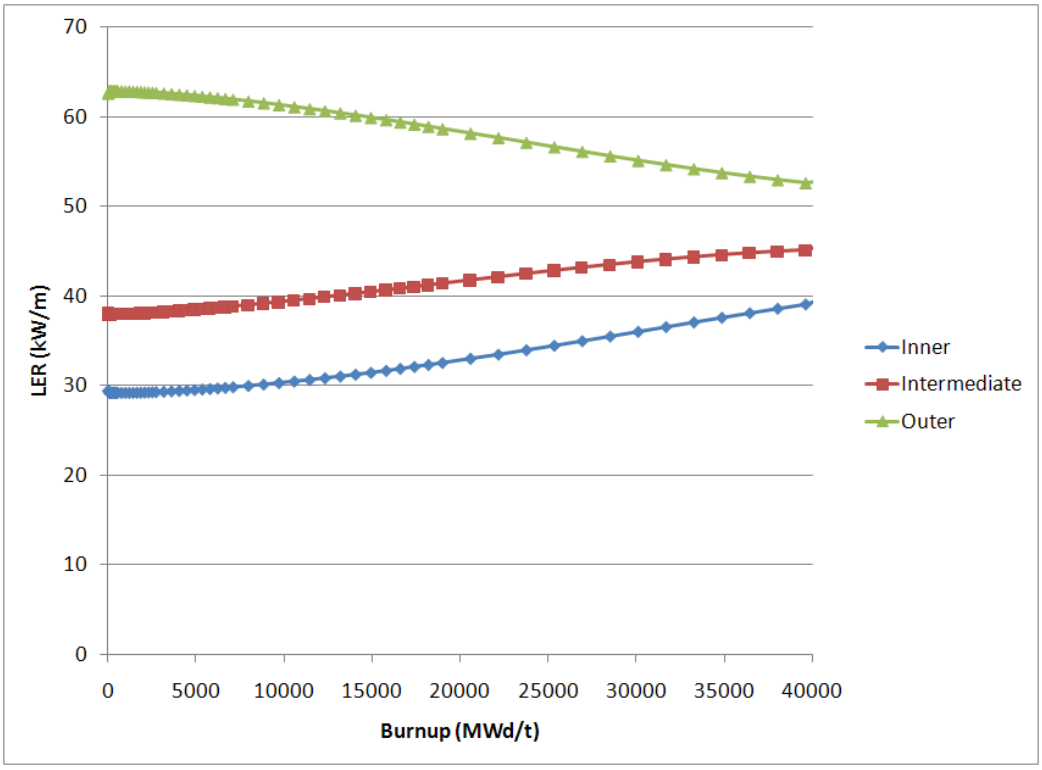

Figure 5.16: Linear Element Rating vs. Burnup for Axial position 2.5 m

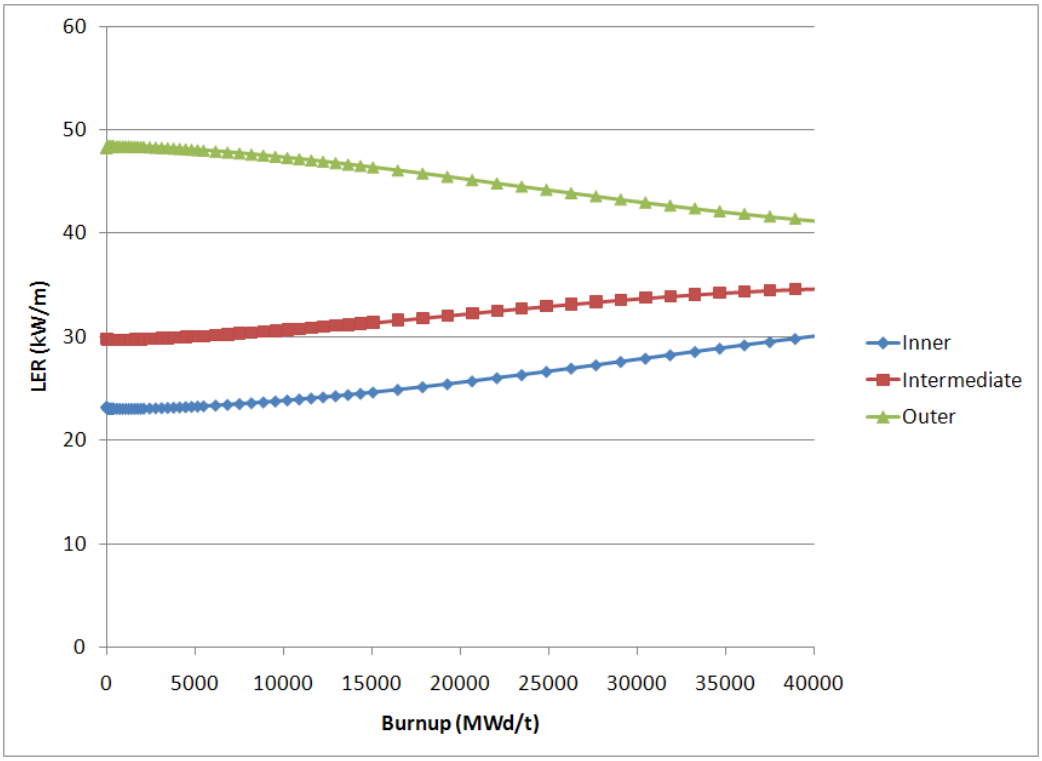

Figure 5.17: Linear Element Rating vs. Burnup for Axial position 3.5 m

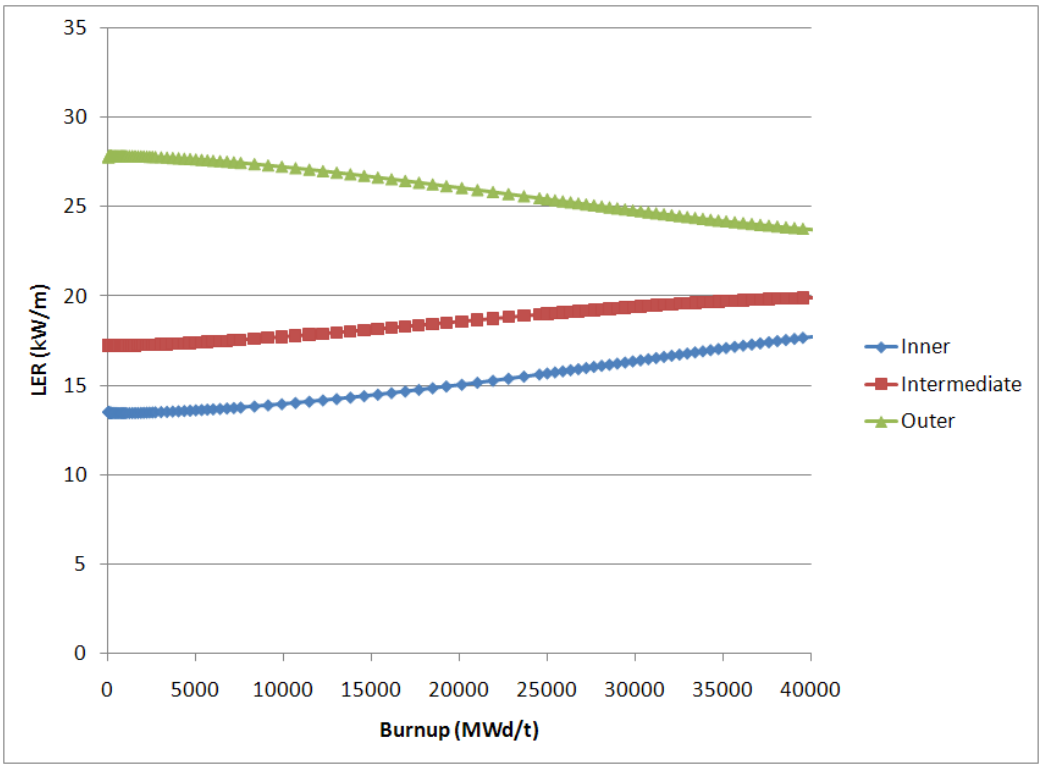

Figure 5.18: Linear Element Rating vs. Burnup for Axial position 4.5 m

Chapter 6

Loss of Regulation Analysis

The loss of regulation analysis is a prediction of the consequences of a reactivity initiated accident (RIA), that is, a transient in reactor power caused by an addition of positive reactivity to the core. This work has been performed with the computer code FUELPIN, a one-dimensional heat transfer code with reactor power transients calculated with a point kinetics model. This code is used to model the hottest fuel element in the reactor core, and predicts the clad and fuel temperatures, which can then be compared to some predetermined temperature limits or criteria. The code also has the capability to simulate shutdown systems in the reactor in great detail by modeling the shutdown system hardware, neutronic detectors and their temporal behavior as well as the associated electronics time response. Within the code, the response of the detectors controlling the reactor trip is determined based on neutron flux, detector construction, and the time response function for the associated electronics. As the shutdown systems for the SCWR are not yet designed, the neutronics trips for current CANDU reactor shutdown systems 1 and 2 were used here assuming the same detector designs and electronics as well as the reactivity insertion rates from the shut-off rods. This is deemed a conservative analysis as, in all likelihood, the SCWR will feature improved detector and shut down systems over current CANDU reactors. This code also contains a model

of fuel temperature reactivity feedback, outlined in [22]. A negative fuel temperature feedback will help to limit a power transient.

6.1 CANDU shutdown systems

Modern CANDU reactors use two fast acting, completely independent shutdown systems (SDS), they are commonly referred to as SDS1 and SDS2. Each system is capable of shutting down the reactor and are effective for all accidents.

SDS1 typically consists of 28 neutron absorbing rods that enter the core from the top of the calandria vessel through gravity. To assist in inserting the rods rapidly, they are spring-loaded and held against the spring by an electromagnetic clutch. Loss of power causes the clutch to disengage and the rods fall into guide tubes penetrating the core. Full insertion of the rods can be accomplished in under two seconds [31].

Shutdown system 2 (SDS2) is a set of six nozzles and perforated tubes that run horizontally through the moderator. Each of these is connected to a tank of a solution of gadolinium nitrate, a strong neutron absorber. Upon a reactor trip, helium from a pressurized tank forces this solution into the moderator rapidly, stopping the nuclear chain reaction and shutting down the reactor.

Each shutdown system uses independent detectors and actuation devices. Also, the design and materials used in each system's detectors are different ensuring complete independence of the two systems and independence from the reactor control system. For the subsequent analysis, both SDS1 and SDS2 trips are simulated, however only the SDS1 shutdown rods are modelled. In practice, it is found that SDS2 acts faster than SDS1, and thus by using only SDS1 in this analysis, the result can be considered conservative. For this work, the inputs for the shutdown system electronics is not changed from the FUELPIN code documentation [22].

6.2 Point Kinetics Data

As the fuel type for this thesis is uranium dioxide, the delayed neutron fractions and decay constants were kept the same as for the CANDU reactor. This information was taken directly from the FUELPIN documentation [22]. Any difference in neutron energy spectrum between CANDU reactor and the SCWR will not affect the delayed neutron fraction, as the delayed neutron yield for U-235 has almost no dependence on the energy of incident neutrons below 4 MeV [32]. In addition, since the moderator is heavy water, an additional nine delayed photoneutron groups were included. One parameter that will be different between the CANDU reactor and the SCWR is the prompt generation time (Λ, in equations 3.5 and 3.6). This can be thought of as the time between "births" of prompt neutrons in two successive generations. It is dependent on the type of moderation and average speed of neutrons, and hence the reactor neutron energy spectrum. As an estimate, the value used in the analysis was 10^{-4} seconds, a value that is somewhere between the CANDU reactor, and a light water reactor. As the moderator is heavy water as in a CANDU reactor, this value may be conservative, and the prompt generation time may be closer to that of a CANDU. An area for future work may be to compute a prompt generation time based on core models of the SCWR. The sensitivity to this value will have a large impact on the reactivity transient analysis. As well, as the current reference fuel is plutonium-thorium, many of the point kinetics parameters will need to be updated for this analysis. The delayed neutron fractions for each group and decay constants are given in Table 6.1. These values are taken from a CANDU 900 reactor with mid-burnup fuel. The final nine rows of the table represent the delayed photoneutron groups.

6.3 Reactor Trip and Shutdown Reactivity Insertion

The reactor trip can be initiated by the code when either of the neutron flux, linear rate of change of power, or log rate of change in power are compared to and exceed user-specified trip setpoints. The

Group Delayed Neutron Fraction (β)	**Group Decay Constant (λ)(1/s)**
1.769×10^{-4}	0.012778
1.1498×10^{-3}	0.031535
1.0191×10^{-3}	0.122197
2.1057×10^{-3}	0.32282
7.726×10^{-4}	1.389289
1.962×10^{-4}	3.778336
Delayed Photoneutron Groups	
1.61×10^{-7}	6.26×10^{-7}
3.23×10^{-7}	3.63×10^{-6}
1.03×10^{-6}	4.37×10^{-5}
7.48×10^{-6}	1.17×10^{-4}
6.61×10^{-6}	4.28×10^{-4}
1.08×10^{-5}	1.50×10^{-3}
2.24×10^{-5}	4.81×10^{-3}
6.52×10^{-5}	1.69×10^{-2}
2.08×10^{-4}	0.277

Table 6.1: Point Kinetics Data for FUELPIN calculations

shutdown reactivity transient is also user-specified and is given in Table 6.2. For points between the times in the table, the code interpolates the reactivity. To simulate shutdown, the code adds the shutdown reactivity to the transient reactivity and this is then used in the point kinetics equations to calculate reactor power.

6.4 Geometry and Initial Conditions

The initial conditions for the simulations are specified below. Of particular importance is the linear element rating. As seen in the previous chapter, there is a need to reduce the linear element rating, however the results presented in this chapter are for linear element ratings of 60 kW/m, which is near the maximum value of 67 kW/m seen in the previous chapter and is close to existing LER ratings for CANDU. Additional sensitivity studies are performed at 50 kW/m, perhaps a more

Time (seconds)	**Reactivity Inserted (mk)**
0	0
0.2	0
0.67	-0.57
0.84	-1.7
0.99	-2.9
1.14	-4.9
1.27	-7.9
1.4	-13.1
1.53	-21.9
1.67	-35.7
1.82	-53.7
2.3	-63.0
3	-63.0
10000	-63.0

Table 6.2: Characteristic shutdown reactivity insertion

realistic target for the maximum LER.

The fuel pellet radius and clad thickness were kept the same as specified in Chapter 4. One change is the addition of a small gap between the fuel pellet and sheath, this gap size was chosen to be 0.15 mm. Current CANDU reactor fuel features a thin fuel sheath, designed to collapse onto the fuel pellet during irradiation. As the fuel for the SCWR will be taken to higher burnups, the collapsible sheath may not be a viable option, and a small gap has been added here, as is common in light water reactor fuel. The fuel density used is 10.12 g/cm^3 and the clad density used is 7.9 g/cm^3. Further work may be required to assess the gap conductance as well as to assess the nature of sheath collapse, if any, in the SCWR fuel behaviour.

For the heat transfer calculation, the coolant temperature and other properties must be specified. As seen in the previous chapter, the maximum linear element rating occurs somewhere near the coolant inlet end of the fuel channel. The heat transfer coefficient at this point is an input to the code. In [17], for a similar 336 channel core with the 54 element assembly design, the heat

Parameter	**Case 1**	**Case 2**	**Case 3**	**Case 4**
Coolant Temperature (°C)	400	400	600	600
Heat Transfer Coefficient ($kW \cdot m^{-2} \cdot K^{-1}$)	12	12	5	5
Linear Element Rating (kW/m)	50	60	50	60

Table 6.3: Cases simulated with FUELPIN code

transfer coefficient at the inlet end is calculated to be 13086 $W \cdot m^{-2} \cdot K^{-1}$, while at the outlet the heat transfer coefficient is reduced to 4470 $W \cdot m^{-2} \cdot K^{-1}$.

For the results presented here, two positions were chosen. First, the most likely location of the peak linear element rating, at a position towards the inlet end of the channel is characterized by a heat transfer coefficient 12 $kW \cdot m^{-2} \cdot K^{-1}$ and a coolant temperature estimated to be 400°C, and secondly, a more unlikely position for the maximum linear element rating further down the channel where the heat transfer has degraded. The heat transfer coefficient used was 5 $kW \cdot m^{-2} \cdot K^{-1}$ and a coolant temperature of 600°C.

The trip setpoints used here are the neutronics trips of neutron overpower (NOP) and log rate. The trip set points for the SDS1 and SDS2 NOP trips were both taken to be 106% full power. Of note, while the NOP setpoints are the same, the design of the SDS1 detector gives a prompt response while the SDS2 detector responds with a slight delay. This is included in the FUELPIN code and it can be seen in the code output that the SDS1 NOP trip always occurs before the SDS2 trip. The log rate setpoints were chosen to be 0.10 s^{-1} for SDS1 and 0.l5 s^{-1} for SDS2 as specified in the code documentation. In the code, the reactor is said to have tripped when any two of these trips are recorded. At this point, the code begins to insert the negative reactivity from the shutoff rods as determined by the lookup table of insertion vs. timing (Table 6.2).

Summarized in Table 6.3 are the combinations of parameters simulated with the FUELPIN code, grouped into four cases.

Each of these cases was simulated with the reactivity insertion rates of 0.01 mk/second, 0.1

Case	**Clad Temperature** (°C)	**Fuel Centerline Temperature** (°C)
Case 1	509	2052
Case 2	530	2502
Case 3	841	2455
Case 4	889	2742

Table 6.4: Temperatures of fuel and clad during normal operation for maximum LER fuel pin in core

mk/second and 1 mk/second.

6.5 Results

It is necessary to compare the temperatures predicted by the code to some temperature limits. The goal for the fuel is that the fuel centerline temperature remain below the melting point of UO_2, that is 2840°C. The sheath temperature limit for stainless steel cladding is recommended in the textbook by Oka [12] to be 740°C for normal operation and 1260°C for design basis accidents. These criteria are used in the subsequent analysis.

The normal operating temperatures are summarized in Table 6.4, for each of the four cases mentioned above.

It is observed that having a fuel element operating at 50 kW/m or 60 kW/m at the lower density coolant region (cases 3 and 4) of the channel presents clad temperatures well in excess of the 740°C limit. Further, the margin to fuel centerline melting is very small (less than 100°C in the 60 kW/m case). Having the highest linear element rating occur near the inlet end of the fuel channel (Case 1 and 2) provides better margin to both fuel clad and fuel centerline temperature limits, although the margin is significantly reduced for the 60 kW/m LER. The fact that the margin is fairly small in the Cases 3 and 4 becomes an issue especially towards the end of the operating cycle, when the axial power peak shifts to this region of the channel, this will cause unacceptably high temperatures.

These considerations provide further motivation to consider an overall reduction of linear element rating for the SCWR core as mentioned in previous chapters.

6.5.1 0.01 mk/s reactivity insertion rate

For the 0.01 mk/sec reactivity insertion rate, the power is seen to increase with time according to Figure 6.1. It is seen to increase relatively slowly, reaching 114% full power (FP) at 25 seconds without the reactor trip. With the reactor trip enabled, 106% full power is reached at approximately 15 seconds, the reactor is tripped by the SDS1 and SDS2 neutron overpower trips at 14.7 seconds and power is reduced quickly thereafter.

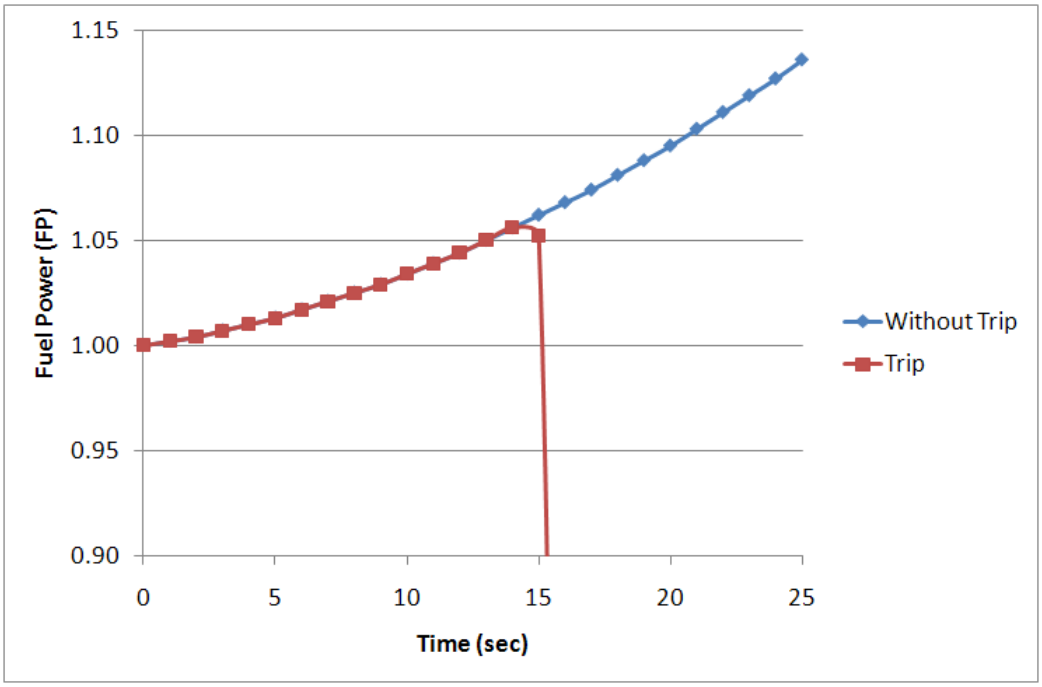

Figure 6.1: Fuel Power vs. Time for 0.01 mk/s reactivity insertion

Shown in Figures 6.2b and 6.2b are the fuel cladding and pellet centerline temperatures for the 0.01 mk/s reactivity insertion rate, with neutronics trips enabled. As observed here, in the case of the clad temperatures, Case 1 and Case 2 are similar, while for the fuel centerline temperature, Case 1 and 3 are similar valued. It can be concluded from this that the clad temperature is mostly

	Case 1	**Case 2**	**Case 3**	**Case 4**
Maximum Clad Temp (°C)	512	534	847	897
Maximum Fuel Centerline Temperature (°C)	2084	2434	2482	2758

Table 6.5: Maximum Temperatures reached for 0.01 mk/s rate

dependent on the coolant temperature, while the fuel centerline temperature is more dependent on the linear element rating.

The maximum temperatures reached are summarized in Table 6.5. Here we see a small margin to fuel centerline melting in Case 3 and 4. In addition, while the clad temperatures in Case 3 and 4 are below the accident limit of 1260°C, they are well above the normal operating temperature limit.

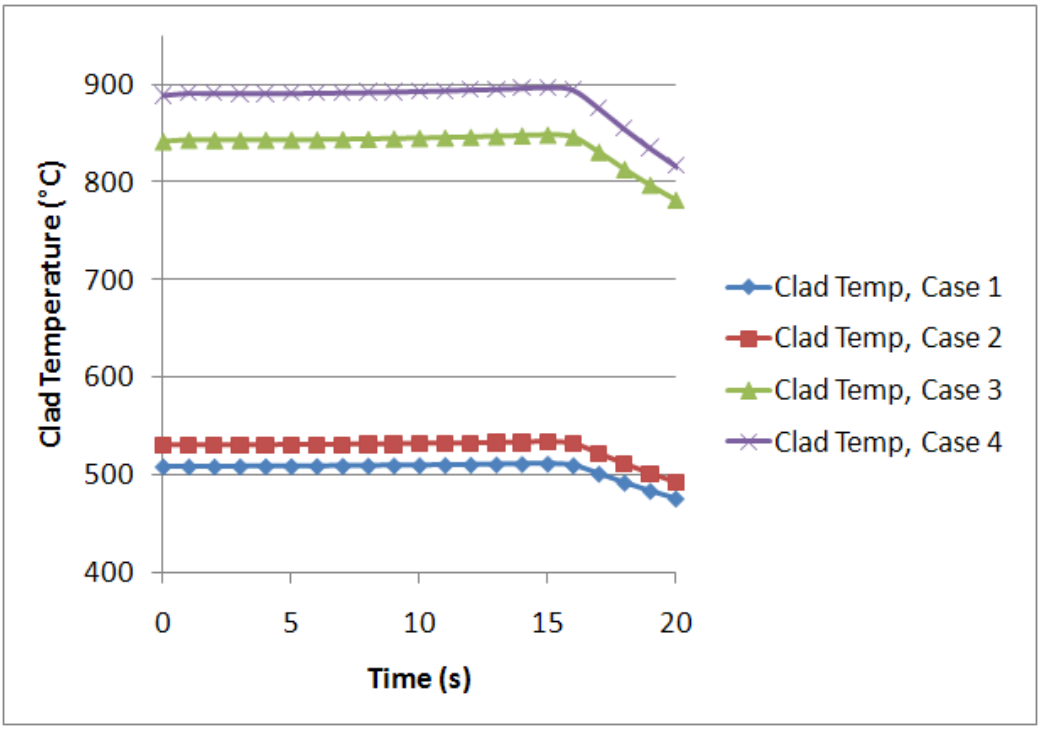

(a) Clad Temperatures for 0.01 mk/s rate

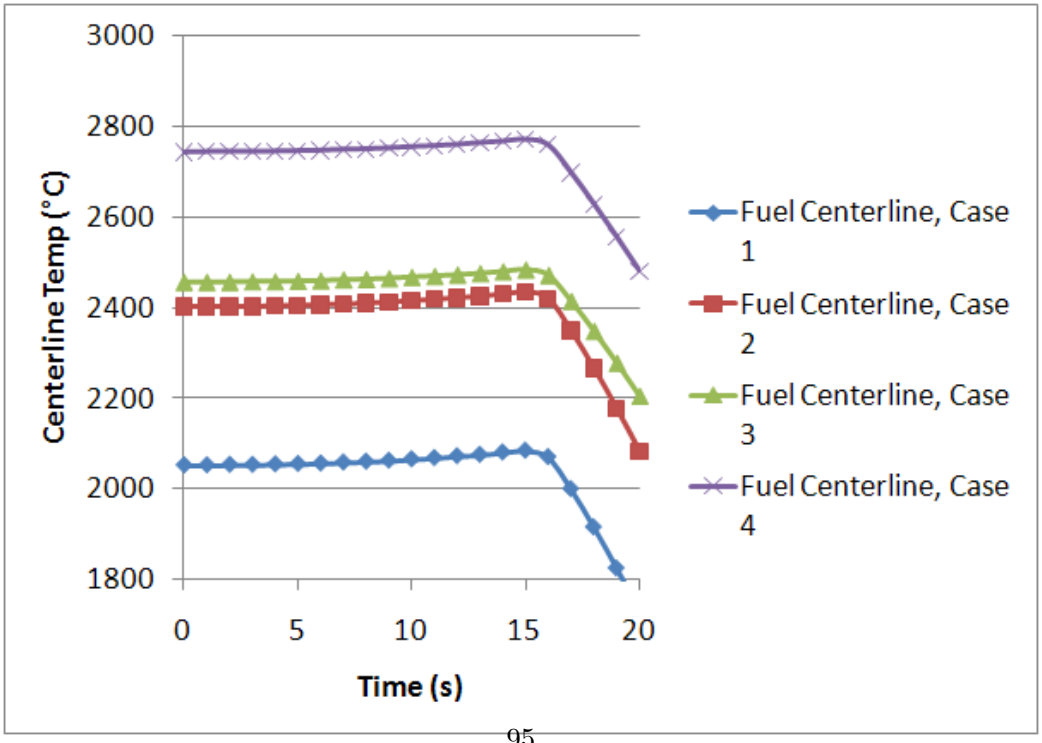

(b) Fuel Centerline Temperature for 0.01 mk/s rate

Figure 6.2: Clad and Centerline Temperatures for 0.01 mk/s rate with trip

6.5.2 0.1 mk/s and 1 mk/s reactivity insertion rates

In the case of the 0.1 mk/s insertion rate, the power is seen to increase to 3.5 times full power by 20 seconds (Figure 6.3). The reactor trip occurs in this case via the neutron overpower trips of SDS1 and SDS2 at 2.7 seconds.

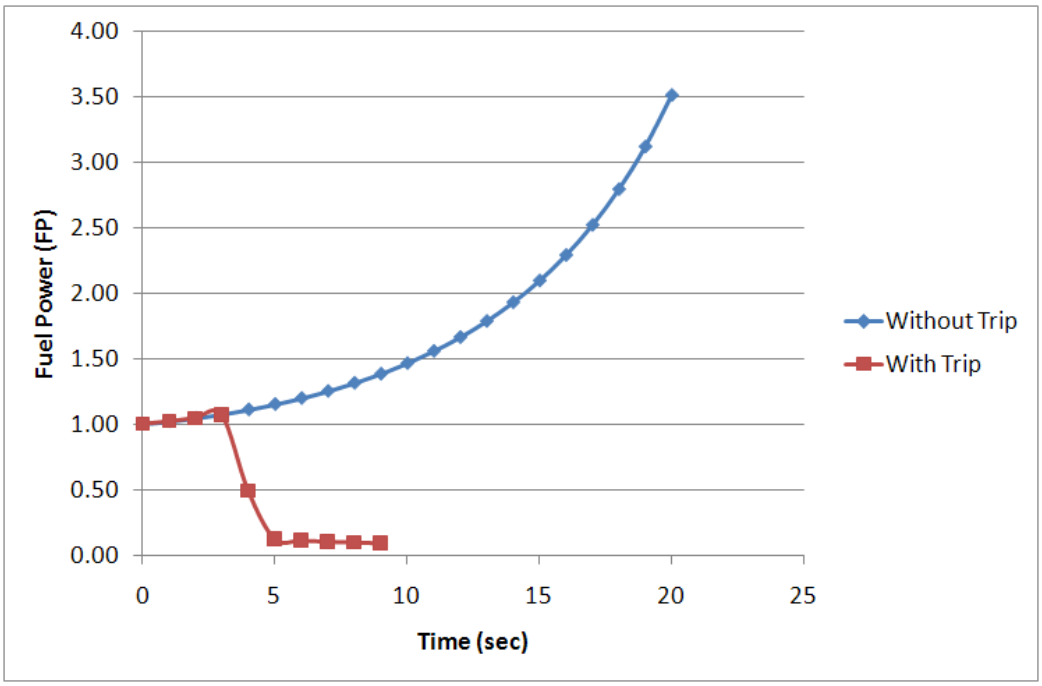

Figure 6.3: Fuel Power vs. Time for 0.1 mk/s reactivity insertion

For the 1 mk/sec reactivity insertion rate, the power is seen to increase rapidly, reaching 13 times full power by 4.5 seconds (Figure 6.4). In this case, the log rate trips become effective, due to the high rate of increase in power. The reactor trip occurs at 0.472 seconds from the SDS1 NOP trip and log rate trips, occuring at 0.462 seconds and 0.472 seconds respectively.

In both of these cases, the maximum temperatures reached are nearly identical, however they are reached at different times. From this, it is concluded that the maximum temperature reached is

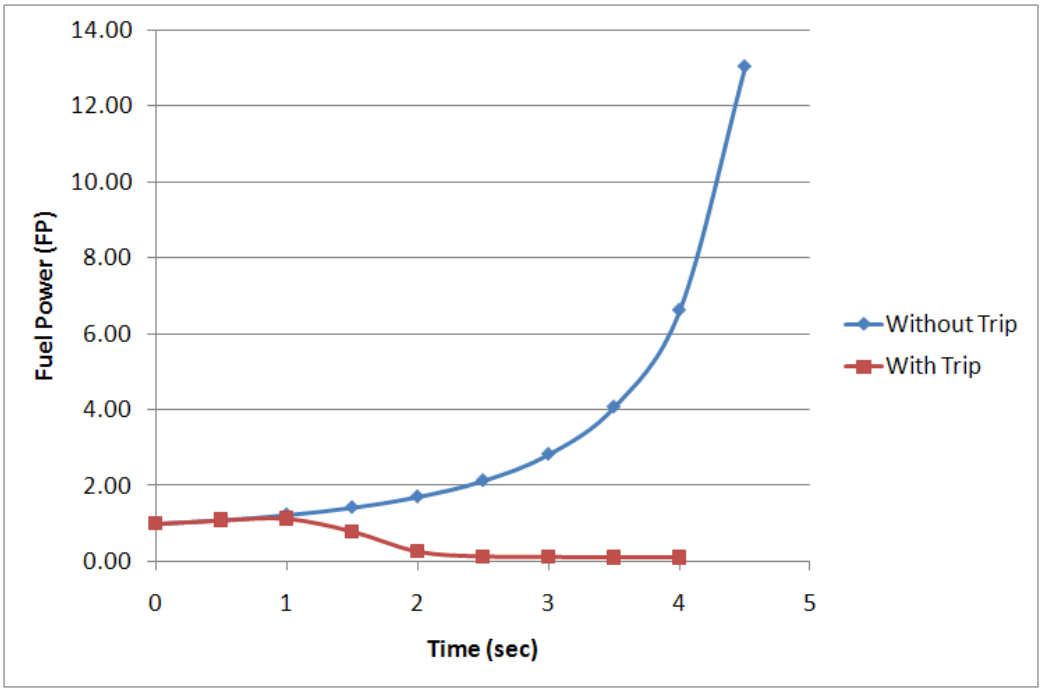

Figure 6.4: Fuel Power vs. Time for 1 mk/s reactivity insertion

governed by the maximum fuel power reached, and thus limited by the trip setpoint. The maximum temperatures occurred at 3 seconds for the 0.1 mk/s rate, while for 1 mk/s they occurred at 1.5 seconds. The maximum temperatures are given in Table 6.6.

	Case 1		**Case 2**		**Case 3**		**Case 4**	
Reactivity Insertion Rate (mk/s)	0.1	1	0.1	1	0.1	1	0.1	1
Linear Element Rating (kW/m)	50	60	50	60	50	60	50	60
Maximum Clad Temp. (°C)	509	510	532	532	844	845	893	894
Maximum Centerline Temp. (°C)	2061	2061	2410	2410	2462	2462	2750	2750

Table 6.6: Maximum fuel clad and centerline temperatures reached for 0.1 mk/s and 1 mk/s reactivity insertion rates

6.5.3 Increased NOP Trip Setpoint

From the previous section, it was found that the clad and centerline temperatures reached were dependent on the power reached rather than the reactivity insertion rate, in particular for slow insertions. The power level reached is in turn limited by the trip setpoint for the case when the transient is sufficiently slow to avoid the log rate trips. A case was run with the slowest reactivity insertion rate from the previous section (0.01 mk/s), and a higher neutron overpower trip setpoint. The slow reactivity insertion rate ensures the log rate trip will not be effective. The NOP trip setpoint for this trial was set at 120% full power for both SDS1 and SDS2. As the margin to fuel centerline melting was already very small with the 60 kW/m linear element rating case, only the 50 kW/m case was simulated here. Both 400°C and 600°C coolant temperatures and corresponding heat transfer coefficients were used (Cases 1 and 3 from previous sections).

In these trials, the reactor reaches 120% full power at 30.5 seconds, and the reactor trip occurs at 31.4 seconds.

In the case of 400°C coolant, the maximum fuel centerline temperature reached was 2227°C while the maximum clad temperature reached was 523°C. For the 600°C coolant, the maximum fuel centerline temperature was 2600°C and the maximum clad temperature reached was 871°C. This represents about a 200 degree margin to centerline melting, and clad temperatures below the accident limit. Further, since the peak linear element rating will most likely occur closer to the 400 degree coolant region, this will provide more margin to the thermal limits. In all cases the transient was arrested and temperatures were kept below their limits for the 50 kW/m LER. As the limit for linear element rating will likely be lower than 50 kW/m, it is seen here that the existing shutdown systems for the CANDU reactor appear adequate for the SCWR.

Chapter 7

Conclusions and Recommendations For Future Work

In this work, simulations of lattice cells and full core models have been performed for the pressure tube supercritical water cooled reactor. Lattice physics calculations performed with WIMS-AECL compared the burnup and coolant void reactivity of assemblies featuring 43 and 54 fuel elements. It was found that the 43 element design achieved greater fuel burnup through its large moderator to fuel ratio, however this came at the expense of large coolant void reactivity values, particularly in the region of of the fuel channel with high coolant density. The CVR values were found to be widely varying throughout the fuel channel for the 43 element design. The 54 element design was found to provide acceptable burnup performance with similar coolant void reactivity performance along the fuel channel and decreasing with burnup. As the reference fuel type for the SCWR is now thorium/plutonium fuel, future investigations may focus on performing similar analyses with this fuel type.

Full core simulations were performed using RFSP using the 54 element design with varying

assembly enrichments. To achieve the burnup target of 30000 MWd/tonne uranium, it was found using WIMS that an enrichment level of between 4-5% is required. In RFSP, the cycle lengths, that is the time between refueling outages, was found to be 250 full power days for a 4% enrichment and 370 full power days for 5% enriched fuel. A refueling scheme was devised that produced a radial core channel peaking factor of 1.26 for 4% initial assembly enrichments, however this factor was much larger in the case of 5% and 6% enrichments. Axial power profiles along the fuel channel were also investigated. It was found that large peaks in power occurred near the 2 m point of the fuel channel. For the maximum power channel, this translated into a maximum linear element rating of nearly 80 kW/m.

Future work in this area may investigate a more precise optimization of refueling schemes. In the investigations here, the optimization was performed manually to achieve a desired low maximum radial channel power factor. Further, the full core simulations were performed assuming the same coolant density profile in all cases. For more accuracy, the coolant density profile should be updated for each type of fuel assembly used and throughout burnup. In addition, while axially graded enrichment was investigated here and found to be an effective way to reduce axial power peaking, other methods, including burnable neutron absorber addition to the fuel, or control rods may be examined.

As well, the full core simulations have been performed using a diffusion code with only two energy groups. While this has been adequate in the past for CANDU analysis, it is not known what effect this has on a reactor like the SCWR. It may be of interest to perform a sensitivity analysis of the calculation results to the number of energy groups used in the code.

Simulations were performed using the FUELPIN code that investigated fuel elements with a maximum linear element rating of 60 kW/m. It was found this LER produced fuel centerline temperatures with little margin to fuel centerline melting during normal operation. It is therefore recommended that the SCWR have a maximum linear element rating below 50 kW/m to provide

adequate safety margins. For additional protection against fission gas release for the high burnups expected for the SCWR, it is further suggested that the maximum LER be kept below 40 kW/m.

Additional simulations using FUELPIN investigated the use of existing CANDU shutdown systems performance during reactivity transients. Various reactivity insertion rates were examined, and in all cases, the existing CANDU shutdown systems were able to prevent temperature limits being exceeded. Additional work in this area can focus on the updating of these results to the use of thorium fuel data. As the point kinetics and physical properties parameters will not be the same for thorium-plutonium fuel, this will affect the results of this section. While this work is a preliminary analysis using CANDU shutdown systems, as the SCWR design becomes more refined, SCWR control and shutdown systems can be simulated.

Bibliography

[1] U.S. DOE Nuclear Energy Research Advisory Committee and Generation IV International Forum (2002). A Technology Roadmap for Generation IV Nuclear Energy Systems. Document GIF-002-00. Accessed from http://www.gen-4.org/PDFs/GenIVRoadmap.pdf.

[2] Chow, C. and Khartabil, H. (2007). Conceptual Fuel Channel Designs for CANDU-SCWR. *Nuclear Engineering and Technology*, Vol. 40, No. 2. pages 139–146.

[3] Rosen, M. A. et al. (2010). Nuclear-based hydrogen production with a thermochemical copperchlorine cycle and supercritical water reactor: equipment scale-up and process simulation. *International Journal of Energy Research*, doi: 10.1002/er.1702.

[4] Duke University Physics Department: Phase Diagram for Water Accessed from: http://www.phy.duke.edu/~hsg/176/table-images/water-phase-diagram.html

[5] Reactor Engineering Development Operation Staff (1959). Supercritical Pressure Power Reactor, A Conceptual Design. HW-59684, General Electric Co., Hanford Atomic Products Operation, Richland, Washington.

[6] Oka, Y. (2000). Review of High Temperature Water and Steam Cooled Reactor Concepts. *The First International Symposium on Supercritical Water-cooled Reactors, Design and Technology.* Paper 104.

[7] Atomic Energy of Canada Ltd. ACR-1000 (Advanced CANDU Reactor). Accessed from: http://www.aecl.ca/Reactors/ACR-1000.htm.

[8] Yetisir, M., Diamond, B., Leung, L., Martin, D., Duffey, R. (2011). Conceptual Mechanical Design for a Pressure-Tube Type Supercritical Water-Cooled Reactor. *Proceedings of The 5 th Int. Sym. SCWR (ISSCWR-5)*. Paper 055.

[9] Pioro, I. and Duffey, R. (2007). Heat Transfer and Hydraulic Resistance at Supercritical Pressures in Power Engineering Applications. New York: ASME Press.

[10] Kamei, K. et al. (2006). Fuel and Core Design of Super Light Water Reactor with Low Leakage Fuel Loading Pattern. *Journal of Nuclear Science and Technology*. Vol 43, No. 2, p. 129-139.

[11] Yamada, K. et al. (2011). Overview of the Japanese SCWR Concept Developed Under the GIF Collaboration. *Proceedings of The 5 th Int. Sym. SCWR (ISSCWR-5)*. Paper 031.

[12] Oka Y, Koshizuka, S., Ishiwatari, Y., Yamaji, A., (2010). "Super Light Water Reactors and Super Fast Reactors - Supercritical-Pressure Light Water Cooled Reactors". Springer Science and Business Media.

[13] Schulenberg, T., et al. (2011). Assessment of the HPLWR Thermal Core Design. *Proceedings of The 5 th Int. Sym. SCWR (ISSCWR-5)*. Paper 057.

[14] Maraczy, C., et al. (2011). HPLWR Equilibrium Core Design with the KARATE Code System. *Proceedings of The 5 th Int. Sym. SCWR (ISSCWR-5)*. Paper 062.

[15] Starflinger, et al. (2010). High performance light water reactor phase 2, Public Final Report - Assessment of the HPLWR Concept. 6th Framework Programme, Contract No. FI60-036230, accessed: www.hplwr.eu.

[16] Boczar, P. et al. (2010). Reactor Physics Studies for a Pressure Tube Supercritical Water Reactor (PT-SCWR). *Proceedings of the 2nd Canada-China Joint Workshop on Supercritical Water-Cooled Reactors*. Paper 088.

[17] McDonald. M. H. et al. (2011). Pre-Conceptual Fuel Design Concepts For The Canadian Super Critical Water-cooled Reactor. *Proceedings of The 5 th Int. Sym. SCWR (ISSCWR-5)*. Paper 134.

[18] Pencer, J. and Hyland, B. (2011). Physics Aspects of the Pressure Tube Type SCWR Preconceptual Design. *Proceedings of The International Conference on the Future of Heavy Water Reactors*. Paper 020.

[19] Altiparmakov, D. V. (2006). WIMS-AECL Version 3.1 Theory Manual. 153-119190-STM-001, FFC-RRP-736. Revision 0.

[20] Liang, T. (2007). WIMS Utilities Version 2.0: User's Manual. 153-119220-UM-001, SQAD-07-5087, Revision 0.

[21] Shen, W. (2006) RFSP-IST Version REL_3-04: Theory Manual. 153-117360-STM-002, SQAD-06-5058.

[22] Rance, F. D. (1982). FUELPIN Engineers' Manual. Report No. 82034, Nuclear Studies and Safety Department, Ontario Hydro.

[23] Driscoll, M. J. et al. (1990). "The Linear Reactivity Model for Nuclear Fuel Management". American Nuclear Society. La Grange Park, Illinois.

[24] Shan, J., Chen, W., Rhee, B. W., Leung, L. K. H., (2010). Coupled Neutronics/thermal-hydraulics analysis of CANDU-SCWR fuel channel. *Annals of Nuclear Energy*. Vol 37. p 58-65.

[25] Magill, M., Pencer, J., Pratt, R., Young, W., Edwards, G.W.R. and Hyland, B., Thorium Fuel Cycles in the CANDU Supercritical Water Reactor. *Proceedings of The 5 th Int. Sym. SCWR (ISSCWR-5)*. Paper 003.

[26] Glasstone, S. and Sesonske, A. (1981). "Nuclear Reactor Engineering". Third Edition. Van Nostrand Reinhold Ltd. New York.

[27] Chen, Y. et al. (1977). Optimal Power Profile Fuel Management. *Annals of Nuclear Energy*. Vol 4. p 407-415.

[28] Chang, Y. and Sesonske, A. (1984). Optimization and Analysis of Low-Leakage Core Management for Pressurized Water Reactors. *Nuclear Technology*. Vol 65. p 292-304.

[29] Floyd, M. R. (2001). Extended-Burnup CANDU Fuel Performance. 7th International CANDU Fuel Conference Proceedings.

[30] Martin-del-Campo, C. et al. (2007). Optimization of BWR fuel lattice enrichment and gadolinia distribution using genetic algorithms and knowledge. *Annals of Nuclear Energy*. Vol. 34. p 248-253.

[31] Snell, V. G. (2001). CANDU Safety #5 - Safety Functions - Shutdown Systems. Canteach Website. http://canteach.candu.org/library/19990105.pdf.

[32] Ott, K. O. and Neuhold, R. J. (1985). Introductory Nuclear Reactor Dynamics. American Nuclear Society, La Grange Park, Illinois, USA.

Appendix A

Sample WIMS-AECL Input File: 43 Element Fuel

```
* M. McDonald
* Jan 6 2011
*
* 43 element bundle geometry + 4% enriched
*
*
Title ‘‘Super Critical Water Reactor 43 Element’’

CELL Cluster
SEQUENCE Pij

plot

SYMMETRY -6 0d 60d * 9-pins in each section

LINES 0.0 2.0 80 13
LINES 2.0 6.80 120 13
LINES 6.80 19.0919 200 13

ANNULUS # 2.113 Coolant2
ANNULUS # 2.225 Coolant2
ANNULUS # 2.485 Coolant2
ANNULUS # 2.745 Coolant2
ANNULUS # 3.005 Coolant2
ANNULUS # 3.265 Coolant2
ANNULUS # 3.525 Coolant2
ANNULUS # 3.638 Coolant2
```

```
ANNULUS # 3.750 Coolant2
ANNULUS # 4.010 Coolant2
ANNULUS # 4.270 Coolant2
ANNULUS # 4.530 Coolant2
ANNULUS # 5.050 Coolant2
ANNULUS # 5.150 Tube2
ANNULUS # 5.4933 Inswet
ANNULUS # 5.9366 Inswet
ANNULUS # 6.15 Inswet
ANNULUS # 6.730 PT
ANNULUS # 7.080 PT
ANNULUS # 7.430 PT
ANNULUS # 7.5500 PT

ANNULUS # 8.2300 moder

ANNULUS # 8.5800 moder
ANNULUS # 8.9300 moder
ANNULUS # 9.2800 moder
ANNULUS # 9.6300 moder
*
ANNULUS # 10.00 moder
ANNULUS # 10.50 moder
ANNULUS # 11.00 moder
ANNULUS # 11.50 moder
ANNULUS # 12.00 moder
ANNULUS # 13.00 moder
ANNULUS # 14.1047 moder * LP = 25.0 cm

NPIJAN #

*-----Fuel and bundle specifications------------------
Array # 1 1 0 0
RODSUB # # .275000 Fuel_1
RODSUB # # .338891 Fuel_1
Rodsub # # 0.4473 Fuel_1
Rodsub # # 0.6326 Fuel_1
Rodsub # # 0.6750 Clad
*
Array # 1 7 1.73000 0
RODSUB # # .275000 Fuel_2
RODSUB # # .338891 Fuel_2
Rodsub # # 0.4473 Fuel_2
Rodsub # # 0.6326 Fuel_2
Rodsub # # 0.6750 Clad
*
Array # 1 14 3.10000 0.224400
RODSUB # # .275000 Fuel_3
RODSUB # # .338891 Fuel_3
Rodsub # # 0.4783 Fuel_3
Rodsub # # 0.5350 Fuel_3
Rodsub # # 0.5723 Clad
*
Array # 1 21 4.400000 0
RODSUB # # 0.275000 Fuel_4
RODSUB # # 0.338891 Fuel_4
```

```
Rodsub # # 0.4783 Fuel_4
Rodsub # # 0.5350 Fuel_4
Rodsub # # 0.5723 Clad

*
newres 4 0.1 -6 0.d 60.d
Tolerance 1e-6
*

FewGroups 1 2 3 4 5 6 7 8 9 $
10 11 12 13 14 15 16 17 18 19 $
20 21 22 23 24 25 26 27 28 29 $
30 31 32 33 34 35 36 37 38 39 $
40 41 42 43 44 45 46 47 48 49 $
50 51 52 53 54 55 56 57 58 59 $
60 61 62 63 64 65 66 67 68 69 $
70 71 72 73 74 75 76 77 78 79 $
80 81 82 83 84 85 86 87 88 89 * 89 group
Suppress 1 1 1 1 1 1 1 1 1 1 -1 1 1 1 0
WATER Coolant2 0.59254 632.35 COOL DD2O = 0.015576
*
Material INSULATOR 5.68 551 Moder $
Zr90 50.7096 $
Zr91 11.1808 $
Zr92 17.2778 $
Zr94 17.8907 $
Zr96 2.9437 $
O16 35.0684
*
Mixture Inswet INSULATOR 0.3 Coolant2 0.7 554.88 Moder
*
Water Moder 1.08509 342.16 Moder dd2o=99.833
*
MATERIAL SS310C 7.750 796.35 CLAD $ * clad at 0.500 m
C = 0.250 $
MN55 = 2.000 $
P31 = 0.045 $
S32 = 0.028414 $
S33 = 0.000231 $
S34 = 0.001351 $
S36 = 0.000003 $
SI28 = 1.377997 $
SI29 = 0.072504 $
SI30 = 0.049498 $
CR50 = 1.043422 $
CR52 = 20.924854 $
CR53 = 2.418398 $
CR54 = 0.613341 $
NI58 = 13.775518 $
NI60 = 5.489068 $
NI61 = 0.242588 $
NI62 = 0.242588 $
NI64 = 0.206671 $
FE54 = 2.860894137 $
FE56 = 46.57122154 $
FE57 = 1.09476965 $
```

```
FE58 = 0.148247254
MATERIAL SS310T 7.750 632.35 CLAD $
C = 0.250 $
MN55 = 2.000 $
P31 = 0.045 $
S32 = 0.028414 $
S33 = 0.000231 $
S34 = 0.001351 $
S36 = 0.000003 $
SI28 = 1.377997 $
SI29 = 0.072504 $
SI30 = 0.049498 $
CR50 = 1.043422 $
CR52 = 20.924854 $
CR53 = 2.418398 $
CR54 = 0.613341 $
NI58 = 13.775518 $
NI60 = 5.489068 $
NI61 = 0.242588 $
NI62 = 0.242588 $
NI64 = 0.206671 $
FE54 = 2.860894137 $
FE56 = 46.57122154 $
FE57 = 1.09476965 $
FE58 = 0.148247254
Mixture Tube2 SS310T 0.3 Coolant2 0.7 632.35 COOL * Liner at 0.500 m
Material Clad2 7.750 632.35 CLAD $ * clad at 0.500 m
C = 0.250 $
MN55 = 2.000 $
P31 = 0.045 $
S32 = 0.028414 $
S33 = 0.000231 $
S34 = 0.001351 $
S36 = 0.000003 $
SI28 = 1.377997 $
SI29 = 0.072504 $
SI30 = 0.049498 $
CR50 = 1.043422 $
CR52 = 20.924854 $
CR53 = 2.418398 $
CR54 = 0.613341 $
NI58 = 13.775518 $
NI60 = 5.489068 $
NI61 = 0.242588 $
NI62 = 0.242588 $
NI64 = 0.206671 $
FE54 = 2.860894137 $
FE56 = 46.57122154 $
FE57 = 1.09476965 $
FE58 = 0.148247254
Material PT 6.515 477.55 Moder $ * PT at 0.500 m
NB93=2.58 $
FE54=0.00266589864 $
FE56=0.042976786 $
FE57=0.00100160658 $
FE58=0.000135886544 $
```

```
CR50=0.000337568856 $
CR52=0.006769656 $
CR53=0.000782319888 $
CR54=0.000198430992 $
NI58=0.002481955 $
NI60=0.00098154 $
NI64=3.6505e-05 $
B10=.00002431 $
ZR90=49.344300082 $
ZR91=10.880521806 $
ZR92=16.813671028 $
ZR94=17.410197266 $
ZR96=2.8645910062
MATERIAL CPin 6.515 632.35 FUEL $ * Centre Pin at 0.500 m
Zr90 = 50.7096 $
Zr91 = 11.1808 $
Zr92 = 17.2778 $
Zr94 = 17.8907 $
Zr96 = 2.9437 $
O16 = 35.0684 $
U235 = 0.0000001

NOBURN CPin

*
Material eUO2 10.12 960.16 Fuel O16=13.44410 U235=4.0 U238=95.994592 U234=0.005408
*
*
*
Material Fuel_1 eUO2
Material Fuel_2 eUO2
Material Fuel_3 eUO2
Material Fuel_4 eUO2
*
Buckling 0.24e-4 0.85e-4 1e-5 1e-5
POWER 8 15427 0.2 1 0.0001
write 1
BEGIN
LEAKAGE -6
BUCKLING 1.0E-4 1.0E-4
BENOIST 1
BEEONE 1
CELLAV
PRINT -2 -2 1 1 1 0
REACTION ALL=0
PARTITION 65 89
MATERIAL 0
BEGIN
POWER 8 -1 0.3 1
WRITE 2
BEGIN
BEGIN
POWER 8 -1 0.4 1
WRITE 3
BEGIN
BEGIN
```

```
POWER 8 -1 0.5 1
WRITE 4
BEGIN
BEGIN
POWER 8 -1 0.7 1
WRITE 5
BEGIN
BEGIN
POWER 8 -1 1 1
```

Appendix B

Sample WIMS-AECL Input File: 54 Element Fuel

```
Title ‘‘Super Critical Water Reactor 54 Element Bundle’’

CELL Cluster
SEQUENCE Pij
plot
SYMMETRY -6 0d 60d * 9-pins in each section

LINES 0.0 2.0 80 13
LINES 2.0 6.80 120 13
LINES 6.80 19.0919 200 13

ANNULUS # 2.113 Coolant2
ANNULUS # 2.225 Coolant2 *Inner radius of fuel ring 1
ANNULUS # 2.485 Coolant2
ANNULUS # 2.745 Coolant2
ANNULUS # 3.005 Coolant2
ANNULUS # 3.265 Coolant2
ANNULUS # 3.525 Coolant2 *Outer radius of fuel ring 1
ANNULUS # 3.638 Coolant2
ANNULUS # 3.750 Coolant2 *Inner radius of fuel ring 2
ANNULUS # 4.010 Coolant2
ANNULUS # 4.270 Coolant2
ANNULUS # 4.530 Coolant2
ANNULUS # 4.790 Coolant2
ANNULUS # 5.050 Coolant2 *Outer radius of fuel ring 2
ANNULUS # 5.163 Coolant2
ANNULUS # 5.275 Coolant2 *Inner radius of fuel ring 3
```

```
ANNULUS # 5.535 Coolant2
ANNULUS # 5.795 Coolant2
ANNULUS # 6.055 Coolant2
ANNULUS # 6.315 Coolant2
ANNULUS # 6.575 Coolant2 *Outer radius of fuel ring 3
ANNULUS # 6.688 Coolant2
ANNULUS # 6.800 Coolant2
*
ANNULUS # 6.900 Tube2 *Liner Tube
*
ANNULUS # 7.160 Inswet
ANNULUS # 7.420 Inswet
ANNULUS # 7.680 Inswet
ANNULUS # 7.900 Inswet
ANNULUS # 8.2600 PT
ANNULUS # 8.5200 PT
ANNULUS # 8.7800 PT
ANNULUS # 9.0400 PT
ANNULUS # 9.3000 PT
*
ANNULUS # 9.500 moder
ANNULUS # 10.00 moder
ANNULUS # 10.50 moder
ANNULUS # 11.00 moder
ANNULUS # 11.50 moder
ANNULUS # 12.00 moder
ANNULUS # 13.00 moder
ANNULUS # 14.1047 moder * LP =25.0 cm

NPIJAN #

*-----Fuel and bundle specifications------------------

ARRAY # 1 1 0.0 0.0
RODSUB # # 1.94 CPin
RODSUB # # 2.00 Clad2

ARRAY # 1 12 2.875 15d
RODSUB # # .275000 Fuel_1
RODSUB # # .338891 Fuel_1
RODSUB # # .476314 Fuel_1
RODSUB # # .550000 Fuel_1
RODSUB # # .620000 Fuel_1
RODSUB # # .680000 Clad
*
ARRAY # 1 18 4.400 10d
RODSUB # # .275000 Fuel_2
RODSUB # # .338891 Fuel_2
RODSUB # # .476314 Fuel_2
RODSUB # # .550000 Fuel_2
RODSUB # # .620000 Fuel_2
RODSUB # # .680000 Clad
*
ARRAY # 1 24 5.925 7.5d
RODSUB # # .275000 Fuel_3
RODSUB # # .338891 Fuel_3
```

```
RODSUB # # .476314 Fuel_3
RODSUB # # .550000 Fuel_3
RODSUB # # .620000 Fuel_3
RODSUB # # .680000 Clad
*
newres 4 0.1 -6 0.d 60.d
Tolerance 1e-6
*

FewGroups 1 2 3 4 5 6 7 8 9 $
10 11 12 13 14 15 16 17 18 19 $
20 21 22 23 24 25 26 27 28 29 $
30 31 32 33 34 35 36 37 38 39 $
40 41 42 43 44 45 46 47 48 49 $
50 51 52 53 54 55 56 57 58 59 $
60 61 62 63 64 65 66 67 68 69 $
70 71 72 73 74 75 76 77 78 79 $
80 81 82 83 84 85 86 87 88 89 * 89 group
Suppress 1 1 1 1 1 1 1 1 1 1 -1 1 1 1 0
*
WATER Coolant2 0.59254 632.35 COOL DD2O = 0.015576 * coolant at 0.500 m

Material INSULATOR 5.68 551 Moder $
Zr90 50.7096 $
Zr91 11.1808 $
Zr92 17.2778 $
Zr94 17.8907 $
Zr96 2.9437 $
O16 35.0684
Mixture Inswet INSULATOR 0.3 Coolant2 0.7 554.88 Moder * insulator at 0.500 m
*
Water Moder 1.08509 342.16 Moder dd2o=99.833
MATERIAL SS310C 7.750 796.35 CLAD $ * clad at 0.500 m
C = 0.250 $
MN55 = 2.000 $
P31 = 0.045 $
S32 = 0.028414 $
S33 = 0.000231 $
S34 = 0.001351 $
S36 = 0.000003 $
SI28 = 1.377997 $
SI29 = 0.072504 $
SI30 = 0.049498 $
CR50 = 1.043422 $
CR52 = 20.924854 $
CR53 = 2.418398 $
CR54 = 0.613341 $
NI58 = 13.775518 $
NI60 = 5.489068 $
NI61 = 0.242588 $
NI62 = 0.242588 $
NI64 = 0.206671 $
FE54 = 2.860894137 $
FE56 = 46.57122154 $
FE57 = 1.09476965 $
FE58 = 0.148247254
```

```
MATERIAL SS310T 7.750 632.35 CLAD $ * clad at 0.500 m
C = 0.250 $
MN55 = 2.000 $
P31 = 0.045 $
S32 = 0.028414 $
S33 = 0.000231 $
S34 = 0.001351 $
S36 = 0.000003 $
SI28 = 1.377997 $
SI29 = 0.072504 $
SI30 = 0.049498 $
CR50 = 1.043422 $
CR52 = 20.924854 $
CR53 = 2.418398 $
CR54 = 0.613341 $
NI58 = 13.775518 $
NI60 = 5.489068 $
NI61 = 0.242588 $
NI62 = 0.242588 $
NI64 = 0.206671 $
FE54 = 2.860894137 $
FE56 = 46.57122154 $
FE57 = 1.09476965 $
FE58 = 0.148247254

Mixture Tube2 SS310T 0.3 Coolant2 0.7 632.35 COOL
Material Clad2 7.750 632.35 CLAD $
C = 0.250 $
MN55 = 2.000 $
P31 = 0.045 $
S32 = 0.028414 $
S33 = 0.000231 $
S34 = 0.001351 $
S36 = 0.000003 $
SI28 = 1.377997 $
SI29 = 0.072504 $
SI30 = 0.049498 $
CR50 = 1.043422 $
CR52 = 20.924854 $
CR53 = 2.418398 $
CR54 = 0.613341 $
NI58 = 13.775518 $
NI60 = 5.489068 $
NI61 = 0.242588 $
NI62 = 0.242588 $
NI64 = 0.206671 $
FE54 = 2.860894137 $
FE56 = 46.57122154 $
FE57 = 1.09476965 $
FE58 = 0.148247254

Material Clad SS310C
Material PT 6.515 477.55 Moder $
NB93=2.58 $
FE54=0.00266589864 $
FE56=0.042976786 $
```

```
FE57=0.00100160658 $
FE58=0.000135886544 $
CR50=0.000337568856 $
CR52=0.006769656 $
CR53=0.000782319888 $
CR54=0.000198430992 $
NI58=0.002481955 $
NI60=0.00098154 $
NI64=3.6505e-05 $
B10=.00002431 $
ZR90=49.344300082 $
ZR91=10.880521806 $
ZR92=16.813671028 $
ZR94=17.410197266 $
ZR96=2.8645910062
MATERIAL CPin 6.515 632.35 FUEL $
Zr90 = 50.7096 $
Zr91 = 11.1808 $
Zr92 = 17.2778 $
Zr94 = 17.8907 $
Zr96 = 2.9437 $
O16 = 35.0684 $
U235 = 0.0000001

NOBURN CPin

*
Material eUO2 10.12 960.16 Fuel O16=13.44410 U235=4.0 U238=95.994592 U234=0.005408
*
*
Material Fuel_1 eUO2
Material Fuel_2 eUO2
Material Fuel_3 eUO2

Buckling 0.24e-4 0.85e-4 1e-5 1e-5
POWER 8 15427 0.2 1 0.0001
write 1
BEGIN
LEAKAGE -6
BUCKLING 1.0E-4 1.0E-4
BENOIST 1
BEEONE 1
CELLAV
PRINT -2 -2 1 1 1 0
REACTION ALL=0
PARTITION 65 89
MATERIAL 0
BEGIN
POWER 8 -1 0.3 1
```

Appendix C

Sample RFSP Input

C.1 Geometry Definition

```
*START M.MCDONALD
BASED ON SCWR
*MODEL SUPER CANDU -- MESH SIZE 52 X 52 X 22
*DATA GEOMETRY
A 52 52 22 20 20 10 0 0 0 0 0 0 300 3000 475
B 0.000 0.000 0.000
C 60.057 60.057 0.000
D 25.000 25.000 50.000
E 1 251 251 221
F 0102030405060708091011121314151617181920
G A B C D E F G H J K L M N O P Q R S T U
H 1 2 3 4 5 6 7 8 910
I 0 0 0 0 0 0 0 0 1 1 1 1 1 1 1 0 0 0 0 0 0 0 0
I 0 0 0 0 0 0 0 1 1 1 1 1 1 1 1 1 0 0 0 0 0 0 0
I 0 0 0 0 0 1 1 1 1 1 1 1 1 1 1 1 1 1 0 0 0 0 0
I 0 0 0 0 1 1 1 1 1 1 1 1 1 1 1 1 1 1 1 0 0 0 0
I 0 0 0 1 1 1 1 1 1 1 1 1 1 1 1 1 1 1 1 1 0 0 0
I 0 0 1 1 1 1 1 1 1 1 1 1 1 1 1 1 1 1 1 1 1 0 0
I 0 0 1 1 1 1 1 1 1 1 1 1 1 1 1 1 1 1 1 1 1 0 0
I 0 1 1 1 1 1 1 1 1 1 1 1 1 1 1 1 1 1 1 1 1 1 0
I 1 1 1 1 1 1 1 1 1 1 1 1 1 1 1 1 1 1 1 1 1 1 1
I 1 1 1 1 1 1 1 1 1 1 1 1 1 1 1 1 1 1 1 1 1 1 1
I 1 1 1 1 1 1 1 1 1 1 1 1 1 1 1 1 1 1 1 1 1 1 1
I 1 1 1 1 1 1 1 1 1 1 1 1 1 1 1 1 1 1 1 1 1 1 1
I 1 1 1 1 1 1 1 1 1 1 1 1 1 1 1 1 1 1 1 1 1 1 1
I 1 1 1 1 1 1 1 1 1 1 1 1 1 1 1 1 1 1 1 1 1 1 1
I 0 1 1 1 1 1 1 1 1 1 1 1 1 1 1 1 1 1 1 1 1 1 0
I 0 0 1 1 1 1 1 1 1 1 1 1 1 1 1 1 1 1 1 1 1 0 0
I 0 0 1 1 1 1 1 1 1 1 1 1 1 1 1 1 1 1 1 1 1 0 0
```

```
I 0 0 0 1 1 1 1 1 1 1 1 1 1 1 1 1 1 0 0 0
I 0 0 0 0 1 1 1 1 1 1 1 1 1 1 1 1 1 0 0 0 0
I 0 0 0 0 0 0 0 1 1 1 1 1 1 1 1 0 0 0 0 0 0
I 0 0 0 0 0 0 0 0 1 1 1 1 1 1 1 0 0 0 0 0 0 0
J A01 U20 ZONE_1
K A01 1 U20 1 SUPER1
K A01 2 U20 2 SUPER1
K A01 3 U20 3 SUPER2
K A01 4 U20 4 SUPER2
K A01 5 U20 5 SUPER3
K A01 6 U20 6 SUPER3
K A01 7 U20 7 SUPER4
K A01 8 U20 8 SUPER4
K A01 9 U20 9 SUPER5
K A0110 U2010 SUPER5
L 20040424 1
X 10.8620 251
X 12.5000 350
Y 10.8620 251
Y 12.5000 350
Z 24.7650 221
M 310.057 310.057 310.057
P 3.1559 3.8545
*PRINT MESH SPACE
*DATA IRRADIATON
C A 08 10
*DATA 2-GROUP
MODEL MOVEPROPS2 ADJGT ADJGT
2GTR1 .0
2GTR2 .0
2GSA1 .0
2GSA2 .0
2GNF1 .0
2GNF2 .0
2GS12 .0
2GS21 .0
2GH1 .0
2GH2 .0
MODEL MOVE DEVS2 ADJGT ADJ01GT 2
A 197.1125 225.6875 .0000 670.8380 352.4150 401.9450
*PRINT FUEL TYPES
*PRINT REGIONS
*READ CARD
BLOCK LATPROPS2GREFLECTOR
FORMAT (2I10)
READ reflector 1 2
FORMAT (6E20.11)
READ reflector 3 13
*READ CARD
BLOCK LATPROPS2GSUPER1
FORMAT (-A10)
READ super1 1 1
FORMAT (2I10)
READ super1 3 4
FORMAT (6E20.11)
READ super1 5 4262
```

```
BLOCK XENONPROP2SUPER1
FORMAT (-A10)
READ super1 1 1
FORMAT (2I10)
READ super1 3 4
FORMAT (6E20.11)
READ super1 5 1166
BLOCK WIMSBURIRRSUPER1
FORMAT (-A10)
READ super1 1 1
FORMAT (I10)
READ super1 3 3
FORMAT (6E20.11)
READ super1 4 262
*READ CARD
BLOCK LATPROPS2GSUPER2
FORMAT (-A10)
READ super2 1 1
FORMAT (2I10)
READ super2 3 4
FORMAT (6E20.11)
READ super2 5 4262
BLOCK XENONPROP2SUPER2
FORMAT (-A10)
READ super2 1 1
FORMAT (2I10)
READ super2 3 4
FORMAT (6E20.11)
READ super2 5 1166
BLOCK WIMSBURIRRSUPER2
FORMAT (-A10)
READ super2 1 1
FORMAT (I10)
READ super2 3 3
FORMAT (6E20.11)
READ super2 4 262
*READ CARD
BLOCK LATPROPS2GSUPER3
FORMAT (-A10)
READ super3 1 1
FORMAT (2I10)
READ super3 3 4
FORMAT (6E20.11)
READ super3 5 4262
BLOCK XENONPROP2SUPER3
FORMAT (-A10)
READ super3 1 1
FORMAT (2I10)
READ super3 3 4
FORMAT (6E20.11)
READ super3 5 1166
BLOCK WIMSBURIRRSUPER3
FORMAT (-A10)
READ super3 1 1
FORMAT (I10)
READ super3 3 3
```

```
FORMAT (6E20.11)
READ super3 4 262
*READ CARD
BLOCK LATPROPS2GSUPER4
FORMAT (-A10)
READ super4 1 1
FORMAT (2I10)
READ super4 3 4
FORMAT (6E20.11)
READ super4 5 4262
BLOCK XENONPROP2SUPER4
FORMAT (-A10)
READ super4 1 1
FORMAT (2I10)
READ super4 3 4
FORMAT (6E20.11)
READ super4 5 1166
BLOCK WIMSBURIRRSUPER4
FORMAT (-A10)
READ super4 1 1
FORMAT (I10)
READ super4 3 3
FORMAT (6E20.11)
READ super4 4 262
*READ CARD
BLOCK LATPROPS2GSUPER5
FORMAT (-A10)
READ super5 1 1
FORMAT (2I10)
READ super5 3 4
FORMAT (6E20.11)
READ super5 5 4262
BLOCK XENONPROP2SUPER5
FORMAT (-A10)
READ super5 1 1
FORMAT (2I10)
READ super5 3 4
FORMAT (6E20.11)
READ super5 5 1166
BLOCK WIMSBURIRRSUPER5
FORMAT (-A10)
READ super5 1 1
FORMAT (I10)
READ super5 3 3
FORMAT (6E20.11)
READ super5 4 262
*DATA FLUX/POWER
A 2 4 2540000.0 1.00000 0.00001 1.5 1.01 0.05 1 100
B 1 1.0 0.5
*simulate SCWR FRESH CORE 0.0 0 0 1 30 0 15 0
2-GROUP
E 0 10 2540000.0 1.00000 0.00001 1.5 1.01 0.05 0 101999
*PRINT POWERS
*PRINT NOTCHRADII
*PRINT DIMENSIONS
*PRINT MESH SPACE
```

```
*PRINT MOVE DEVS2
*MAKE DAF SCWRSETUP

*CLOSE NORMAL TERMINATION
```

C.2 Irradiation Iteration Input

```
*USE DAF SCWRSETUP
*START M.McDONALD
*MODEL SCWR
*READ CARD
BLOCK SIMULDATA SCWR 0 0FUEL IRRAD
FORMAT (10F7.4)
READ irr01.out 1 3000
*PRINT FUEL IRRAD
$
$ step 1
$
*SIMULATE SCWR 0 0.0 0 30 15
2-GROUP
E 0 10 2540000.0 1.00000 0.00001 1.500 1.01 0.05 0 999
*PRINT POWERS
$
$ step 2
$
*SIMULATE SCWR 999999999 10.0 0 30 15
2-GROUP
E 0 10 2540000.0 1.00000 0.00001 1.500 1.01 0.05 0 999
*PRINT POWERS
$
$ step 3
$
*SIMULATE SCWR 999999999 10.0 0 30 15
2-GROUP
E 0 10 2540000.0 1.00000 0.00001 1.500 1.01 0.05 0 999
*PRINT POWERS
$
$ step 4
$
*SIMULATE SCWR 999999999 20.0 0 30 15
2-GROUP
E 0 10 2540000.0 1.00000 0.00001 1.500 1.01 0.05 0 999
*PRINT POWERS
$
$ step 5
$
*SIMULATE SCWR 999999999 20.0 0 30 15
2-GROUP
E 0 10 2540000.0 1.00000 0.00001 1.500 1.01 0.05 0 999
*PRINT POWERS
$
$ step 6
$
```

```
*SIMULATE SCWR 999999999 20.0 0 30 15
2-GROUP
E 0 10 2540000.0 1.00000 0.00001 1.500 1.01 0.05 0 999
*PRINT POWERS
$
$ step 7
$
*SIMULATE SCWR 999999999 20.0 0 30 15
2-GROUP
E 0 10 2540000.0 1.00000 0.00001 1.500 1.01 0.05 0 999
*PRINT POWERS
$
$ end of 100 FPD
$
$ step 8
$
*SIMULATE SCWR 999999999 20.0 0 30 15
2-GROUP
E 0 10 2540000.0 1.00000 0.00001 1.500 1.01 0.05 0 999
*PRINT POWERS
$
$ step 9
$
*SIMULATE SCWR 999999999 20.0 0 30 15
2-GROUP
E 0 10 2540000.0 1.00000 0.00001 1.500 1.01 0.05 0 999
*PRINT POWERS
$
$ step 10
$
*SIMULATE SCWR 999999999 20.0 0 30 15
2-GROUP
E 0 10 2540000.0 1.00000 0.00001 1.500 1.01 0.05 0 999
*PRINT POWERS
$
$ step 11
$
*SIMULATE SCWR 999999999 20.0 0 30 15
2-GROUP
E 0 10 2540000.0 1.00000 0.00001 1.500 1.01 0.05 0 999
*PRINT POWERS
$
$ step 12
$
*SIMULATE SCWR 999999999 20.0 0 30 15
2-GROUP
E 0 10 2540000.0 1.00000 0.00001 1.500 1.01 0.05 0 999
*PRINT POWERS
$
$ end of 200 FPD
$
$ step 13
$
*SIMULATE SCWR 999999999 20.0 0 30 15
2-GROUP
E 0 10 2540000.0 1.00000 0.00001 1.500 1.01 0.05 0 999
```

```
*PRINT POWERS
$
$ step 14
$
*SIMULATE SCWR 999999999 20.0 0 30 15
2-GROUP
E 0 10 2540000.0 1.00000 0.00001 1.500 1.01 0.05 0 999
*PRINT POWERS
$
$ step 15
$
*SIMULATE SCWR 999999999 20.0 0 30 15
2-GROUP
E 0 10 2540000.0 1.00000 0.00001 1.500 1.01 0.05 0 999
*PRINT POWERS
$
$ step 16
$
*SIMULATE SCWR 999999999 20.0 0 30 15
2-GROUP
E 0 10 2540000.0 1.00000 0.00001 1.500 1.01 0.05 0 999
*PRINT POWERS
$
$ step 17
$
*SIMULATE SCWR 999999999 20.0 0 30 15
2-GROUP
E 0 10 2540000.0 1.00000 0.00001 1.500 1.01 0.05 0 999
*PRINT POWERS
*PRINT FUEL IRRAD
*PRINT FUELBURNUP
$
$ end of 300 FPD
$ step 18
$
*SIMULATE SCWR 999999999 20.0 0 30 15
2-GROUP
E 0 10 2540000.0 1.00000 0.00001 1.500 1.01 0.05 0 999
*PRINT POWERS
$
$ END OF 320 FPD
$
*PRINT MASS
*rite card
FORMAT (10F7.4)
BLOCK IRRADIATONFUEL IRRAD
WRITE irrad02
$
$
*CLOSE NORMAL TERMINATION
```

Appendix D

Perl Refueling Irratiation Script

```
#!/usr/bin/perl -w
use strict;
use warnings;

#
# PERL SCRIPT TO PERFORM REFUELLING
# By:  M. McDonald
# November 23, 2010
#

open(my $scheme, '<scheme.txt') or die qq{Cannot open data.txt:  $!};
open(my $sym, '<symmetric.txt') or die qq{Cannot open symmetric.txt:  $!};
print(''Input filename:  '');
my $in =<STDIN>;
open(my $irrad, ''$in'') or die qq{Cannot open irrad:  $!};
open(my $core, 'core.txt');
print(''Output filename:  '');
my $out=<STDIN>;
open(my $output,''>$out'') or die qq{Cannot open out};

my $line;
my $cellinquad1;
my $rest;
my %hoa;
my %cells;
my %irrads;
my @chanlist;
my @array;


# Get equivalent channels
```

```
while (my $line = <$sym>){
chomp $line;
if($line =~m/^’/){next;} #skips line if it’s a comment
else{
($cellinquad1, $rest) = split ‘ ’, $line, 2;
my @fields=split ‘ ’, $rest;
$hoa{$cellinquad1}=[@fields];
}
}


# Get list of channels corresponding to RFSP output

my $x=0;
while (my $line = <$core>){
chomp $line;
if($line =~m/^’/){next;} #skips line if it’s a comment
else{
my @cells= split ‘ ’, $line;
for(my $p=1; $p<10; $p++){
if($cells[$p]==1){$chanlist[$x]=‘‘$cells[0]0$p’’;$x++;}
}
for(my $p=10; $p<($#cells +1); $p++){
if($cells[$p]==1){$chanlist[$x]=‘‘$cells[0]$p’’;$x++;}
}
}
}
my $channumber = $#chanlist + 1;

# Read in irradiations
my $i=0;
while (my $line = <$irrad>){
chomp $line;
if($line = ~m/^’/){next;} #skips line if it’s a comment


else{
$irrads{$chanlist[$i]} = $line;
$i++;
}}


######################### # Swap assemblies in each quadrant according to scheme.txt
while (my $line = <$scheme>){
chomp $line;
@array = split ‘ ’, $line;
if($line = m/^’/){next;} #skips line if it’s a comment
else{
if($array[1] eq ‘fff’){
$irrads{$array[0]}=(‘‘ 0.0000 0.0000 0.0000 0.0000 0.0000 0.0000 0.0000 0.0000 0.0000 0.0000’’);
$irrads{$hoa{$array[0]}[0]}=(‘‘0.0000 0.0000 0.0000 0.0000 0.0000 0.0000 0.0000 0.0000 0.0000 0.0000’’);
$irrads{$hoa{$array[0]}[1]}=(‘‘ 0.0000 0.0000 0.0000 0.0000 0.0000 0.0000 0.0000 0.0000 0.0000 0.0000’’);
$irrads{$hoa{$array[0]}[2]}=(‘‘0.0000 0.0000 0.0000 0.0000 0.0000 0.0000 0.0000 0.0000 0.0000 0.0000’’);
}
else{
$irrads{$array[0]} = $irrads{$array[1]};
$irrads{$hoa{$array[0]}[0]} = $irrads{$hoa{$array[1]}[0]};
$irrads{$hoa{$array[0]}[1]} = $irrads{$hoa{$array[1]}[1]};
```

```
$irrads{$hoa{$array[0]}[2]} = $irrads{$hoa{$array[1]}[2]};
}
}
}

# Print out new file irr.out

for(my $i=0; $i< $channumber; $i++){
printf $output (``$irrads{$chanlist[$i]} \n'');
}

# DONE!


close($scheme);
close($sym);
close($irrad);
close($output);
close($core);
```

Appendix E

Sample FUELPIN Input

```
DRFLAG : 01
VRFLAG : 00
SDFLAG : 00
MWFLAG : 01
PFFLAG : 00
DSFLAG : 01
FLAG1 :  00
N16 :  00
DELTAT : +0.100000000E-02
REA0 :  +0.000000000E+00
N0 :  +0.100000000E+01
RPIN0 : +0.103000000E+01
QN0 :  +0.500000000E+02
TC0 :  +0.400000000E+03
HB : +0.120000000E+02
HP : +0.100000000E+02
ATFB : +0.000000000E+00
PDRY : +0.117600000E-05
HDRY : +0.120000000E+02
PSAT : +0.100000000E+03
TCSAT : +0.310000000E+03
RAD : +0.632600000E-02
TG : +0.150000000E-03
TCLAD : +0.424000000E-03
ROF : +0.101200000E+05
ROC : +0.790000000E+04
BETA : +0.100000000E+01
LSTAR : +0.100000000E-03
GROUPNO : 15
LAM(1) :  +0.127780000E-01
LAM(2) :  +0.315350000E-01
LAM(3) :  +0.122197000E+00
```

```
LAM(4) :  +0.322820000E+00
LAM(5) :  +0.138928900E+01
LAM(6) :  +0.377833600E+01
LAM(7) :  +0.626000000E-06
LAM(8) :  +0.363000000E-05
LAM(9) :  +0.437000000E-04
LAM(10) :  +0.117000000E-03
LAM(11) :  +0.428000000E-03
LAM(12) :  +0.150000000E-02
LAM(13) :  +0.481000000E-02
LAM(14) :  +0.169000000E-01
LAM(15) :  +0.277000000E+00
B(1) :  +0.176900000E-03
B(2) :  +0.114980000E-02
B(3) :  +0.101910000E-02
B(4) :  +0.210570000E-02
B(5) :  +0.772600000E-03
B(6) :  +0.196200000E-03
B(7) :  +0.161000000E-06
B(8) :  +0.323000000E-06
B(9) :  +0.103000000E-05
B(10) :  +0.748000000E-05
B(11) :  +0.661000000E-05
B(12) :  +0.108000000E-04
B(13) :  +0.224000000E-04
B(14) :  +0.652000000E-04
B(15) :  +0.208000000E-03
NUMPTS : 03
LAMH(1) :  +0.103680000E+00
LAMH(2) :  +0.142000000E-03
LAMH(3) :  +0.476000000E-02
GAM(1) :  +0.226000000E-01
GAM(2) :  +0.231100000E-01
GAM(3) :  +0.207800000E-01
NTRPS : 02
SRDELA : +0.000000000E+00
NUMTRPPRM: 06
TDELAY(1):  +0.100000000E+00
TDELAY(2):  +0.580000000E-01
TDELAY(3):  +0.100000000E+00
TDELAY(4):  +0.100000000E+00
TDELAY(5):  +0.100000000E+00
TDELAY(6):  +0.100000000E+00
TCONST(1):  +0.000000000E+00
TCONST(2):  +0.600000000E-01
TCONST(3):  +0.200000000E+00
TCONST(4):  +0.000000000E+00
TCONST(5):  +0.200000000E+00
TCONST(6):  +0.200000000E+00
TRPSP(1) :  +0.106000000E+01
TRPSP(2) :  +0.999900000E+04
TRPSP(3) :  +0.100000000E+00
TRPSP(4) :  +0.106000000E+01
TRPSP(5) :  +0.150000000E+00
TRPSP(6) :  +0.999900000E+04
NRTP : 14
```

```
SHUTDOWN : +0.000000000E+00 +0.000000000E+00 +0.100000000E+01
:  +0.200000000E+00 +0.000000000E+00 +0.100000000E+01
:  +0.670000000E+00 -0.570000000E+00 +0.100000000E+01
:  +0.840000000E+00 -0.170000000E+01 +0.100000000E+01
:  +0.990000000E+00 -0.290000000E+01 +0.100000000E+01
:  +0.114000000E+01 -0.490000000E+01 +0.100000000E+01
:  +0.127000000E+01 -0.790000000E+01 +0.100000000E+01
:  +0.140000000E+01 -0.131000000E+02 +0.100000000E+01
:  +0.153000000E+01 -0.219000000E+02 +0.100000000E+01
:  +0.167000000E+01 -0.357000000E+02 +0.100000000E+01
:  +0.182000000E+01 -0.537000000E+02 +0.100000000E+01
:  +0.230000000E+01 -0.631000000E+02 +0.100000000E+01
:  +0.300000000E+01 -0.630000000E+02 +0.100000000E+01
:  +0.100000000E+04 -0.630000000E+02 +0.100000000E+01
NUMPTS1 :  05
NUMPTS2 :  05
ALPHA(1) :  -0.100000000E-01
ALPHA(2) :  -0.400000000E-02
ALPHA(3) :  -0.330000000E-01
ALPHA(4) :  -0.150000000E-02
ALPHA(5) :  +0.000000000E+00
TAU(1) :  +0.952400000E+02
TAU(2) :  +0.153846000E+04
TAU(3) :  +0.133333300E+05
TAU(4) :  +0.333333330E+06
TAU(5) :  +0.000000000E+00
TAMP : +0.150000000E-01
ALPHA2(1):  +0.150000000E-01
ALPHA2(2):  +0.230000000E-01
ALPHA2(3):  +0.160000000E-01
ALPHA2(4):  +0.450000000E-01
ALPHA2(5):  +0.140000000E-01
TAU2(1) :  +0.390000000E+01
TAU2(2) :  +0.300000000E+02
TAU2(3) :  +0.250000000E+03
TAU2(4) :  +0.240000000E+04
TAU2(5) :  +0.170000000E+06
IOPT : 00
CC1 :  +0.500000000E-01
NUMPTS1 :  01
NUMPTS2 :  01
DK1(1) :  0.0000000000E+00
DTAU1(1) :  0.0000000000E+00
DK2(1) :  0.0000000000E+00
DTAU2(1) :  0.0000000000E+00
NUMPTS : 04
N16TC(1) :  +0.000000000E+00
N16TC(2) :  +0.000000000E+00
N16TC(3) :  +0.000000000E+00
N16TC(4) :  +0.000000000E+00
NUMPTS : 04
CC(1) :  +0.900000000E-02
CC(2) :  +0.700000000E-02
CC(3) :  +0.330000000E-01
CC(4) :  +0.120000000E-01
GAIN : +0.100000000E+01
```

```
DELT(1) :  +0.300000000E+01
DELT(2) :  +0.300000000E+02
DELT(3) :  +0.300000000E+03
DELT(4) :  +0.300000000E+04
LTAU(1) :  +0.300000000E+02
LTAU(2) :  +0.250000000E+03
LTAU(3) :  +0.240000000E+04
LTAU(4) :  +0.160000000E+06
F : +0.000000000E+00
PRINT : +0.100000000E+00
NTALB1 :  26
RVOID : +0.134000000E+02
DRIVING : +0.000000000E+00 +0.000000000E+01 +1.000000000E+00
:  +0.100000000E+01 +0.010000000E+00 +1.000000000E+00
:  +0.200000000E+01 +0.020000000E+00 +1.000000000E+00
:  +0.300000000E+01 +0.030000000E+00 +1.000000000E+00
:  +0.400000000E+01 +0.040000000E+00 +1.000000000E+00
:  +0.500000000E+01 +0.050000000E+00 +1.000000000E+00
:  +0.600000000E+01 +0.060000000E+00 +1.000000000E+00
:  +0.700000000E+01 +0.070000000E+00 +1.000000000E+00
:  +0.800000000E+01 +0.080000000E+00 +1.000000000E+00
:  +0.900000000E+01 +0.090000000E+00 +1.000000000E+00
:  +0.100000000E+02 +0.100000000E+00 +1.000000000E+00
:  +0.110000000E+02 +0.110000000E+00 +1.000000000E+00
:  +0.120000000E+02 +0.120000000E+00 +1.000000000E+00
:  +0.130000000E+02 +0.130000000E+00 +1.000000000E+00
:  +0.140000000E+02 +0.140000000E+00 +1.000000000E+00
:  +0.150000000E+02 +0.150000000E+00 +1.000000000E+00
:  +0.160000000E+02 +0.160000000E+00 +1.000000000E+00
:  +0.170000000E+02 +0.170000000E+00 +1.000000000E+00
:  +0.180000000E+02 +0.180000000E+00 +1.000000000E+00
:  +0.190000000E+02 +0.190000000E+00 +1.000000000E+00
:  +0.200000000E+02 +0.200000000E+00 +1.000000000E+00
:  +0.210000000E+02 +0.210000000E+00 +1.000000000E+00
:  +0.220000000E+02 +0.220000000E+00 +1.000000000E+00
:  +0.230000000E+02 +0.230000000E+00 +1.000000000E+00
:  +0.240000000E+02 +0.240000000E+00 +1.000000000E+00
:  +0.250000000E+02 +0.250000000E+00 +1.000000000E+00
NUMBER : 00
CHANGE : +0.000000000E+00 +0.000000000E+00 +0.000000000E+00
```